Bio-nanocapsules for Oriented Immobilization of Biological Sensing Molecules

生物由来センサー分子の整列化を行う
バイオナノカプセルに関する研究

IIJIMA Masumi
飯嶋　益巳

October, 2011

Contents

Chapter I

General Introduction

Immunoassay techniques, such as enzyme immunoassay (EIA) [1], radio immunoassay (RIA) [2], and fluorescence immunoassay (FIA) [3], have been widely used for the detection and quantitation of the immunocomplex in samples. Recently, immunosensors [4] (*e.g.*, surface plasmon resonance (SPR) [5], quartz crystal microbalance (QCM) [6]) have been utilized for the high-throughput screening of immunocomplex. In order to improve the sensitivity and specificity of these immunoassays systems, the oriented immobilization of antibodies has been considered as one of the important issues [7, 8].

For EIA, two types of strategies using macromolecules have been utilized in the reaction with antibody to improve the sensitivity. One type of macromolecule allows the clustering of antibodies and labeling molecules (enzyme, radioactive material, fluorophore). For examples, polymeric horseradish peroxidase (HRP)-streptavidin conjugate [9], 3DNA dendrimer [10], and IgG-poly-D-glutamic acid-$(HRP)_n$ conjugate [11] have been used previously. However, these macromolecules require chemical modification of antibodies, and do not allow the oriented immobilization of antibodies [8], which improves the avidity and antigen recognition of antibodies [12]. In general, chemical modification is considered to reduce the stability or antigen-binding activity of antibodies. Another type of macromolecule is expected to permit the oriented immobilization of antibodies. For examples, nanoparticles have been used for displaying antibodies on their surface, *e.g.*, streptavidin-conjugated nanobeads [13] and biotin-coated liposomes [14]. Because biotinylation occurred randomly at free amino groups on the surface of antibodies, these nanoparticles partially accomplished oriented immobilization of antibodies using a biotin-avidin complex. These results encouraged us to develop macromolecules that can assemble antibodies and labeling molecules without chemical modification, in the manner of oriented immobilization.

On the other hands, for immunosensors, the immobilization of antibodies on the solid phase (*e.g.*, gold surface) is accomplished by chemical crosslinking without any control of orientation through single or mixed self-assembled monolayers (SAMs) [15], an immunoglobulin (Ig) G Fc-interacting protein A or G [7, 8], a biotin/(strept)avidin complex [16], or synthetic polymers [17–19]. Since these immobilization methods often utilize agents that react nonspecifically with the protein

amino groups for tethering antibodies or other interacting molecules to the sensor surface, the IgG Fv regions are not always oriented to the solvent. While several methods have been reported for the oriented immobilization of an antibody (*e.g.*, a Fab′ fragment grafted with a thiol group [8]), almost all methods are necessary to modify the IgG antibody by chemical treatment. Thus, it has been paid much attention to develop the new method that is able to improve the sensing techniques without using chemical modification of antibodies.

In 1992, our group developed bio-nanocapsules (BNCs) which are hollow particles of about 50 nm in diameter consisting of HBsAg (hepatitis B virus surface antigen) L proteins and phospholipids, and are efficiently synthesized in the recombinant yeast *Saccharomyces cerevisiae* (up to about 40% (w/w) of total soluble proteins) [20]. In 2003, our group succeeded in loading payloads, such as drugs, polystyrene beads and DNAs, into the inside of BNCs by electroporation [21], and in 2008 by liposome-mediated fusion [22]. By exploiting the infection mechanism of HBV (hepatitis B virus), these BNCs have been used to deliver payloads to human hepatocyte-derived cells *ex vivo* and to a mice *xenograft* model *in vivo* [21-24]. Additionally, the tropism of BNCs can be altered from human liver cells to other cell types, such as epidermal growth factor (EGF) receptor-expressing cells by genetic substitution of EGF for the pre-S1 region of BNC [21, 24]. Recently, our collaborators have made a derivative of BNC in which the N-terminal region (amino acid residue from 51 to 159) of L protein is replaced with a tandem sequence of the IgG Fc-interacting region (Z domain) derived from *Staphylococcus aureus* protein A [25] and designated it ZZ-BNC (*see* Figure 3.1A) [26]. The ZZ-BNC allowed us to display antibodies on its surface and to deliver various therapeutic materials to tissues of interest in an antibody-dependent manner [26]. Hence, all IgG Fc domains are expected to spontaneously attach onto the surface of ZZ-BNC as well as displaying all the IgG Fv regions outwardly for effective binding of antigens. These situations led me to evaluate the ZZ-BNC could adsorb antibodies onto its surface in the manner of oriented immobilization and consequently improve the sensitivity and specificity of antibodies in various immunoassays.

When I started the study, it has been inefficient and time-consuming to obtain the large amounts of BNCs. Since the previous purification method for BNC involved two ultracentrifugational steps, both rotor volume and running time of ultracentrifugation have limited the mass scalability and the time efficiency of this purification process, respectively. Furthermore, due to the trace amount of contaminated yeast-derived proteinases, the functional domains displayed onto the surface of BNC are

often degraded during the long-term storage. In Chapter II, I demonstrated that the combination of heat treatment and sulfated cellulofine column chromatography significantly improved the efficiency of time and mass scalability of BNC production and the purity and yield of purified BNC. In addition, the lyophilization in the presence of an excipient (*e.g.*, sucrose) was also found to greatly prolong the lifetime of BNC without impairing their function. These improvements should facilitate the use of BNCs (including ZZ-BNCs) in a wide variety of biomaterials. Next, in Chapter III, I examined if ZZ-BNCs could contribute to signal enhancement of enzyme-linked immunosorbent assays (ELISAs) and western blot analysis through the formation of IgG-ZZ-BNC complexes. The addition of ZZ-BNCs in the aqueous phase was found to enhance the sensitivity of antigen detection significantly. In combination with the avidin–biotin complex (ABC) system, biotinylated ZZ-BNCs showed more significant signal enhancement in ELISAs and western blot analyses. These results suggested that ZZ-BNC contributes not only to the clustering of antibodies and labeling molecules but also presumably to the oriented immobilization of antibodies. This data led me to decipher the directions of antibodies adsorbed onto ZZ-BNC in Chapter IV. In the previous study conducted by my colleagues, BNC could adsorb onto a mica surface without disrupting its particle structure [27], strongly suggesting that ZZ-BNC is applicable for the scaffold for oriented immobilization of antibodies in the solid phase of various immunoassay systems. In Chapter IV, I evaluated the robustness of ZZ-BNC onto gold surface and then examined if the ZZ-BNC could enhance the sensitivities and antigen-binding capacities of antibodies in the immunosensor chips of QCM and SPR. Furthermore, I analyzed the effect of ZZ-BNC on the affinity of antibodies to corroborate the oriented immobilization of the antibodies. In Chapter V, I prepared the ZZ-BNCs labeled with distinct fluorophores as bio-imaging probes to expand the applications of ZZ-BNC in immunofluorescence techniques. The fluorophore-labeled ZZ-BNCs were found not only to enhance both sensitivity and signal intensity of various immunological assays but also to facilitate the simultaneous immunolabeling of multiple antigens. Even if the available antibodies are derived from the same animal species, the fluorophore-labeled ZZ-BNCs enable the simultaneous detection of multiple antigens in western blot analysis, immunocytochemistry, and flow cytometric analysis. Taken together, these findings described in this thesis indicated that ZZ-BNC is a unique biomaterial facilitating the oriented immobilization of the antibodies, which allows us to improve various immunosensing techniques.

1.2. References

1. Luquin RM. Enzyme immunoassay (EIA)/enzyme-linked immunosorbent assay (ELISA). Clinical Chem 2005;51:2415–2418.
2. Yallow RS, Berson SA. Immunoassay of endogenous plasma insulin in man. Clin Invest 1960;39:1157–1175.
3. Soini E, Hemmilä I. Fluoroimmunoassay: present status and key problems. Clin Chem 1979;25:353–61.
4. Gizeli E, Lowe CR. Immunosensors. Curr Opin Biotechnol 1996;7:66–71.
5. Liedberg B, Nylander C, Lundström I. Biosensing with surface plasmon resonance-how it all standard. Biosens Bioelectron 1995;10:i-ix.
6. Shons A, Dorman F, Najarian JJ. An immunospecific miclobalance. J Biomed Mater Res 1972;6:565–570.
7. Lu B, Smyth MR, O'Kennedy R. Oriented immobilization of antibodies and its applications in immunoassays and immunosensors. Analyst 1996;121:29R–32R.
8. Rao SV, Anderson KW, Bachas LG. Oriented immobilization of proteins. Mikrochim Acta 1998;128:127–143.
9. Vasilov RG, Tsitsikov EN. An ultrasensitive immunoassay for human IgE measurement in cell-culture supernatant. Immunol Lett 1990;26:283–284.
10. Mora JR, Zielinski TL, Nelson BP, Getts RC. Protein detection enhanced by 3DNA dendrimer signal amplification. BioTechniques 2008;44:815–818.
11. Simons B, Kaplan H, Hefford MA. Novel cross-linked enzyme–antibody conjugates for Western blot and ELISA. J Immunol Methods 2006;315:88–98.
12. Lipman NS, Jackson LR, Trudel LJ, Weis-Garcia F. Monoclonal versus polyclonal antibodies: distinguishing characteristics, applications, and information resources. ILAR J 2005;46:258–268.
13. Teramura Y, Arima Y, Iwata H. Surface plasmon resonance-based highly sensitive immunosensing for brain natriuretic peptide using nanobeads for signal amplification. Anal Biochem 2006;357:208–215.
14. Wink T, van Zuilen SJ, Bult A, van Bennekom WP. Liposome-mediated enhancement of the sensitivity in immunoassays of proteins and peptides in surface plasmon resonance spectrometry. Anal Chem 1998;70:827–832.
15. Wink T, van Zuilen SJ, Bult A, van Bennkom WP. Self-assembled monolayers for biosensors. Analyst 1997;122:43R–50R.
16. Johnsson B, Löfås S, Lindquist G, Edström A, Müller Hillgren RM, Hansson A. Comparison of methods for immobilization to carboxymethyl dextran sensor

surfaces by analysis of the specific activity of monoclonal antibodies. J Mol Recog 1995;8:125–131.

17. Geckeler KE, Müller B. Polymer materials in biosensors. Naturwissenschaften 1993;80:18–24.
18. Suzuki N, Quesenberry MS, Wang JK, Lee RT, Kobayashi K, Lee YC. Efficient immobilization of proteins by modification of plate surface with polystyrene derivatives. Anal Biochem 1997;247:412–416.
19. Jordan CE, Corn RM. Surface plasmon resonance imaging measurement of electrostatic biopolymer adsorption onto chemically modified gold surfaces. Anal Chem 1997;69:1449–1456.
20. Kuroda S, Otaka S, Miyazaki T, Nakao M, Fujisawa Y. Hepatitis B virus envelope L protein particles. J Biol Chem. 1992;267:1953–1961.
21. Yamada T, Iwasaki Y, Tada H, Iwabuki H, Chuah MKL, VandenDriessche T, Fukuda H, Kondo A, Ueda M, Seno M, Tanizawa K, Kuroda S. Nanoparticles for the delivery of genes and drugs to human hepatocytes. Nat Biotechnol 2003;21:885–890.
22. Jung J, Matsuzaki T, Tatematsu K, Okajima T, Tanizawa K, Kuroda S. Bio-nanocapsule conjugated with liposomes for *in vivo* pinpoint delivery of various materials. J Control Release 2008;126:55–264.
23. Kasuya T, Jung J, Kinoshita R, Goh Y, Matsuzaki T, Iijima M, Yoshimoto N, Tanizawa K, Kuroda S. Bio-nanocapsule–liposome conjugates for *in vivo* pinpoint drug and gene delivery. Methods Enzymol 2009;464:147–166.
24. Iwasaki Y, Ueda M, Yamada T, Kondo A, Seno M, Tanizawa K, Kuroda S, Sakamoto M, Kitajima M. Gene therapy of liver tumors with human liver-specific nanoparticles. Cancer Gene Ther 2007;14:74–81.
25. Nilsson B, Moks T, Jansson B, Abrahmsén L, Elmblad A, Holmgren E, et al. A synthetic IgG-binding domain based on staphylococcal protein A. Protein Eng 1987;1:107–113.
26. Kurata N, Shishido T, Muraoka M, Tanaka T, Ogino C, Fukuda H, Kondo A. Specific protein delivery to target cells by antibody-displaying bionanocapsules. J Biochem 2008;144:701–707.
27. Kanno T, Yamada T, Iwabuki H, Tanaka H, Kuroda S, Tanizawa K, Kawai T. Size distribution measurement of vesicles by atomic force microscopy. Anal Biochem 2002;309:196–199.

Chapter II

Efficient and Rapid Purification of Drug- and Gene-Carrying Bio-nanocapsules, Hepatitis B Virus Surface Antigen L particles, from Saccharomyces cerevisiae

2.1. Introduction

Hepatitis B virus (HBV) is a 42-nm DNA virus that infects the human liver and causes hepatitis, cirrhosis and hepatocarcinoma [1]. Its envelope (*env*) proteins consist of three HBV surface antigen (HBsAg) proteins: (1) S (small) protein, the major constituent (226 amino acid residues (aa)) of the HBV *env* protein; (2) M (middle) protein, containing an additional 55 aa (pre-S2 region) at the N-terminus of the S protein; (3) L (large) protein, containing a further 108 (subtype *y*) or 119 (subtype *d*) aa (pre-S1 region) at the N-terminus of the M protein [2]. The pre-S1 region is indispensable for HBV infection in human and chimpanzee hepatocytes [3, 4]. Bio-nanocapsules (BNC) are hollow particles of about 50 nm in diameter consisting of HBsAg L proteins and phospholipids, and are efficiently synthesized in the recombinant yeast *Saccharomyces cerevisiae* (up to about 40% (w/w) of total soluble proteins) [5]. In 2003, our group succeeded in loading payloads, such as drugs, polystyrene beads and DNAs, into the inside of BNCs by electroporation [6], and in 2008 by liposome-mediated fusion [7]. These BNCs have been used to deliver payloads to human hepatocyte-derived cells *ex vivo* and to a mice *xenograft* model *in vivo* [6-9]. Additionally, the tropism of BNCs can be altered from human liver cells to other cell types, such as epidermal growth factor (EGF) receptor-expressing cells by genetic substitution of EGF for the pre-S1 region of BNC [6, 9].

As an immunogen of recombinant HBV vaccine, HBsAg S and M particles (BNC-related particles) have been produced in various cells (*e.g., Saccharomyces cerevisiae*, *Pichia pastoris*, Chinese hamster ovary (CHO) cells, and insect cells) for the last 30 years [10-13]. In particular, *S. cerevisiae*-derived S particles have been widely used in clinical fields for reasons of safety, cost-effectiveness, and scalability for mass production [11, 14]. These situations led us to develop *S. cerevisiae*-derived BNCs as a potential drug delivery system (DDS) and as a gene delivery system (GDS) carrier for nanomedicines.

In 1992, our group succeeded in producing HBsAg L particles (BNCs) in *S. cerevisiae* AH22R$^-$ strain carrying the BNC-expression plasmid pGLDLIIP39-RcT [5].

The BNCs were then purified by fractionation with polyethylene glycol (PEG), followed by one CsCl equilibrium and two sucrose density gradient ultracentrifugation steps [15]. However, because of the sequential ultracentrifugation steps, preparation of BNC from wet cells took at least 1 week. Furthermore, the volume capacity of the ultracentrifuge rotor prevented us from expanding the production scale. Although the overall yield of BNCs from wet cells was estimated to be <20% [15], the BNC preparation was sufficient for an immunogen of HB vaccine, but sometimes showed cytotoxic effect on cultured cells (unpublished observation), prompting us to further purify BNC by gel filtration before use as DDS and GDS carriers (Table 2.1). Finally, by using this purification protocol, only about 3% of the BNCs expressed in yeast cells could be used as DDS and GDS carriers. Unexpectedly, the BNC-surface pre-S region degraded during long-term storage; presumably because of trace contamination with yeast proteinases (*see* Figure 2.4A). Taken together, the process used to purify BNCs was time-consuming, had limited scalability for mass production, and did not completely remove contaminating yeast-derived proteinases. These factors might adversely affect the development of promising BNC-based nanomedicines.

Here, I demonstrate that a combination of heat treatment and sulfated cellulofine column chromatography significantly improved the purity and yield of BNC preparations. Lyophilization in the presence of an excipient (*e.g.*, sucrose) was also found to greatly prolong the storage of BNC without impairing their function. These improvements should facilitate the use of BNCs in DDS and GDS.

Table 2.1 Purification of BNC from yeast cells harboring pGLDLIIP39-RcT using the original protocol

Purification steps	Protein (mg) [a]	BNC antigenicity (unit) [b]	Purification (fold-change)	Yield (%)
Crude extract	5,970	225,000	1.0	100
PEG 6000 precipitate	2,770	55,800	5.3	25
CsCl (10–40%) equilibrium ultracentrifugation	54.7	34,600	16.8	15
Sucrose (10–50%) density gradient ultracentrifugation	37.9	24,400	17.0	11
Gel filtration	10.3	7,120	18.3	3

[a]The protein concentration was determined by the BCA assay using BSA as a standard.

[b]BNC antigenicity was measured with an IMx HBsAg assay kit using BNC as a standard.

2.2. Experimental Procedures

2.2.1. Physicochemical analyses of BNC

The protein concentrations of BNCs were determined at each step using BCA protein assay reagent (Sigma) with bovine serum albumin as a standard. The antigenicity of BNC was measured using commercial IMx HBsAg enzyme immunoassays (Abbott), which is based on a sandwich enzyme-linked immunosorbent assay utilizing anti-HBsAg S antibody as solid phase antibody, horseradish peroxidase-labeled anti-HBsAg S antibody as aqueous phase antibody, and purified BNCs as standard. The samples were analyzed by (sodium dodecyl sulfate polyacrylamide gel electrophoresis (SDS-PAGE) followed by silver staining and western blotting using mouse anti-BNC polyclonal antibodies (mouse monoclonal anti-S antibody clone 824; Institute of Immunology). The average diameter of the BNCs was determined in water at 25°C by dynamic light scattering using a Zetasizer Nano-ZS (Malvern).

2.2.2. Original purification protocol for recombinant yeast-derived BNC

The original purification protocol is described in more detail elsewhere [15]. Briefly, the yeast *S. cerevisiae* AH22R$^-$ harboring pGLDLIIP39-RcT was disrupted with glass beads. The crude extract was mixed with a PEG 6000 solution to concentrate the L particles, and was then separated in the CsCl equilibrium ultracentrifugation (10–40%, w/v). In the original procedure, sucrose density gradient ultracentrifugation (10–50%, w/v) was performed twice. However, here, I performed it once to provide better separation and yield. The sample was further purified by gel filtration chromatography using a Sephacryl S-500 HR column.

2.2.3. New purification protocol for recombinant yeast-derived BNC

Step 1. Preparation of the crude extract

The yeast *S. cerevisiae* AH22R$^-$ harboring pGLDLIIP39-RcT [5] was cultured in 2 L of 8S5N-P400 medium for 72 h, as previously described [15]. Yeast cells in the stationary growth phase were harvested by centrifugation at 4,450 ×*g* for 15 min 4°C. The wet cells (35 g) were then suspended in 240 mL of buffer A (7.5 M urea, 0.1 M Tris-HCl, pH 7.4, 50 mM NaH_2PO_4, 15 mM EDTA, 0.1% (v/v) Tween80) and 4 mM

phenylmethylsulfonyl fluoride (PMSF, Sigma). The yeast cells were then disrupted with 0.5-mm glass beads (175 mL) using a Bead-Beater (Biospec) with five sets of disruption for 2 min and a 1-min interval. The whole cell extract (215 mL) was obtained by centrifugation at 34,780 ×*g* for 30 min at 4°C, and dialyzed twice against 5 L of phosphate-buffered saline (PBS; 137 mM NaCl, 2 mM KCl, 8 mM Na_2HPO_4, 1.5 mM KH_2PO_4) containing 1 mM EDTA for 2 h at 4°C. Finally, the extract was dialyzed overnight against 10 L of PBS containing 1 mM EDTA at 4 °C.

Step 2. Heat treatment

The dialyzed extract (275 mL) was divided into approximately 40-mL portions in 50-mL CORNING tubes, incubated at 70°C for 20 min in a water bath, and immediately chilled on ice. Insoluble materials were removed by centrifugation at 34,780 ×*g* for 30 min at 4°C, and then filtered using a 0.45-μm PVDF filter (Millex-HV, Millipore).

Step 3. Sulfated cellulofine column chromatography

The filtered solution (250 mL) was applied onto the sulfated cellulofine column (1.6 × 20 cm; Cellufine™ sulfate, Chisso) equipped on an AKTA system (GE Healthcare) and equilibrated with 10 mM PBS (pH7.2) and 0.15 M NaCl. After extensive washing with the equilibration buffer, the BNC fractions were eluted by stepwise increases in the NaCl concentration using 0.15, 1.0, and 2.0 M NaCl (flow rate, 4 mL/min). The active fractions were combined and concentrated to approximately 5 mL by ultrafiltration (Amicon ultra, NMWL 100K, Millipore).

Step 4. Gel filtration

The concentrated solution (5 mL) was filtered using a 0.45-μm PVDF filter (Millex-HV), and applied onto a Sephacryl S-500 HR column (1.6 × 60 cm; GE Healthcare) equipped on an AKTA system (GE Healthcare) and equilibrated with buffer B (PBS, 1 mM EDTA, 0.005% Tween 80), which was. The BNC fractions were eluted with buffer B (flow rate, 0.5 mL/min), combined, and filtered with a 0.2-μm PVDF filter (Minisart RC-15, Sartorius).

Step 5. Lyophilization

Aliquots (about 250 μL) of purified BNCs (100 μg of protein) were mixed with 10 μL of 50% (w/v) sucrose in a 2-mL polypropylene tube. The mixture was frozen by immersion into liquid nitrogen, lyophilized *in vacuo* (~5 Pa) at –40°C for 4 h using a centrifugal concentrator model CC-105 (TOMY), and then stored at 4°C in a desiccator.

2.2.4. Ex vivo *transfection of HepG2 cells using BNC-containing fluorescent beads*

Two milliliters of 0.2% (w/v) FluoSpheres beads (FITC-labeled 100-nm polystyrene beads; Molecular Probe) were mixed with 61 mg of lyophilized anionic liposomes (COATSOME EL-01-A; NOF) according to the manufacturer's instructions. Next, 12 μL of the bead/liposome solution and 88 μL of distilled water were dissolved in freeze-dried BNCs (100 μg protein). Human hepatocellular carcinoma HepG2 cells were seeded (2×10^4 cells/well) on a 24-well plate in Dulbecco's modified eagle medium (DMEM) supplemented with 10% (v/v) fetal bovine serum (FBS), and cultured for 24 h. Three microliters of the BNC/bead/liposome mixture was added to each well. The cells were cultured for 16 h in a humidified atmosphere at 37°C under 5% (v/v) CO_2. The cells were observed under a confocal laser-scanning microscope (LSM5 PASCAL, Carl Zeiss).

2.2.5. Ex vivo *transfection of Huh7 and HEK293 cells using BNCs containing the luciferase gene*

Luciferase expression plasmid (pGL3 control, Promega; 252 μg in 1 mL water) was mixed with 1.51 mg of freeze-dried cationic liposomes (Coatsome-El-01-D, NOF) according to the manufacturer's instructions. Then, 100 μL of the liposome-plasmid complex (lipoplex) was mixed with lyophilized BNC (100 μg protein) and incubated at room temperature for 15 min. Human hepatocellular carcinoma Huh7 cells were seeded (2×10^4 cells/well) on a 24-well plate in DMEM supplemented with 10% FBS. The BNC-lipoplex mixture containing 30 ng of the plasmid was added to each well. The cells were cultured for 48 h in a humidified atmosphere at 37°C under 5% CO_2. Luciferase activity of cell lysates was determined by a luciferase assay system (Promega). Human embryonic kidney 293 (HEK293) cells and commercial transfection reagent FuGENE6 (Roche) were used as negative controls.

2.2.6. Immunization of Balb/c mice with BNC

Purified and lyophilized BNCs (1 μg/mouse) were reconstituted with water, and then intravenously administrated once a month for 6 months to 5-week-old male Balb/c mice (CREA Japan, Inc.). One week after each administration, blood was taken from the orbital vein, and the plasma was collected by centrifugation at 5,000 ×*g* for 15 min at room temperature. The plasma anti-S antibody titer was measured using an

anti-HBs enzyme immunoassay (Immunis, Institute of Immunology Co., Ltd.) by according to the manufacturer's protocol, which is based on the sandwich enzyme-linked immunosorbent assay using HBsAg S particles as solid phase antigen and horseradish peroxidase-labeled HBsAg S antigen as aqueous phase antigen. The cutoff index (COI) was defined as (test plasma A_{490nm}) / (2.5 × negative control A_{490nm}). Plasma samples with anti-HBsAg antibody titers >1 × COI were considered seropositive.

2.3. Results

2.3.1. Heat treatment

When the HBsAg M particle was purified from recombinant yeast cells, the pre-S2 region displayed on the surface was often degraded by yeast-derived proteinases during purification and storage [16]. To inhibit yeast proteinases, it was necessary to add 7.5 M urea as a denaturant to the crude extract [10]. However, for purification of BNCs (HBsAg L particle), 7.5 M urea was not sufficient to completely inhibit proteinase activity. Thus, contamination with trace amounts of yeast proteinase in the BNC preparations hindered long-term storage of BNCs, also as shown later (*cf.* Figure 2.4A). On the other hand, plasma-derived HB vaccines have been produced from blood of HB patients and the contaminated HBV was inactivated by heat treatment (at 101°C for 90 s) [17], indicating excellent heat stability of HBsAg. Our previous study revealed that about 90% (w/w) of the BNCs retain their structure after heat treatment at 80°C for 5 min [15]. Therefore, I introduced heat treatment to the purification of BNCs to inactivate yeast proteinases. After the crude extract from *S. cerevisiae* overexpressing BNCs was prepared in the presence of 7.5 M urea, the samples were heated to 60–90°C for 10–20 min and the supernatants were subjected to SDS-PAGE followed by silver staining (data not shown). Although the degradation of the BNCs was repressed, the cellular impurities were not efficiently removed in any condition, suggesting that urea enhances the solubilization of impurities. Next, the crude extract was dialyzed in PBS containing EDTA and subjected to heat treatment at varying temperature, time and pH. When the crude extract was heated to 70°C for 15 min at various pH, the BNCs were precipitated in acidic conditions (pH 3–5) while the impurities were not precipitated in alkaline conditions (pH 8–10). Accordingly, pH 7.4 was chosen for further optimization. Finally, I found that neither the remaining amount of intact BNC nor the removal of impurities was significantly changed by varying the temperature between 70 and 80°C for 20–50 min; the optimal condition for heat treatment was thus pH 7.4 at 70°C for 20 min. The heat-treated crude extract predominantly contained the ~52-kDa HBsAg L protein (Figure 2.1A, *lane 2*), which was recognized by anti-BNC polyclonal antibodies (Figure 2.1B, *lane 2*). The protein of ~100-kDa observed in Figure 2.1B is a homodimer of HBsAg L proteins, and has a similar ternary structure to that of endogenous HBsAg proteins. Based on the BNC antigenicity determined by commercial IMx HBsAg enzyme immunoassays, the recovery yield of BNCs after heat treatment was estimated to be 77% (Table 2.2).

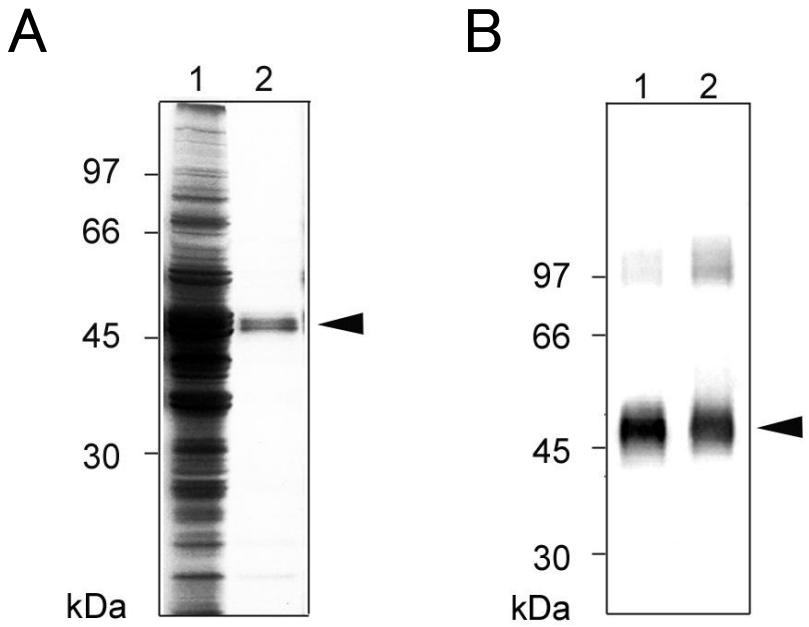

Figure 2.1 SDS-PAGE and western blot analyses of the heat-treated crude extract. The crude extracts of *S. cerevisiae* harboring pGLDLIIP39-RcT were incubated at 70°C for 20 min at pH 7.4, and centrifuged at 34,780 ×*g* for 30 min at 4°C. The supernatant was subjected to 12.5% SDS-PAGE followed by silver staining (A) or western blotting with anti-BNC antibodies (B). Lane 1, crude extract (2 μg protein); lane 2, heat-treated sample derived from crude extract (2 μg protein). The 52-kDa band corresponding to the BNCs is indicated with an arrowhead.

2.3.2. Sulfated cellulofine column chromatography

Sulfated cellulofine columns have been used to purify various viral particles because the mammalian-derived carbohydrate moieties of viral *env* proteins often show high affinity to sulfate residues [18]. Therefore, the heat-treated sample was applied onto the sulfated cellulofine column, and the absorbance of fractions at 280 nm was monitored spectrophotometrically (Figure 2.2A). SDS-PAGE followed by silver staining confirmed the presence of the ~52-kDa HBsAg L protein in fractions 5–7 (Figure 2.2B). Based on the antigenicity of BNCs, the recovery yield of BNCs by sulfated cellulofine column chromatography was estimated to be 42% (Table 2.2). The *N*-linked 6-kDa or *O*-linked 3-kDa carbohydrate moieties of BNCs [10] may bind to the sulfated cellulofine, indicating that the sulfated cellulofine is applicable not only for mammalian-derived carbohydrate moieties but also yeast-derived moieties. Thus, if the BNCs are fully modified with carbohydrates on production in yeast cells, the recovery

yield of BNCs could be improved.

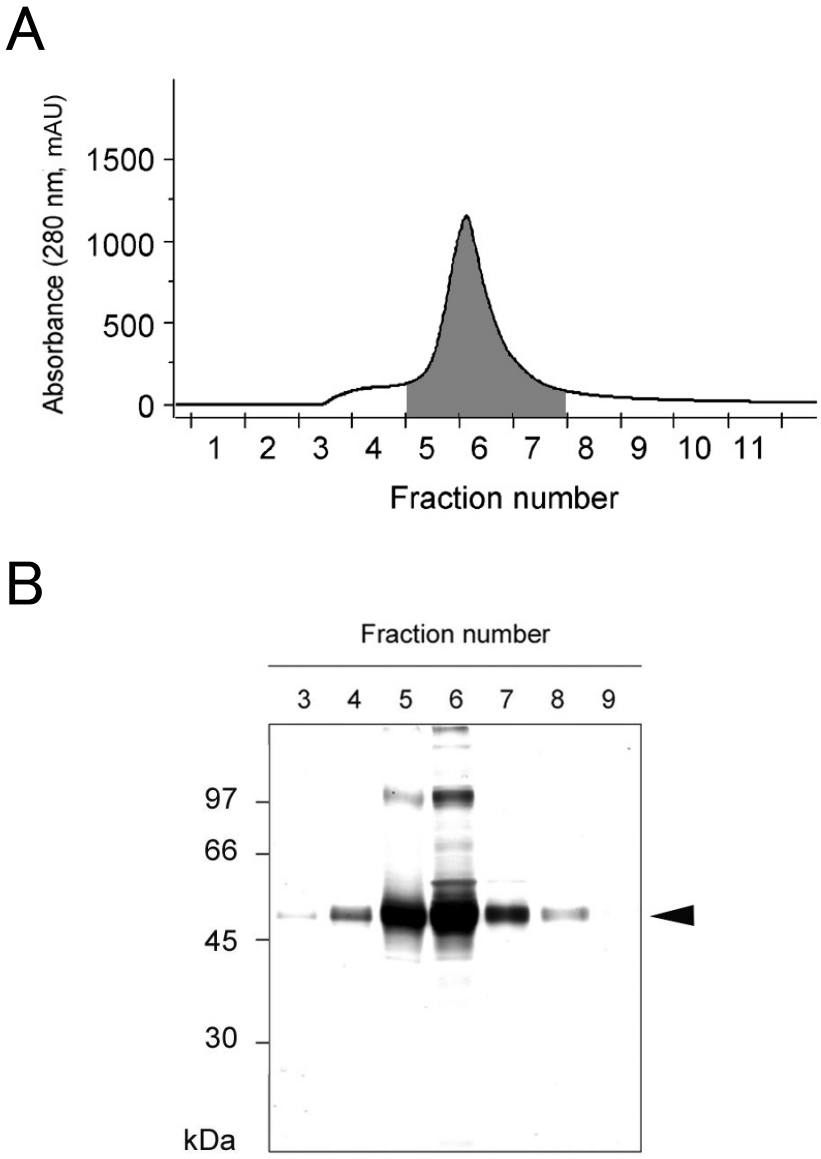

Figure 2.2 Purification of BNCs by sulfated cellulofine column chromatography. (A) Elution profile obtained on a sulfated cellulofine column (40 mL). The absorbance at 280 nm (solid line) is shown. After increasing the concentration of NaCl from 0.15 M to 1 M at fraction number 1, a major peak was collected (fraction volume, 5 mL). Fractions 5–7 (shaded area) were combined, concentrated by ultrafiltration, and subjected to gel-filtration column chromatography. (B) Each fraction was subjected to 12.5% SDS-PAGE followed by silver staining. The 52-kDa band corresponding to the BNCs is indicated with an arrowhead.

2.3.3. Gel filtration column chromatography

The sample was applied onto the Sephacryl S-500 column, and the absorbance of fractions at 280 nm was monitored spectrophotometrically (Figure 2.3A). SDS-PAGE followed by silver staining confirmed that fractions 17–24 exclusively contained the ~52-kDa HBsAg L protein (Figure 2.3B). The protein bands could be detected by western blotting using anti-BNC antibodies (Figure 2.3C). The purity of BNC was >95%, comparable to that of the original purification protocol [15] (Table 2.1). The recovery yield for the gel filtration column was about 50%, and the recovery yield for the complete purification process was about 16% (Table 2.2). These results indicate that the BNCs were efficiently purified using this new protocol involving fewer purification steps than the original protocol.

Table 2.2 Purification of BNCs from yeast cells harboring pGLDLIIP39-RcT using the new protocol

Purification steps	Protein (mg) [a]	BNC antigenicity (unit) [b]	Purification (fold-change)	Yield (%)
Crude extract	1,090	41,000	1.0	100
Heat treatment	130	31,700	6.5	77
Sulfated cellulofine	18.4	13,100	18.9	32
Gel filtration	9.1	6,540	19.2	16

[a]The protein concentration was determined by the BCA assay using BSA as a standard.

[b]BNC antigenicity was measured with an IMx HBsAg assay kit using BNC as a standard.

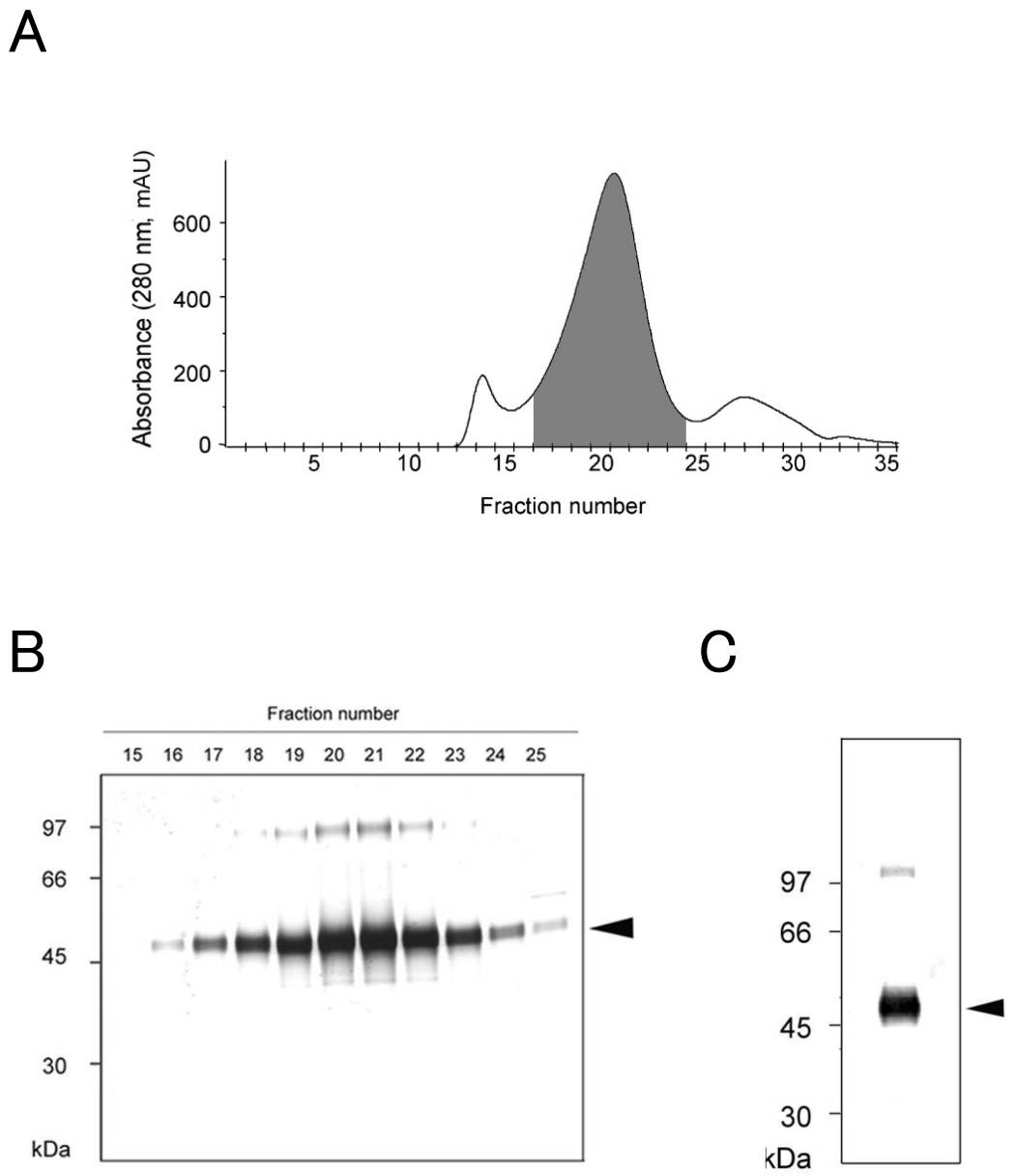

Figure 2.3 Purification of BNCs by gel-filtration column chromatography. (A) Elution profile obtained on a Sephacryl S-500 HR gel filtration column (120 mL). The absorbance at 280 nm (solid line) is shown. The eluate was fractionated into 5-mL tubes. Fractions 17–24 (shaded area) were combined, concentrated by ultrafiltration, sterilized with a 0.2-μm PVDF filter, and lyophilized. (B) Each fraction was subjected to 12.5% SDS-PAGE followed by silver staining. The 52-kDa band corresponding to BNCs is indicated with an arrowhead. (C) The concentrated BNC fractions were subjected to western blotting analysis with anti-BNC antibodies. The 52-kDa band corresponding to the BNCs is indicated with an arrowhead.

2.3.4. Stability of BNCs in solution

When the BNCs purified by the original purification protocol were stored at 4°C or 37°C for 16 h, the ~52-kDa HBsAg L protein was degraded to 43- and 31-kDa proteins at 37°C (Figure 2.4A; SDS-PAGE followed by silver staining), which was thought to be caused by contamination with trace amounts of yeast-derived proteinases. N-terminal analyses of these proteins revealed that the yeast-derived proteinases digest the polypeptide bonds at Ala^{60}-Gly^{61} and Leu^{139}-Tyr^{140} within the pre-S region of the BNC, and digestion at these sites was assumed to generate the 43- and 31-kDa proteins, respectively. Under the same conditions, the BNCs purified by the new protocol were stable at 4°C and at 37°C for 16 h (Figure 2.4B). Thus, the combination of heat treatment and sulfated cellulofine column chromatography might facilitate the complete removal of yeast-derived proteinases from the BNC preparations.

2.3.5. Lyophilization

To develop BNCs as a carrier of nanomedicines, it is important that the BNC maintain their functional activity for at least 1 year. BNCs in solution may be damaged by various physical stresses (*e.g.*, heat, oxidation and dryness) during long-term storage. Since the CHO cell-derived HB vaccine was lyophilized for long-term storage [19], I examined the effects of lyophilization of BNCs with or without sugar (glucose, sucrose, trehalose and mannose) as an excipient. We measured the BNC antigenicity, which reflects the formation of particulate structures [15], and the size of the BNC, which should be maintained at around 100 nm for efficient *in vivo* delivery of the BNCs [7]. The antigenicity of BNCs was >90% for 6 months at 4°C in the presence of 5% (w/v) glucose, 10% sucrose or 10% trehalose, but was <50% and <10% in 10% mannose and the negative control, respectively. Furthermore, the particle size of BNC increased by approximately 3-fold after lyophilization with 10% mannose and without an excipient followed by storage for 3 months at 4°C. Thus, I chose sucrose as the excipient for further optimization. By changing the concentration of sucrose (3, 5 or 10%), I measured the antigenicity and particle size of lyophilized BNCs after storage for 6 months at 4°C. Storage in 10% sucrose slightly decreased the BNC antigenicity, while 3% sucrose increased the particle size several-fold. Thus, I chose 5% sucrose as the excipient for long-term storage of BNC. In fact, storage of lyophilized BNCs for 14 months at 4°C did not affect the molecular mass (Figure 2.4C). Furthermore, the ζ-average diameter of BNCs (91.7 nm at 0 months; polydispersity index (PDI) = 0.25 at

0 month) was not significantly affected by long-term storage for 14 months (95.8 nm; PDI = 0.23).

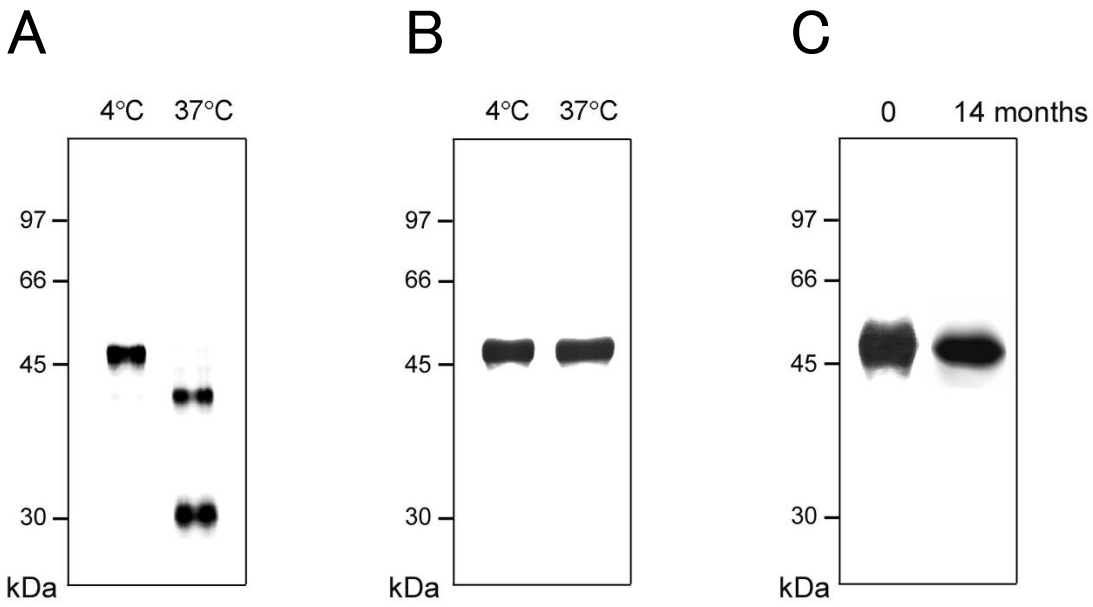

Figure 2.4 Stability of BNC obtained from the original and new protocols. BNCs were purified by the original protocol (A) or the new protocol (B) and stored at 4°C or 37°C for 16 h, and separated by 12.5% SDS-PAGE followed by silver staining (2 μg protein/lane). (C) BNCs purified by the new protocol were lyophilized in the presence of 5% sucrose, and stored at 4°C for 0 or 14 months, and subjected to 12.5% SDS-PAGE followed by silver staining (2 μg protein/lane).

2.3.6. Ex vivo *transfection efficiency of BNC*

The anionic liposomes containing 100-nm FITC-labeled beads were conjugated with lyophilized BNCs obtained by the original or the new purification protocols. The BNCs-beads-liposome mixture was applied to the culture medium of HepG2 cells. After 16 h, the beads were incorporated into the cells by the action of the BNCs [7] (Figure 2.5A). The transfection efficiency of the BNCs produced by the original purification protocol was 91.7 ± 2% (n = 3; 1000 cells per measurement) versus 97.9 ± 2% for BNCs obtained by the new protocol (n = 3; 1000 cells per measurement). Next, the cationic liposomes containing the lipoplex were conjugated with each type of

lyophilized BNC, and were applied to the culture medium of Huh7 cells (BNC target cells) and HEK293 cells (non-target cells). After 48 h, the crude cell lysates were subjected to luciferase assays (n = 5; Figure 2.5B). Compared with the commercial transfection reagent FeGENE6, which is based on cationic liposomes, both types of BNC showed excellent transfection efficiency in Huh7 cells but not in HEK293 cells. These data indicate that the new protocol, as well as the original protocol, does not affect the transfection efficiency or the human liver-specificity of BNC, suggesting that the conformation of the pre-S region is not damaged by the purification process.

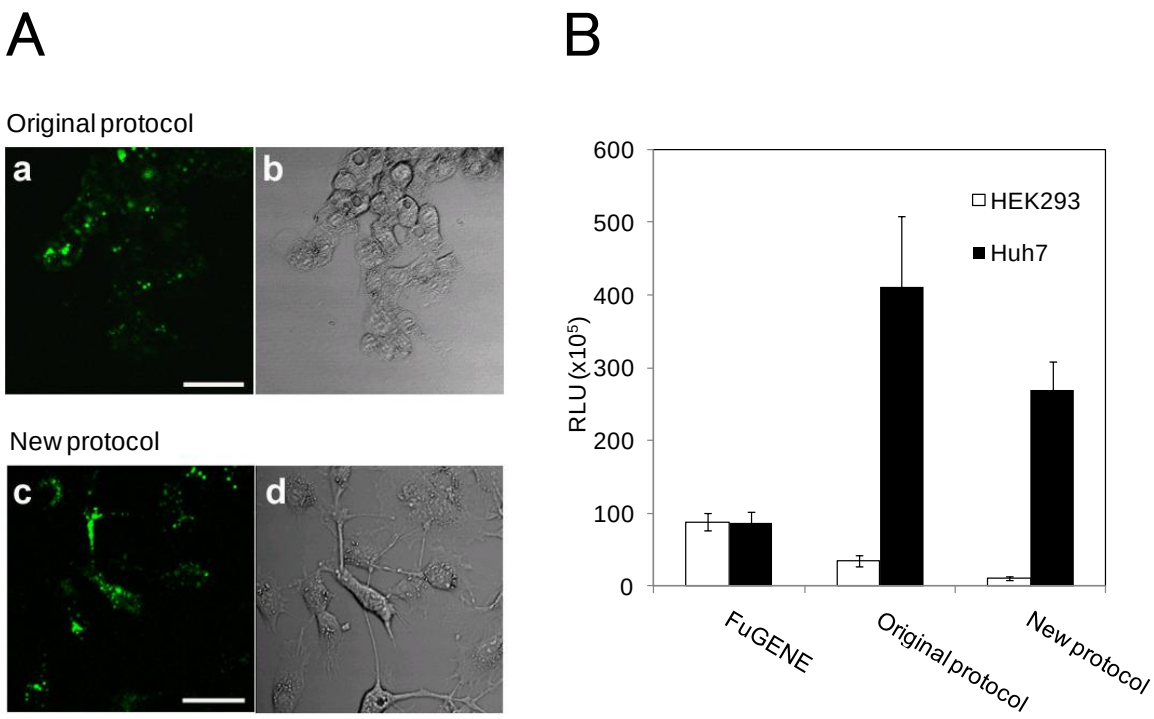

Figure 2.5 *Ex vivo* transfection using BNCs. (A) BNCs purified by the original or the new protocol were conjugated with anionic liposomes containing 100-nm FITC-labeled beads, and then added to the medium of HepG2 cells grown on a 24-well plate. After 16 h, the cells were observed under a confocal laser scanning microscope. Scale bar, 100 μm. (B) BNCs purified by the original or the new protocol were conjugated with cationic liposomes containing luciferase expression plasmid (30 ng/well), and then added to the medium of Huh7 and HEK293 cells grown on a 24 well plate. After 16 h, the cell lysates were subjected to luciferase assay (n = 5). FuGENE6, a commercial cationic liposome, was used as a control.

2.3.7. Antigenicity of BNC

When BNCs are used as a drug/gene carrier, the administration route in humans is likely to be intravenous. Thus, the antigenicity of intravenously injected BNC, purified by the new protocol, is an important factor. Therefore, immediately after the addition of water to the lyophilized BNCs, five Balb/c mice were intravenously injected with 1 μg/mouse of BNC (without an adjuvant) once a month for 6 months (24 weeks). Plasma samples were collected at 0, 1, 5, 9, 13, 17, 21 and 25 weeks, and were subjected to an enzyme immunoassay for the anti-S antibody, the major protective antibody to HBV, to determine the COI values (Figure 2.6). Seropositivity was first identified in some mice at 5 weeks (1 week after the second injection), and all mice were seropositive after 13 weeks (1 week after the fourth injection). After the sixth injection, the anti-S antibody titer was significantly increased in several mice. These data indicated that BNC can be used for a carrier of nanomedicines several times but repetitive injections should be avoided. Since the epitope of anti-S antibody is conformational [20], the S region of the BNCs purified by new protocol is likely to have the correct conformation, which is similar to that of endogenous HBsA

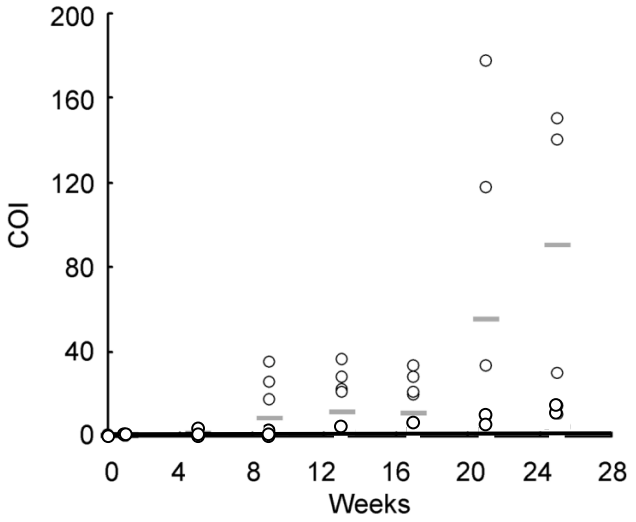

Figure 2.6 Antigenicity of BNC purified by the new protocol. The purified and lyophilized BNCs were reconstituted with water, and the BNCs (1 μg/mouse) were immediately injected intravenously. Five Balb/c mice were administrated once a month for 6 months (arrows indicate the intravenous injections). One week after administration, plasma anti-S antibodies were measured by enzyme immunoassays (n = 2). The cutoff index (COI) was determined as (plasma A_{490nm}) / (2.5 × negative plasma A_{490nm}). The gray bars show the average COI values (n = 10).

2.4. Discussion

The new protocol for purifying BNC was established by utilizing heat treatment and affinity chromatography. This approach improved the yield and purity of BNCs, and shortened the time for purification from 1 week to 2 days. In addition, I found that lyophilization with sucrose preserved the function of BNC for at least 14 months. When preparing the crude extract of yeast cells expressing HBsAg M particles (BNC-related particles) at 4°C, I found that protease inhibitors (*e.g.*, PMSF, EDTA) are not sufficient to fully inhibit the degradation of the pre-S region by yeast-derived proteinases [16]. Therefore, I genetically modified the pre-S region by deleting six aa encoding Ser^{44}–Thr^{49}, a region that is particularly susceptible to proteinases. In addition, I found that the addition of 7.5 M urea effectively suppressed proteinase activity in the crude extract. The modified HBsAg M particles and 7.5 M urea facilitated the purification of HBsAg M particles from yeast cells, which was used as an immunogen of hepatitis B vaccine in humans [21]. Similar activity of yeast proteinases was reported in the purification of HBsAg S particles by other researchers [22]. In this study, owing to the excellent heat stability of the BNCs [15], heat treatment at 70°C at pH 7.4 for 20 min completely removed the yeast proteinases from the crude extract (Figures 2.1 and 2.4). BNCs in the heat-treated supernatant were confirmed to be stable for >1 week, even when stored at 37°C. When PEG6000 precipitation was changed to heat treatment, the yield of BNCs from the pretreated crude extract was improved from 25% (Table 2.1) to 77% (Table 2.2). In the original protocol, the pretreated crude extract was further processed by one CsCl equilibrium step and one sucrose density gradient ultracentrifugation step, which usually took about 4 days. Furthermore, the use of an ultracentrifuge rotor prevented us from adapting the original protocol for mass production of BNCs. In the new protocol, the use of affinity column chromatography allowed us to complete the processing of the pretreated crude extract within 3 h, representing a simple, time-saving, cost-effective and easily adaptable approach suitable for larger-scale production. The overall purification efficiency of this new protocol (16%) was higher than that of other protocols used to purify HBsAg S and M particles produced in *S. cerevisiae* (3–13%) [10, 14, 23]. Since HBsAg has been successfully expressed in a particulate form in a number of different eukaryotic hosts, including *S. cerevisiae*, *Pichia pastoris* [12, 24], *Hansenula polymorpha* [25], mammalian cells [13], insect cells [26] and plants [27], the new protocol could be applied to purify HBsAg from these hosts. Furthermore, to maximize BNC recovery, the following two problems need to be solved. First, the content of BNCs containing carbohydrates could be

enhanced by optimizing the yeast cells and the culture conditions for efficient adsorption to affinity column chromatography, as described above. Second, the *in vitro* conditions of L particle (BNC) formation should be optimized. Although the synthesized L proteins comprised >40% of the total soluble proteins in the yeast cells [5, 15], a large proportion of the L proteins did not assemble into L particles during the preparation of crude extract in the presence of a surfactant. About 80% of the synthesized L proteins were estimated to exist in a disassembled form [24]. Thus, it is essential to optimize the conditions for cell disruption, particularly the use of surfactants to enhance the formation of the liposomal structure of BNCs.

To produce biopharmaceuticals by recombinant organisms for clinical use, it is essential to completely remove any host-derived proteins and DNA. For HBsAg M particles produced by *S. cerevisiae* as an HB vaccine [10], sequential chromatography steps using three gel-filtration columns and one immunoaffinity column are necessary to obtain highly purified antigens. In particular, immunoaffinity column chromatography is indispensable to completely remove host-derived materials (*i.e.*, yeast-derived DNAs and proteins). However, some of the immunoglobulin was released from the column and was present in the eluate, which has prompted us to search for other resins that specifically interact with HBsAg. In this study, I found that sulfated cellulofine interacts with BNC, presumably the carbohydrate moieties of BNC, and may substitute for the immunoaffinity column in the production of biopharmaceuticals, at least for HB vaccines. Our results indicate that the new purification protocol is rapid and efficient for the purification of BNCs and is suitable for mass-production of BNCs. I also optimized the conditions for long-term preservation of functional BNCs and demonstrated that BNCs lyophilized with 5% sucrose are stable for up to 14 months at 4°C, without impaired transfection efficiency.

In summary, the new purification and preservation protocols reported here will increase the availability of BNCs and should promote the use of BNCs as a carrier in DDS and GDS in clinical fields.

2.5. References

1. Tiollais P, Christine P, Dejean A. The hepatitis B virus, Nature 1985;317:489–495.
2. Heermann KH, Goldmann U, Schwartz W, Seyffarth T, Baumgarten H, Gerlich WH. Large surface proteins of hepatitis B virus containing the pre-S sequence. J Virol 1984;52:396–402.
3. Hong HJ, Ryu CJ, Hur H, Kim S, Oh HK, Oh MS, Park SY. *In vivo* neutralization of hepatitis B virus infection by an anti-preS1 humanized antibody in chimpanzees. Virology 2004;318:134–141.
4. Neurath AR, Kent SB, Stick N, Parker K. Identification and chemical synthesis of a host cell receptor binding site on hepatitis B virus. Cell 1986;46:429–436.
5. Kuroda S, Otaka S, Miyazaki T, Nakao M, Fujisawa Y. Hepatitis B virus envelope L protein particles. J Biol Chem. 1992;267:1953–1961.
6. Yamada T, Iwasaki Y, Tada H, Iwabuki H, Chuah MKL, VandenDriessche T, Fukuda H, Kondo A, Ueda M, Seno M, Tanizawa K, Kuroda S. Nanoparticles for the delivery of genes and drugs to human hepatocytes. Nat Biotechnol 2003;21:885–890.
7. Jung J, Matsuzaki T, Tatematsu K, Okajima T, Tanizawa K, Kuroda S. Bio-nanocapsule conjugated with liposomes for *in vivo* pinpoint delivery of various materials. J Control Release 2008;126:55–264.
8. Kasuya T, Jung J, Kinoshita R, Goh Y, Matsuzaki T, Iijima M, Yoshimoto N, Tanizawa K, Kuroda S. Bio-nanocapsule–liposome conjugates for *in vivo* pinpoint drug and gene delivery. Methods Enzymol 2009;464:147–166.
9. Iwasaki Y, Ueda M, Yamada T, Kondo A, Seno M, Tanizawa K, Kuroda S, Sakamoto M, Kitajima M. Gene therapy of liver tumors with human liver-specific nanoparticles. Cancer Gene Ther 2007;14:74–81.
10. Kobayashi M, Asano T, Utsunomiya M, Itoh Y, Fujisawa Y, Nishimura O, Kato K, Kakinuma A. Recombinant hepatitis B virus surface antigen carrying the pre-S2 region derived from yeast: purification and characterization. J Biotech 1998;8:1–22.
11. Ohmura T, Ohmizu A, Sumi A, Ohtani W, Uemura Y, Arimura H, Nishida M, Kohama Y, Okabe M, Mimura T, Heldebrant CM. Properties of recombinant hepatitis B vaccine. Biochem Biophys Res Commun 1987;149:1172–1178.
12. Hardy E, Martinez E, Diago D, Diaz R, Gonzalez D, Herrera L. Large-scale production of recombinant hepatitis B surface antigen form *Pichia pastoris*. J Biotech 2000;77:157–167.
13. Belew M, Mei Y, Li B, Berglof JH, Janson JC. Purification of recombinant

Hepatitis B surface antigen (r-HBsAg) produced by transformed CHO cells grown in culture. Bioseparation 1991;1:397–408.

14. Stephenne J. Recombinant versus plasma derived hepatitis B vaccines: issues of safety, immunogenecity and cost-effectiveness. Vaccine 1998;6:299–303.
15. Yamada T, Iwabuki H, Kanno T, Tanaka H, Kawai T, Fukuda H, Kondo A, Seno M, Tanizawa K, Kuroda S. Physicochemical and immunological characterization of hepatitis B virus envelope particles exclusively consisting of the entire L (pre-S1+pre-S2+S) protein. Vaccine 2001;19:3154–3163.
16. Itoh Y, Fujisawa Y. Synthesis in yeast of hepatitis B virus surface antigen modified P31 particles by gene modification. Biochem Biophys Res Commun. 1986;141:942–948.
17. Lelie PN, Reesink HW, Th S. De Jong-van Manen, Dees PJ, Reerink-brongers EE. Immnunogenicity and safety of a plasma-derived heat-inactived hepatitis B vaccine (CLB). Am J Epidemiol 1984;120:694–702.
18. Sugawara K, Nishiyama K, Ishikawa Y, Abe M, Sonoda K, Komatsu K, Horikawa Y, Takeda K, Honda T, Kuzuhara S, Kino Y, Mizokami H, Mizuno K, Oka T, Honda K. Development of vero cell-derived inactivated Japanese encephalitis vaccine. Biologicals 2002;30:303–314.
19. Diminsky D, Moav N, Gorecki M, Barenholz Y. Physical, chemical and immunological stability of CHO-derived hepatitis B surface antigen (HBsAg) particles. Vaccine 2000;18:3–17.
20. Ionescu-Matiu I, Kennedy RC, Sparrow JT, Culwell AR, Sanchez Y, Melnick JL, Dreesman GR. Epitopes associated with a synthetic hepatitis B surface antigen peptide. J Immunol 1983;130:1947–1952.
21. Kuroda S, Fujisawa Y, Iino S, Akahane Y, Suzuki H. Induction of protection level of anti-pre-S2 antibodies in humans immunized with a novel hepatitis B vaccine consisting of M (pre-S2 + S) protein particles (a third generation vaccine). Vaccine 1991;9:163–169.
22. Gimenez JA, Monkovic DD, Dekleva ML. Identification and monitoring of protease activity in recombinant *Saccharomyces cerevisiae*. Biotechnol Bioeng 2000;67:245–251.
23. Valenzuela P, Medina A, Rutter WJ, Ammerer G, Hall BD. Synthesis and assembly of hepatitis B virus surface antigen particles in yeast. Nature 1982;298:347–351.
24. Han X, Ye L, Li B, Bo G, Cai W, Hong Z, She Y, Li Y, Kong L, Wu Z. Expression, purification and characterization of the hepatitis B virus entire envelope large protein in *Pichia pastoris*. Protein Express Purif 2006;49:168–175.

25. Huang Y, Bi J, Zhang Y, Zhou W, Li Y, Zhao L, Su Z. A highly efficient integrated chromatographic procedure for the purification of recombinant hepatitis B surface antigen from *Hansenula polymorpha.* Protein Express Purif 2007;56:301–310.
26. Kang CY, Bishop DH, Seo JS, Matsuura Y, Choe M. Secretion of particles of hepatitis B surface antigen from insect cells using a baculovirus vector. J Gen Virol 1987;68:2607–2613.
27. Mason HS, Lam DM, Arntzen CJ. Expression of hepatitis B surface antigen in transgenic plants. Proc Natl Acad Sci USA 1992;891:1745–11749.

Chapter III

Bio-nanocapsule-Based Enzyme–Antibody Conjugates for Enzyme-Linked Immunosorbent Assay

3.1. Introduction

Enzyme immunoassay (EIA), radioimmunoassay (RIA), and fluoroimmunoassay (FIA) have been widely used for high-throughput screening of immunocomplexes. To increase the sensitivity of these immunoassays, two types of macromolecules have been utilized in the reaction with antibody. One type of macromolecule allows for clustering of antibodies and labeling molecules (enzyme, radioactive material, fluorescence). For examples, polymeric horseradish peroxidase (HRP)-streptavidin conjugate [1], 3DNA dendrimer [2], and IgG-poly-D-glutamic acid-$(HRP)_n$ conjugate [3] have previously been used. However, these macromolecules require chemical modification of antibodies, and do not allow the oriented immobilization of antibodies [4], which improves the avidity and antigen recognition of antibodies [5]. In general, chemical modification is considered to reduce the stability or antigen-binding activity of antibodies. Another type of macromolecule is expected to permit the oriented immobilization of antibodies. For examples, nanoparticles have been used for displaying antibodies on their surface, *e.g.*, streptavidin-conjugated nanobeads [6] and biotin-coated liposomes [7]. Because biotinylation occurred randomly at free amino groups on the surface of antibodies, these nanoparticles partially accomplished oriented immobilization of antibodies using a biotin-avidin complex. These results encouraged us to develop macromolecules that can assemble antibodies and labeling molecules without chemical modification, in the manner of oriented immobilization.

On the other hand, our group previously developed a yeast-derived hollow nanoparticle applicable for pinpoint delivery of drugs and genes [8]. The nanoparticle (bio-nanocapsule; later abbreviated as “BNC”) has a diameter of about 30 nm and is composed of hepatitis-B virus (HBV) surface antigen (HBsAg) L-proteins embedded in a liposome [9]. The L-protein is a three membrane-spanning protein possessing a pre-S region at the N-terminal of the S region (*see* Figure 3.1A) [10]. BNCs can incorporate various therapeutic materials (drugs, genes) by electroporation [8] and liposome fusion [11], and deliver them specifically to the human liver [8] based on the liver-specific recognition ability of the pre-S region [12]. Recently, in order to alter the tissue

specificity of BNC, our collaborators made a derivative of BNC by replacing the pre-S region with a tandem sequence of the IgG Fc-interacting region (Z domain) derived from *Staphylococcus aureus* protein-A [13] and designated it "ZZ-BNC" [14] (Figure 3.1A). The ZZ-BNC allowed us to display antibodies on its surface and to deliver various therapeutic materials to tissues of interest in an antibody-dependent manner [14].

These properties led us to imagine that ZZ-BNC spontaneously adsorbs antibodies in the manner of oriented immobilization. In the present study, I examined if ZZ-BNCs could contribute to signal enhancement of ELISA through formation of IgG-ZZ-BNC complexes.

3.2. Experimental Procedures

3.2.1. ZZ-BNCs

ZZ-BNCs were overexpressed in *Saccharomyces cerevisiae* AH22R$^-$ carrying the ZZ-BNC-expression plasmid pGLD-ZZ50 [14]. According to the preparation method for BNCs [8], ZZ-BNCs were extracted by the disruption with glass beads, and purified using an AKTA chromatography system (GE Healthcare, Amersham, UK) by affinity chromatography on porcine IgG and gel filtration.

3.2.2. Transmission electron microscopy (TEM)

ZZ-BNCs (1 μg as protein) were mixed with 10-nm gold particle-labeled goat total IgG (50 μL, Sigma Aldrich, Saint Louis, MO), adsorbed onto a carbon-coated copper grid (JEOL, Tokyo, Japan), negatively stained using 2% (w/v) phosphotungstic acid (pH 7.0), and subjected to TEM using a model JEM1011 (JEOL, Tokyo, Japan).

3.2.3. ELISA for ovalbumin (OVA) on solid phase

OVA (100 μL, 0-6.25 ng/mL; Sigma-Aldrich, St. Louis, MO) was adsorbed to each well of a Nunc-Immuno Plate II (96 wells; Nalge Nunc International K.K., Rochester, NY). The plate was kept at 4°C overnight, and washed three times with 200 μL of phosphate buffered saline (PBS; 137 mM NaCl, 2.7 mM KCl, 10 mM Na_2PO_4, 2 mM KH_2PO_4, pH 7.4) containing 0.05% (V/V) Tween-20 (PBST). Antibodies were diluted with PBST containing 5% (W/V) skimmed milk (Nacalai Tesque, Kyoto, Japan). A primary antibody, a mouse anti-OVA IgG_1 antibody (100 μL, 0.4 μg/mL; Abcam, Cambridge, UK), was added to each well, incubated at room temperature for 1.5 h, and washed three times with PBST. A secondary antibody, HRP-conjugated rabbit anti-mouse IgG (100 μL, 2 μg/mL; Sigma-Aldrich), was added to each well, incubated at room temperature for 1.5 h, and washed three times with PBST. When biotinylated rabbit anti-mouse IgG (100 μL, 2 μg/mL; Sigma-Aldrich) was used as the secondary antibody, the avidin-biotin complex (ABC) system (ABC peroxidase staining kit, Pierce) was used for the labeling with HRP. The colorimetric reaction was carried out at room temperature for 15 min in 100 μL per well of a 3,3',5,5'-tetramethylbenzidine (TMB) substrate kit (Pierce, Rockford, IL). The reaction was stopped with 100 μL of 2N H_2SO_4. Absorbance at 450 nm was measured on a Varioskan microplate reader

(Thermo Fisher Scientific, Waltham, MA) using absorbance at 690 nm as the reference. When the calibration curve was generated using 0-6.25 ng/mL OVA (n = 8), the wells containing 0 ng/mL OVA were defined as blank wells for subtracting background.

3.2.4. ELISA for anti-OVA IgE antibodies in aqueous phase

OVA (100 μL, 15 μg/mL) was adsorbed onto each well of a Nunc-Immuno Plate II. The plate was kept at 4°C overnight, and washed three times with 200 μL of PBST. Mouse anti-OVA IgE antibody (0-6.25 ng/mL, 100 μL, AbD Serotec, Oxford, UK) diluted with PBST containing 5% skimmed milk was added to each well, incubated at room temperature for 1.5 h, and washed three times with PBST. An HRP-conjugated rabbit anti-mouse IgE Fc antibody (100 μL, 5 μg/mL, Nordic Immunological Laboratories, Tilburg, The Netherlands) was added to each well, incubated at room temperature for 1.5 h, and washed three times with PBST. When biotin-labeled rabbit anti-mouse IgE Fc antibody (100 μL, 5 μg/mL, Nordic Immunological Laboratories) was used as the secondary antibody, the ABC peroxidase staining kit was used for the labeling with HRP. The colorimetric reaction was carried out at room temperature for 15 min in 100 μL per well of a TMB substrate kit. The reaction was stopped with 100 μL of 2N H_2SO_4. Absorbance at 450 nm was measured on a Varioskan microplate reader using absorbance at 690 nm as the reference. When the calibration curve was generated using 0-6.25 ng/mL anti-OVA IgE (n = 8), the wells containing 0 ng/mL anti-OVA IgE were defined as blank wells for subtracting background.

3.2.5. Western blot analysis

One μL of OVA (0.001-10 mg/mL) was blotted onto a PVDF membrane (Millipore, Billerica, MA), and dried at room temperature for 30 min. The membrane was blocked with 5% skimmed milk in TBST (20 mM Tris-HCl, 140 mM NaCl, 0.05% Tween-20, pH 7.4) at room temperature for 30 min, and then incubated at room temperature for 1 h with the mouse anti-OVA IgG_1 antibody (1 μg/mL) diluted with TBST. The membrane was washed three times with TBST, incubated with the HRP-conjugated rabbit anti-mouse IgG (1 μg/mL) at room temperature for 1 h. When biotinylated rabbit anti-mouse IgG (1 μg/mL) was used as the secondary antibody, the ABC system was used for the labeling with HRP. After washing three times with TBST, the membrane was treated with ECL Western blotting detection reagents (GE Healthcare), and then the immunoreactive spots were visualized under a luminescence

image analyzer LAS-4000mini (Fujifilm, Tokyo, Japan).

3.3. Results and Discussion

3.3.1. Display of antibodies on the ZZ-BNC surface

BNC is a yeast-derived hollow nanocapsule consisting of about 110 HBsAg L proteins embedded in a liposome [8]. Recently, our group replaced the N-terminal region of L protein (pre-S region) with a tandem sequence of protein A-derived IgG Fc-binding domain (Z domain) and designated it ZZ-BNC [14] (Figure 3.1A). When mixed with anti-EGFR (epidermal growth factor receptor) antibody, the ZZ-BNCs labeled with EGFP (enhanced green fluorescent protein) accumulated on the surface of human cervical carcinoma HeLa cells, which express EGFR abundantly [14]. I therefore mixed ZZ-BNC with 10-nm gold particle-labeled goat total IgG, and observed it under TEM. As shown in Figure 3.1B, approximately 30-nm ZZ-BNCs were surrounded by several molecules of 10-nm gold particle-labeled goat total IgG. This result strongly suggested that ZZ domains surrounding on the ZZ-BNC surface tether the IgG Fc domains to display all IgG Fv regions outwards for effective antigen binding. Thus, ZZ-BNC was expected to cluster antibodies on its surface in the manner of oriented immobilization, which might improve the avidity and antigen recognition of antibodies [5].

A

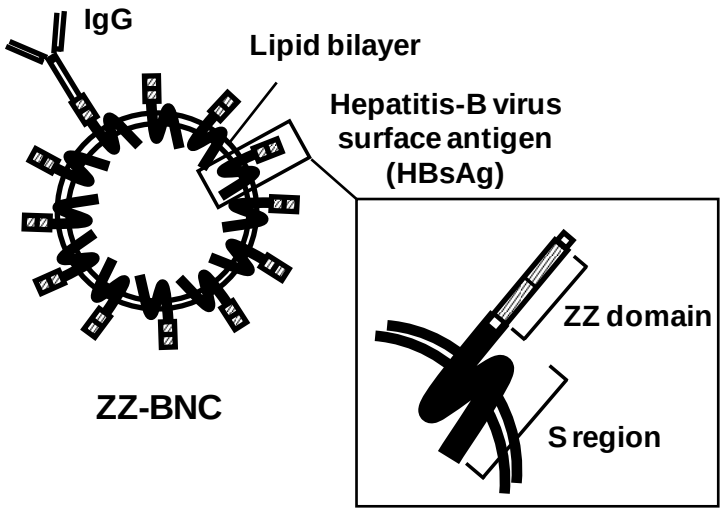

B

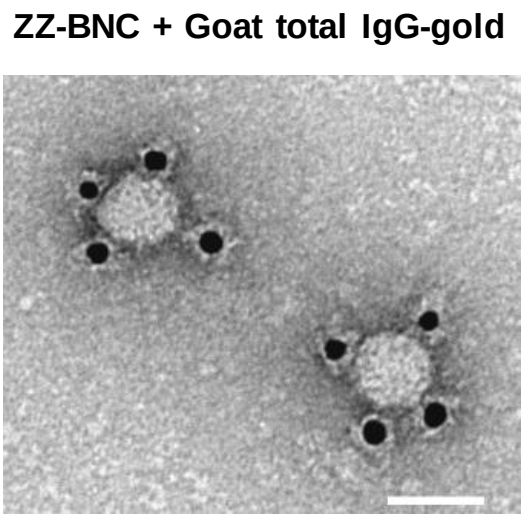

Figure 3.1 Structures and properties of ZZ-BNCs. (A) Schematic structure of a ZZ-BNC. (B) TEM images of ZZ-BNC conjugated with 10-nm gold particle-labeled goat total IgG. Bar, 40 nm.

3.3.2. ELISA for antigens on solid phase

The enhancement of the sensitivity was examined in the detection of antigen (ovalbumin (OVA)) by ELISA with or without ZZ-BNCs (*see* Figure 3.2A, panels 1 and 2). As described in **Materials and methods,** OVA (0-6.25 ng/mL) was adsorbed onto each well of immunoplate, contacted with primary antibody, and then contacted with secondary antibody (*see* Figure 3.2A, panel 1). When the purified ZZ-BNCs (2 μg/mL as protein) were preincubated with the secondary antibody (2 μg/mL) at room temperature for 30 min and then added to each well (*see* Figure 3.2A, panel 2), the signal at 3.125 ng/mL of OVA was about 10-fold higher than that without ZZ-BNCs (Figure 3.2B, lines 1 & 2). The avidin-biotin complex (ABC) system has been widely used for the enhancement of ELISA signals because it forms a tetrameric avidin-based complex of biotinylated antibodies and biotinylated HRP (*see* Figure 3.2A, panel 3). The signal at 3.125 ng/mL of OVA with the ABC system was about 4-fold higher than that with the conventional ELISA (Figure 3.2B, lines 1 & 3). When ZZ-BNC (2 μg/mL as protein) was preincubated with the biotinylated secondary antibody (2 μg/mL) at room temperature for 30 min and then added to each well (100 μL, *see* Figure 3.2A, panel 4), the signal at 3.125 ng/mL of OVA was about 13-fold higher than that without ZZ-BNCs or ABC system (Figure 3.2B, lines 1 & 4). Next, biotinylated ZZ-BNCs (2 μg/mL as protein) were prepared with EZ-Link Sulfo-NHS-Biotin (Pierce) according to the manufacturer's protocol and added to the secondary antibody instead of ZZ-BNCs (*see* Figure 3.2A, panel 5). The signal at 3.125 ng/mL of OVA was about 19-fold higher than that without ZZ-BNCs or ABC system (Figure 3.2B, line 1 & 5). The sensitivity for ELISA is defined by the limit of detection (LOD, mean ± 3SD) and the limit of quantitation (LOQ, mean + 10SD) [15] at the lowest end of the quantifiable concentration range of OVA (n = 20). As shown in Table 3.1, the LOD and LOQ of ELISA (*see* Figure 3.2A, panel 1; 750 pg/mL and 1500 pg/mL, respectively) were decreased by 47% using ZZ-BNCs (*see* Figure 3.2A, panel 2; 350 pg/mL and 700 pg/mL, respectively), indicating that the two sensitivities (LOD and LOQ) were increased 2.1-fold. The ABC complex enhanced the two sensitivities 2.5- and 20-fold in the presence of ZZ-BNCs (*see* Figure 3.2A, panel 4) and biotinylated ZZ-BNCs (*see* Figure 3.2A, panel 5), respectively.

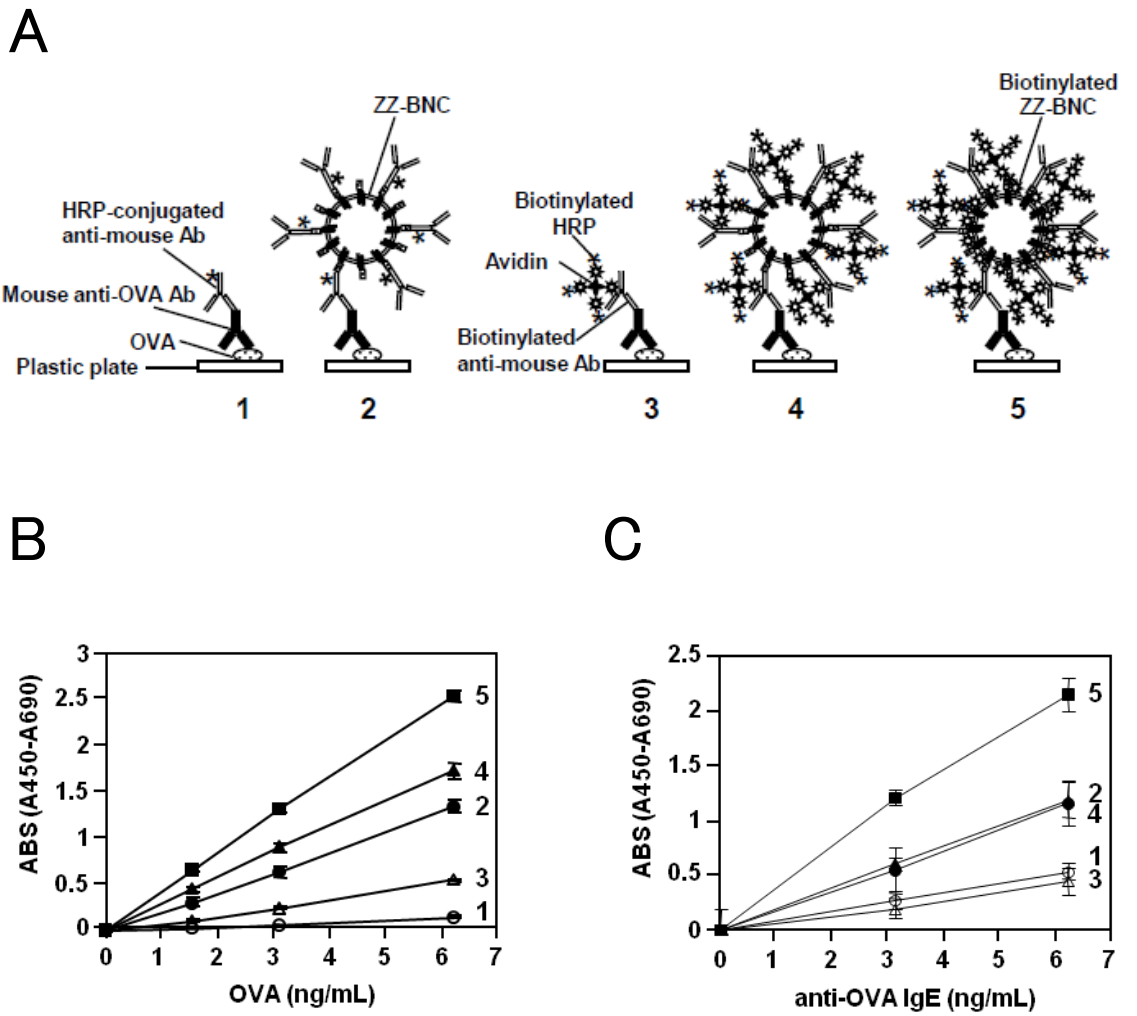

Figure 3.2 Sensitivities of various ELISA systems for OVA. (A) Schematic representations of various ELISA systems for OVA detection. 1, conventional ELISA using an anti-OVA antibody and an HRP-conjugated anti-mouse IgG antibody; 2, conventional ELISA in the presence of ZZ-BNC; 3, conventional ELISA with the ABC system; 4, conventional ELISA with the ABC system in the presence of ZZ-BNCs; 5, conventional ELISA with the ABC system in the presence of biotinylated ZZ-BNC. Abbreviations: OVA, ovalbumin; Ab, antibody. (B) Detection of OVA (solid phase) by various ELISA systems. Results are means ± SD (n = 8). Numbers correspond to the methods shown in (A). (C) Detection of anti-OVA IgE (aqueous phase) by various ELISA systems. Results are means ± SD (n = 8). Numbers correspond to the methods shown in (A).

3.3.3. ELISA for antibodies in aqueous phase

I investigated the enhancement of the sensitivity of detection of the primary antibody by ELISA using ZZ-BNCs and biotinylated ZZ-BNCs. OVA adsorbed onto each well was contacted with primary antibody (0-6.25 ng/mL), and then contacted with secondary antibody (*see* **Materials and methods** and Figure 3.2A, panel 1). When ZZ-BNC (1.25 μg/mL as protein) was preincubated with the secondary antibody (5 μg/mL) at room temperature for 30 min and then added to each well (*see* Figure 3.2A, panel 2), the signal at 3.125 ng/mL of mouse anti-OVA IgE antibody was 2.3-fold higher than that without ZZ-BNCs (Figure 3.2C, lines 1 & 2). Next, with the concurrent use of biotinylated secondary antibody (5 μg/mL), biotinylated ZZ-BNCs (2.5 μg/mL as protein), and ABC system, the signal at 3.125 ng/mL of mouse anti-OVA IgE antibody was 4.4-fold higher than that of conventional ELISA (Figure 3.2C, lines 1 & 5). Furthermore, the sensitivity for ELISA is defined by LOD and LOQ [15] at the lowest end of the quantifiable concentration range of anti-OVA IgE (n = 20). LOD was decreased by 50% and 8% using ZZ-BNCs and biotinylated ZZ-BNCs, respectively (Table 3.1).

Table 3.1 Sensitivities of various ELISA systems for OVA

Methods	LOD (pg/mL) Mean ± 3SD	CV (%)	LOQ (pg/mL) Mean + 10SD	CV (%)
For detection of antigen (OVA)				
Conventional ELISA	750	4.5	1500	3.4
+ ZZ-BNC	350	6.4	700	6.9
+ ABC	500	3.0	1000	3.1
+ ABC + ZZ-BNC	300	5.3	600	11.8
+ ABC + bio-ZZ-BNC	40	3.5	80	4.3
For detection of primary antibody (anti-OVA IgE)				
Conventional ELISA	500	5.0	ND[b]	ND
+ ZZ-BNC	250	5.4	500	4.6
+ ABC + bio-ZZ-BNC	40	4.2	130	3.6

[a] Abbreviations: OVA, ovalbumin; ABC, avidin–biotin complex system; bio-, biotinylated-.

[b] Not detected.

3.3.4. Western blot analysis

Signal enhancement of ELISA for antigens on solid phase by ZZ-BNCs led us to examine if they are applicable for Western blot analysis. The dot-blot containing OVA (from 1 ng/spot to 10 μg/spot) was incubated with the primary antibody at room temperature for 1 h, incubated with the secondary antibody at room temperature for 1 h, and then subjected to the chemiluminescence detection (*see* **Material and methods**). When ZZ-BNCs (1 μg/mL as protein) were preincubated with the secondary antibody (1 μg/mL) at room temperature for 30 min, the spot containing 10 ng OVA could be detected, which was about 50-fold higher than that without ZZ-BNCs (Figure 3.3, lanes 1 & 2). Next, the use of ABC system and biotinylated secondary antibody facilitated us to detect the spot containing 50 ng OVA (lane 3). The adaptation of ZZ-BNCs (1 μg/mL as protein) and biotinylated ZZ-BNCs (1 μg/mL as protein) to this system achieved approximately 5- and 10-folds higher sensitivity (lanes 4 & 5, respectively), comparable to 50- and 100-folds enhancements from the conventional method (lane 1). It was confirmed that the combinated use of ABC system and biotinylated ZZ-BNCs significantly enhanced the sensitivity of not only ELISA but also Western blot analysis. Furthermore, ZZ-BNCs might be applicable for the signal enhancement of immunohistochemical analysis.

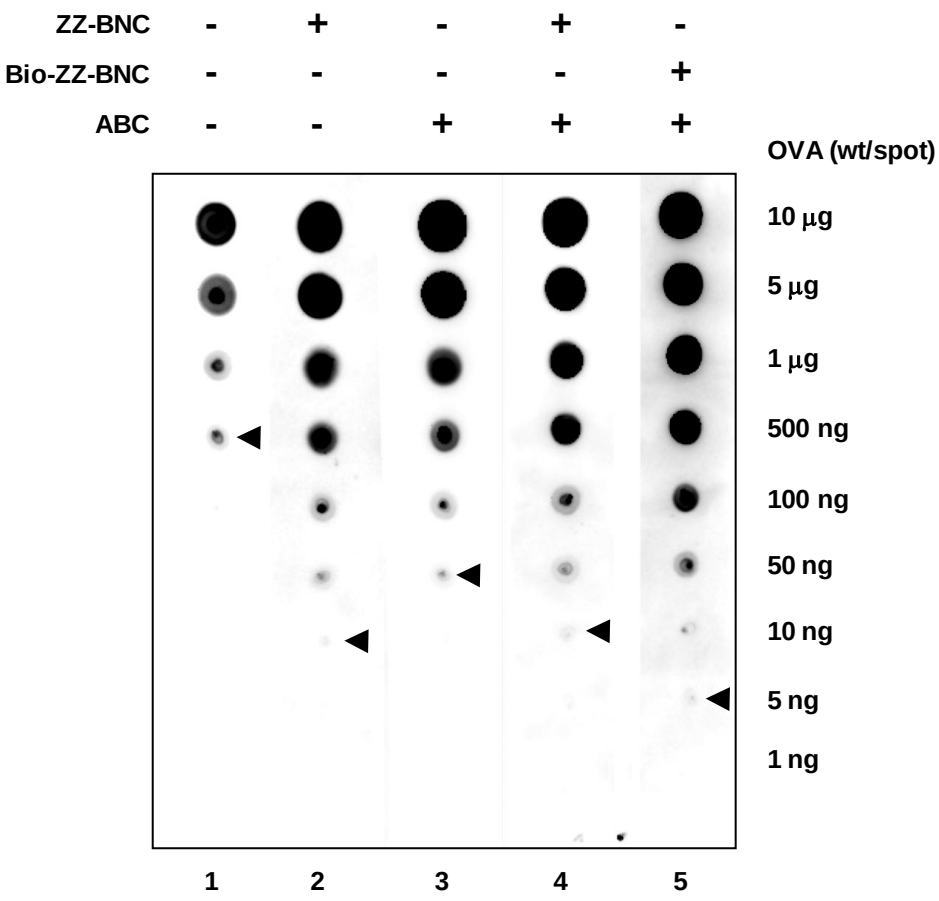

Figure 3.3 Western blot analyses of spotted OVA by various detection methods. Lane numbers correspond to the methods shown in Figure 3.2 (A). The minimum OVA amounts detectable by each method are indicated with arrow heads.

3.3.5. Conclusions

It has been demonstrated that ZZ-BNCs could assemble antibodies on their surface even without chemical modification. ZZBNCs could then enhance the signals in the detection of antigens and antibodies when added to the aqueous phase of conventional ELISA and Western blot analysis. A combination of the ABC system and biotinylated ZZ-BNCs significantly improved the sensitivity of conventional ELISA and Western blot analysis. In Figure 3.1B, ZZ-BNCs are shown to tether the Fc regions of IgG on the ZZ domain so that all of the Fv regions are displayed outward for effective formation of immunocomplexes. Thus, oriented immobilization of antibodies has presumably been achieved on the surface of ZZ-BNCs. As mentioned above, BNCs

(including ZZ-BNCs) can incorporate various materials by electroporation and liposome fusion. This indicated that ZZ-BNCs may be applicable for RIA and FIA. BNCs could be adsorbed onto a mica surface without the disruption of its particle structure [16]. Therefore, ZZ-BNCs would also be applicable for the oriented immobilization of antibodies in the solid phase of various immunoassay systems.

3.4. References

1. Vasilov RG, Tsitsikov EN. An ultrasensitive immunoassay for human IgE measurement in cell-culture supernatant. Immunol Lett 1990;26:283–284.
2. Mora JR, Zielinski TL, Nelson BP, Getts RC. Protein detection enhanced by 3DNA dendrimer signal amplification. BioTechniques 2008;44:815–818.
3. Simons B, Kaplan H, Hefford MA. Novel cross-linked enzyme–antibody conjugates for Western blot and ELISA. J Immunol Methods 2006;315:88–98.
4. Rao SV, Anderson KW, Bachas LG. Oriented immobilization of proteins. Mikrochim Acta 1998;128:127–143.
5. Lipman NS, Jackson LR, Trudel LJ, Weis-Garcia F. Monoclonal versus polyclonal antibodies: distinguishing characteristics, applications, and information resources. ILAR J 2005;46:258–268.
6. Teramura Y, Arima Y, Iwata H. Surface plasmon resonance-based highly sensitive immunosensing for brain natriuretic peptide using nanobeads for signal amplification. Anal Biochem 2006;357:208–215.
7. Wink T, van Zuilen SJ, Bult A, van Bennekom WP. Liposome-mediated enhancement of the sensitivity in immunoassays of proteins and peptides in surface plasmon resonance spectrometry. Anal Chem 1998;70:827–832.
8. Yamada T, Iwasaki Y, Tada H, Iwabuki H, Chuah MK, VandenDriessche T, Fukuda H, Kondo A, Ueda M, Seno M, Tanizawa K, Kuroda S. Nanoparticles for the delivery of genes and drugs to human hepatocytes. Nat Biotechnol 2003;21:885–890.
9. Kuroda S, Otaka S, Miyazaki T, Nakao M, Fujisawa Y. Hepatitis B virus envelope L protein particles. J Biol Chem 1992;267:1953–1961.
10. Nagaoka T, Fukuda T, Yoshida S, Nishimura H, Yu D, Kuroda S, Tanizawa K, Kondo A, Ueda M, Yamada H, Tada H, Seno M. Characterization of bio-nanocapsule as a transfer vector targeting human hepatocyte carcinoma by disulfide linkage modification. J Control Release 2007;118:348–356.
11. Jung J, Matsuzaki T, Tatematsu K, Okajima T, Tanizawa K, Kuroda S. Bio-nanocapsule conjugated with liposomes for in vivo pinpoint delivery of various materials. J Control Release 2008;126:255–264.
12. Neurath AR, Kent SB, Strick N, Parker K. Identification and chemical synthesis of a host cell receptor binding site on hepatitis B virus. Cell 1986;46:429–436.
13. Nilsson B, Moks T, Jansson B, Abrahmsén L, Elmblad A, Holmgren E, Henrichson C, Jones TA, Uhlén M. A synthetic IgG-binding domain based on staphylococcal

protein A. Protein Eng 1987;1:107–113.

14. Kurata N, Shishido T, Muraoka M, Tanaka T, Ogino C, Fukuda H, Kondo A. Specific protein delivery to target cells by antibody-displaying bionanocapsules. J Biochem 2008;144:701–707.
15. MacDougall D, Crummett WB. Guidelines for data acquisition and data quality evaluation in environmental chemistry. Anal Chem. 1980;52:2242–2249.
16. Kanno T, Yamada T, Iwabuki H, Tanaka H, Kuroda S, Tanizawa K, Kawai T. Size distribution measurement of vesicles by atomic force microscopy. Anal Biochem 2002;309:196–199.

Chapter IV

Nanocapsules Incorporating IgG Fc-Binding Domain Derived from Staphylococcus aureus *Protein A for Displaying IgGs on Immunosensor Chips*

4.1. Introduction

Oriented immobilization of the antibody on the surface of a sensor chip is one of the important criteria for improving the sensitivity and specificity of immunosensors [1–3]. In general, immobilization of antibodies on the solid phase (*e.g.*, gold surface) is accomplished by chemical crosslinking without any control of orientation through single or mixed self-assembled monolayers (SAMs) [4], an immunoglobulin (Ig) G Fc-interacting protein A or G [1–3], a biotin/(strept)avidin complex [5], or synthetic polymers [6–8]. These immobilization methods often utilize agents that react nonspecifically with the protein amino groups for tethering antibodies or other interacting molecules to the sensor surface, so the IgG Fv regions are not always oriented to the solvent for antigens to access easily. Several methods have been reported for the oriented immobilization of an antibody (*e.g.*, a Fab′ fragment grafted with a thiol group [2]), but chemical modification of IgG is necessary.

Our group previously developed a yeast-derived novel nanocapsule applicable for pinpoint delivery of drugs and genes [9]. The nanocapsule (abbreviated later as BNC) has a diameter of ~30 nm and is composed of hepatitis B virus surface antigen (HBsAg) L proteins embedded in liposomes [10]. The L protein is a transmembrane protein possessing pre-S1 and pre-S2 regions at the N-terminal of the S region (Figure 4.1A) [9]. Our collaborators recently made a derivative of BNCs by replacing the pre-S1+pre-S2 region with a tandem sequence of the IgG Fc-interacting region (Z domain) derived from *Staphylococcus aureus* protein A [11] and designated it ZZ-BNC (Figures 4.1A and B) [12, 13]. Hence, all IgG Fc domains are expected to spontaneously attach onto the surface of ZZ-BNC as well as displaying all the IgG Fv regions outwardly for effective binding of antigens. In conventional enzyme-linked immunosorbent assays (ELISAs) and western blot analyses, the addition of ZZ-BNCs in the aqueous phase was found to enhance the sensitivities of antigen detection by 10-fold and 50-fold, respectively [14]. In combination with the avidin–biotin complex (ABC) system, biotinylated ZZ-BNCs showed more significant signal enhancement in ELISAs and western blot analyses. These results suggested that ZZ-BNC contributes not only to

the clustering of antibodies and labeling molecules, but also presumably to the oriented immobilization of antibodies. To expand the applications of ZZ-BNC in various immunoassays, I attempted to utilize it as a scaffold of antibodies for immunosensors. An inspiration for this application was derived from our earlier finding that BNCs were observed by atomic force microscopy (AFM) as a monolayer crammed with dome-shaped nanocapsules on the mica substrate [15]. ZZ-BNC (as well as BNC) is considered to be mechanically stable upon treatment with heat or detergent [16]. In the present study, I examined if ZZ-BNCs enhance the sensitivities and antigen-binding capacities of immunosensors due to oriented immobilization of antibodies.

4.2. Experimental Procedures

4.2.1. BNCs

ZZ-BNCs are overexpressed in *Saccharomyces cerevisiae* AH22R$^-$ cells carrying the ZZ-BNC-expression plasmid pGLD-ZZ50 [10, 13]. According to the preparation method for BNC [16], ZZ-BNCs were extracted by disruption with glass beads and purified using an AKTA™ (GE Healthcare, Amersham, UK) by affinity chromatography on porcine IgG and gel filtration.

4.2.2. Reagents

The following materials were obtained commercially. Total IgGs derived from mouse, human, rabbit, sheep, goat, and rat; human IgG1–4; mouse IgG1, 2a, 2b, and 3; anti-actin mouse-derived monoclonal IgG2a; anti-chicken IgY rabbit polyclonal IgG; and actin were purchased from Sigma–Aldrich (Saint Louis, MO, USA). Anti-β-tubulin mouse-derived monoclonal IgG2b was obtained from Millipore Corporation (Billerica, MA, USA). Chicken IgY was from R&D Systems (Minneapolis, MN, USA). Skimmed milk was purchased from Nacalai Tesque (Kyoto, Japan) and tubulin was from Cytoskeleton Incorporated (Denver, CO, USA). The 19-kDa C-terminal region of the *Plasmodium falciparum* merozoite surface protein 1 ($MSP1_{19}$) and mouse-derived anti-$MSP1_{19}$ antiserum are described elsewhere [17].

4.2.3. Transmission electron microscopy (TEM)

ZZ-BNCs (1 μg as protein) were mixed with 10-nm gold particle-labeled goat-derived anti-rabbit total IgG (50 μL, Sigma–Aldrich). They were adsorbed onto a carbon-coated copper grid (JEOL, Tokyo, Japan), negatively stained using 2% (w/v) phosphotungstic acid (pH 7.0), and subjected to TEM using model JEM1011 (JEOL).

4.2.4. AFM

Surface topology images of the fabricated surfaces of immunosensors were analyzed by an AFM model SPA-300 (SII NanoTechnology Inc., Chiba, Japan). Raw AFM images were undertaken in non-contact mode in air at room temperature. The scanning rate was modulated for 1 Hz for a 200 × 200 cm^2 scale image. The average

surface roughness (R_a) for each AFM image was calculated by means of the software provided with the instrument.

4.2.5. Static light scattering (SLS)

The molecular mass (M_r) of ZZ-BNC was measured by a SLS model Zetasizer Nano ZS (Malvern Instruments, Worcestershire, UK) with a constant scattering angle of 173°. The apparent M_r and second virial coefficient (A_2) were estimated from the relationship:

$$KC/R_\theta = (1/ M_r + 2 A_2 C) P_\theta$$

where K, C, R_θ, and P_θ are the optical constant, protein concentration, Rayleigh ratio, and scattering angle, respectively. By measuring R_θ at a series of protein concentrations, apparent values of M_r and A_2 were obtained from Debye plots. Measurements were carried out in triplicate.

4.2.6. Quartz crystal microbalance (QCM)

The amount of IgG bound to ZZ-BNC was determined by a QCM model Twin-Q (As One Corp., Osaka, Japan). The sensor chip of the QCM consisted of a 9-mm-diameter disk made from an AT-cut 27-MHz quartz crystal with gold electrodes on both sides (diameter, 2.5 mm; area, 4.9 mm^2). A frequency change (ΔF) of 1 Hz corresponds to a weight change of 0.6 ng/cm^2. The temperature of the measuring bath (~600 μL) was kept at 25°C with mixing at 600 rpm with a stirring tube. Protein samples were dissolved in 500 μL of phosphate-buffered saline (PBS, 137 mM NaCl, 10 mM Na_2PO_4 and 2 mM KH_2PO_4, pH 7.4). Measurements were done until a stable frequency (less than ± 3 Hz) was observed for >1 min in triplicate.

4.2.7. Preparation of the gold surface

Five microliters of ZZ-BNC (1 mg/mL as protein) were spotted onto the gold surface (Auro sheet (111) HS; Tanaka Kikinzoku Kogyo K.K., Tokyo, Japan). The gold surface was incubated for 30 min at room temperature, washed with distilled water, and dried in air. It was then incubated with 5 μL of anti-β-tubulin mouse IgG2b (1 mg/mL) at room temperature for 1 h, washed thoroughly in distilled water, and dried in air. As a

control, 5 μL of protein A (1 mg/mL) were spotted onto a bare surface or a dithiobis-succinimide propionate (DSP; Thermo Fisher Scientific Inc., Rockford, IL, USA)-modified gold surface [18], incubated at room temperature for 30 min, washed with distilled water, and dried in air. The gold surface was incubated at room temperature for 1 h with 5 μL of anti-β-tubulin mouse IgG2b (1 mg/mL), washed thoroughly in distilled water, and dried in air.

4.2.8. Fluorescence imaging

Aliquots (0.01, 0.1, 1, 10 μg) of Alexa Fluor 546-labeled goat-derived anti-mouse IgG (Invitrogen, Carlsbad, CA, USA) were spotted onto four types of gold surface (*i.e.*, bare gold; protein A-coated; DSP-protein A-coated; ZZ-BNC-coated) and kept at room temperature for 1 h. After washing three times with phosphate-buffered saline (PBS), immunoreactive spots were visualized under a fluorescence image analyzer model OV-100 (Olympus, Tokyo, Japan).

4.2.9. Surface plasmon resonance (SPR)

SPR measurements were performed with a gold sensor chip (PS-01; ICx Nomadics, Inc., Oklahoma City, OK, USA) equipped with an automated SPR-based instrument for biomolecular interaction analyses (SensíQ Pioneer; ICx Nomadics, Inc.) at 25°C. Assay data files were analyzed with Qdat analysis software (ICx Nomadics, Inc. and BioLogic Software).

4.3. Results and Discussion

4.3.1. Structure of ZZ-BNC on the gold surface

I first studied the physical properties of ZZ-BNC. Its molecular mass (M_r) was determined to be 6.57 ± 0.73 MDa (n = 7) by SLS [19], which agrees well with the value previously reported for BNC [16]. Based on the composition of BNC (~90% (w/w) L glycoprotein and 10% (w/w) yeast endoplasmic reticulum membrane-derived lipid bilayer) [20], one particle of ZZ-BNC was estimated to contain ~120 molecules of ZZ domain-substituted L (ZZ-L) protein (M_r, 48 kDa) (*see* Figure 4.1B). TEM analyses showed that ZZ-BNCs of diameter 32.4 ± 4.0 nm (n = 50) were surrounded by several molecules of 10-nm gold particle-labeled goat total IgG (Figure 4.1C, right). This confirmed that ZZ domains are displayed on the surface of ZZ-BNC. Moreover, the topology image of individual ZZ-BNCs (2.5 ng as protein per spot) on the gold surface was analyzed by AFM. This showed dome-shaped nanocapsules with a smooth surface (10.2 ± 0.5 nm in height (n = 40); 44.3 ± 1.2 nm in diameter (n = 10); 0.56 ± 0.11 nm in average surface roughness (R_a) (n = 5)) (Figure 4.1D). Assuming that a ZZ-BNC on a gold surface has a dome-shaped capsule structure, the volume and the surface area of the ZZ-BNC were calculated to be 3410 nm^3 and 8449 nm^2, respectively. These values correspond to those of a spherical particle of ~30 nm in diameter, which agrees well with the diameter obtained by TEM (32.4 nm). The thickness of a lipid bilayer is ~5 nm [21], so the height of a ZZ-BNC on a gold surface (10.2 nm) is sufficient for double lipid bilayers. Thus, it is considered that a ZZ-BNC is in contact with a gold surface without disrupting its capsule structure as well as displaying its ZZ domains outwards.

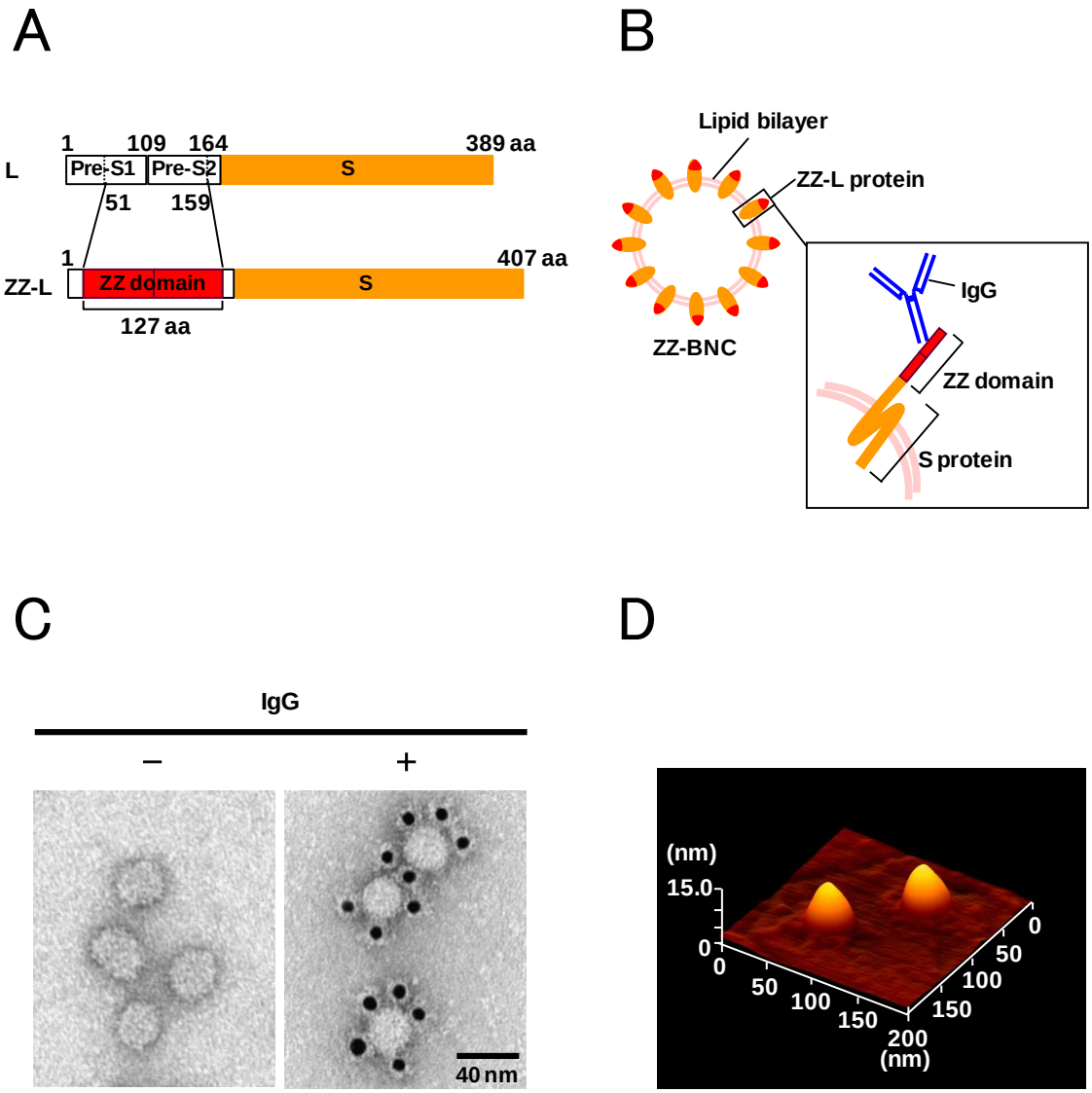

Figure 4.1 Structure and properties of ZZ-BNCs. (A) Schematic structure of original L protein (upper) and ZZ-L protein (lower). (B) Capsular structure of ZZ-BNCs. One ZZ-BNC particle consists of ~120 ZZ-L proteins and a lipid bilayer. (C) TEM images of ZZ-BNC with (+) and without (–) 10-nm gold particle-labeled goat total IgG. Scale bar = 40 nm. (D) AFM image of two ZZ-BNC particles on a gold surface.

4.3.2. Interaction of ZZ-BNC with various IgG molecules

I then measured the binding capacity of ZZ-BNCs for IgG molecules from various species and subclasses using a QCM [22]. The sensor chip in the measuring bath was first treated with ZZ-BNC (10 μg/mL as protein), then blocked with skimmed milk (2.0×10^3 μg/mL), and finally reacted with excess amounts of various IgG molecules (n = 3). As shown in Figure 4.2B, 2387 ± 44 ng/cm^2 of ZZ-BNCs were bound on the sensor chip as estimated from the initial frequency change (ΔF) of –3979 ± 74 Hz. After repeated injection (five times) onto the skimmed milk-blocked sensor chip, 3284 ± 146 ng/cm^2 (corresponding to ΔF of –5473 ± 244 Hz) of mouse total IgG (M_r, *ca.* 150 kDa) was adsorbed (≤95% adsorption was accomplished after the third injection). Under the same condition, 111 ± 5 ng/cm^2 (corresponding to ΔF of –185 ± 8 Hz) of mouse total IgG was adsorbed non-specifically onto the gold surface in the absence of ZZ-BNCs (Figure 4.2A). These data indicated that a maximum of ~0.5 mol of mouse total IgG was bound per mol of ZZ-L protein. Assuming that only about half of the surface of ZZ-BNC bound to the sensor chip was available for IgG binding, this result suggested that each ZZ-L protein can bind one molecule of IgG. This corresponds to binding ~60 molecules per single ZZ-BNC. Thus, the ZZ domains show a 'half-of-the-sites reactivity'. If an IgG molecule binds to one Z domain, another IgG cannot bind to the neighboring Z domain contained in the same ZZ-L protein (*see* Figure 4.1B), presumably due to steric hindrance.

In the same way, fifteen types of IgG molecule (derived from seven species) were examined by QCM for adsorbing onto ZZ-BNC, and the amounts of IgG bound to ZZ-L protein were calculated on a molar basis (n = 3, Table 4.1). Total IgG from humans, mice, rabbits, sheep and goats exhibited similar high binding affinities to ZZ-L protein (0.34–0.49 mol of IgG per mol of ZZ-L protein), whereas rat total IgG and chicken IgY showed much lower affinities (0.05 and 0.01 mol of IgG per mol of ZZ-L protein, respectively). With respect to subclasses of IgG molecules, human IgG1, IgG2, IgG4, and mouse IgG3 showed high binding affinities; mouse IgG2a and IgG2b showed moderate affinities, and human IgG3 and mouse IgG1 had very low affinities. The IgG-binding properties of ZZ-L protein reflect those of protein A [23].

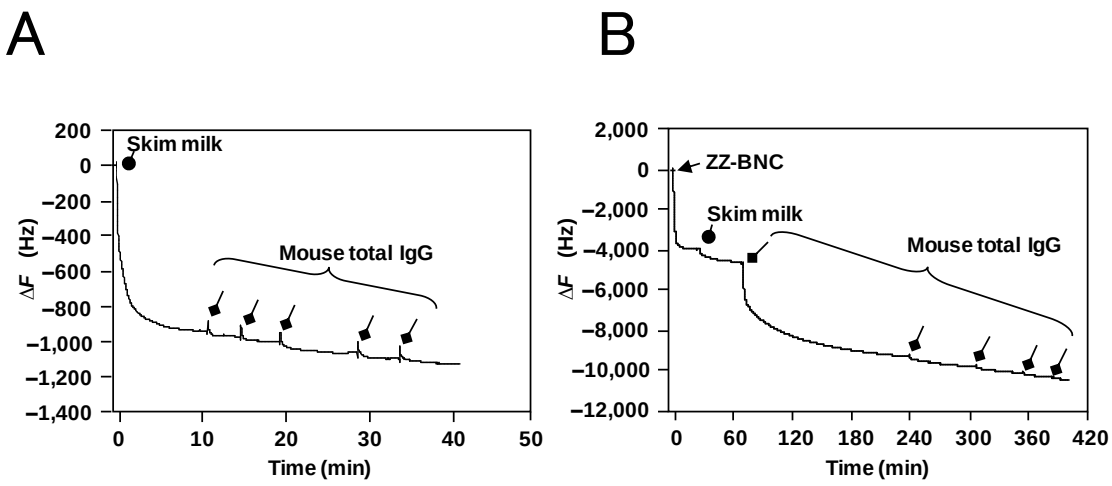

Figure 4.2 QCM analyses for the interaction of ZZ-BNCs with mouse total IgG. The frequency changes (Δ*F*) upon successive injections of ZZ-BNC (triangle), skimmed milk (circle), and mouse total IgG (200 μg × 5; squares) were recorded. (A) Without ZZ-BNC. (B) With ZZ-BNC.

Table 4.1 Binding capacity of the ZZ domain to various IgG molecules determined by QCM

Species	Subclass of antibody	IgG/ZZ domain*
Human	Total IgG	0.39 ± 0.04
	IgG1	0.30 ± 0.03
	IgG2	0.28 ± 0.02
	IgG3	0.01 ± 0.00
	IgG4	0.35 ± 0.03
Mouse	Total IgG	0.49 ± 0.01
	IgG1	0.03 ± 0.01
	IgG2a	0.14 ± 0.02
	IgG2b	0.15 ± 0.04
	IgG3	0.47 ± 0.02
Rabbit	Total IgG	0.47 ± 0.08
Sheep	Total IgG	0.34 ± 0.03
Goat	Total IgG	0.41 ± 0.07
Rat	Total IgG	0.05 ± 0.01
Chiken	IgY	0.01 ± 0.00

* Number (mol) of IgG molecules bound per mol of the ZZ domain.

4.3.3. IgG-binding capacity of ZZ-BNC-coated gold surface

The IgG-binding capacity of ZZ-BNC led us to examine the ZZ-BNC-coated gold surface as immunosensors. I coated bare gold surfaces with protein A (5 μg per spot, Figure 4.3B), with DSP and subsequently protein A (5 μg per spot, Figure 4.3C), and with ZZ-BNC (5 μg as protein per spot, Figure 4.3D). Then, the gold surfaces were treated with anti-β-tubulin mouse IgG2b, which shows moderate binding affinity to ZZ-BNC (*see* Table 4.1). The topology images of each gold surface were acquired at 200 × 200 nm^2 by AFM (n = 3). The height and R_a of the bare gold surface were 1.04 ± 0.32 nm and 0.14 ± 0.01 nm, respectively. After modification with protein A and DSP-protein A, heights were increased by 1.33 nm and 4.37 nm, respectively, with small increase in R_a (Figure 4.3, line 2). Modification with ZZ-BNC significantly increased height and R_a. Protein A on a mica surface in air showed a highly extended shape of 1.5 × 25 nm to 1.5 × 30 nm [24]. The linker length of DSP is ~1.2 nm. The height of ZZ-BNC on a gold surface was 10.2 ± 0.5 nm (Figure 4.1D). Thus, the increases of each height were consistent with the sizes of protein A , DSP, and ZZ-BNC.

When anti-β-tubulin mouse IgG2b was applied onto each gold surface (Figure 4.3, line 3), the heights of bare, protein A-coated, and DSP-protein A-coated gold surface were increased by 1.14 nm, 0.68 nm, and 1.07 nm with a small increase in R_a (0.31 nm, 0.19 nm, and 0.43 nm), respectively. AFM observation of IgG molecules on a mica surface in air have shown that the hinge region of IgG is sufficiently flexible so that two Fab regions can rotate about their axes to present its side to the mica surface with deposition of the Fc region to opposite side (triangular form, ~10 nm of each side; ~1.3 nm in height) [25], so the restrained configuration of IgG2b molecules might result in a change in their heights of ~1 nm on each gold surface. Next, the height of the ZZ-BNC-coated gold surface was significantly increased by 10.98 nm by the adsorption of IgG2b molecules with small decrease in R_a (0.38 nm). These results could be because the change in height by IgG2b molecules on the ZZ-BNC-coated gold surface was much higher than that of the bare, protein A-, or DSP-protein A-coated gold surface (10.98 nm *vs.* 0.68–1.14 nm), presumably due to the upward disposition of Fab regions. The small decrease in R_a by IgG2b molecules on the ZZ-BNC-coated gold surface (which was not observed in other gold surfaces) may be caused by the oriented immobilization of IgG molecules.

I also examined the IgG-binding capacity on each gold surface by fluorescence imaging (Figure 4.3, line 4). When aliquots (0.01–10 μg) of Alexa Fluor 546-labeled goat-derived IgG were spotted onto each gold surface, the ZZ-BNC-coated gold surface

could capture the largest amounts of IgG compared with other gold surfaces. The minimum amount of IgG necessary to be detected on ZZ-BNC-coated gold surfaces was 0.01 μg, whereas those of bare, protein A-coated, and DSP-protein A-coated gold surfaces were 10 μg, 1 μg, and 10 μg, respectively. These results indicated that ZZ-BNC allows the binding of more IgG molecules (>100 times) than protein A and DSP-protein A, indicating that ZZ-BNC plays as an efficient scaffold for IgG molecules for immunosensors probably by reducing steric hindrance due to oriented immobilization.

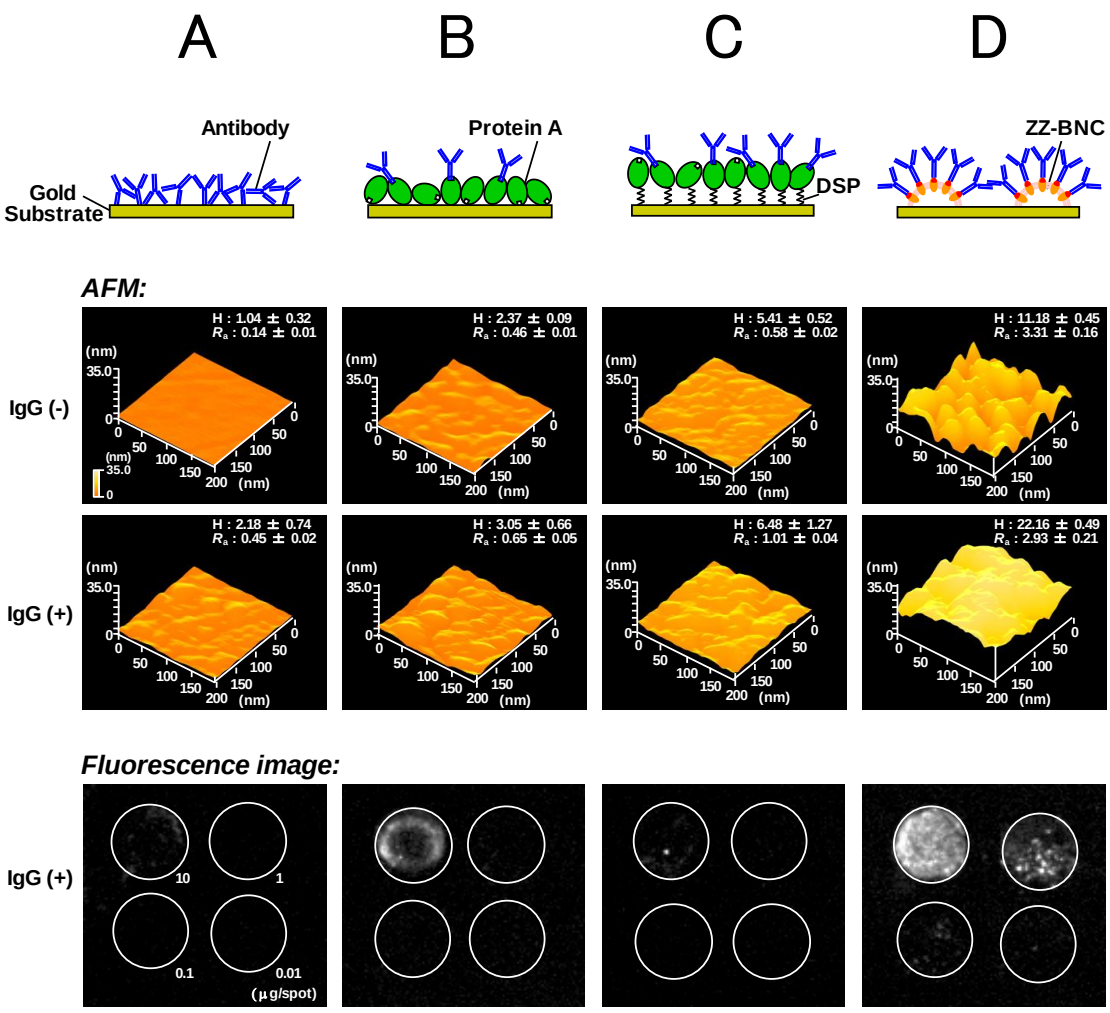

Figure 4.3 IgG-binding capacity of the ZZ-BNC-coated gold surface. Line 1, schematic representation of antibody immobilization on the gold surface. Lines 2 and 3, AFM images of gold surfaces without (–) and with (+) IgG, respectively. H, height (nm); R_a, roughness (nm). Line 4, fluorescence images of gold surfaces with IgG. Row A, antibody alone; row B, protein A-coated; row C, DSP-protein A-coated; row D, ZZ-BNC-coated.

4.3.4. Effect of ZZ-BNC on the sensitivity and antigen-binding capacity in QCM

I assessed the effect of ZZ-BNC on the sensitivity and antigen-binding capacity of immunosensors in QCM. Antigen binding to the sensor chip was studied with four arbitrarily chosen antigens (tubulin, actin, chicken IgY, malaria merozoite surface protein 1 ($MSP1_{19}$)) for which antibodies were readily available (anti-β-tubulin mouse IgG2b, anti-actin mouse IgG2a, anti-chicken IgY rabbit polyclonal IgG, and anti-$MSP1_{19}$ mouse antiserum, respectively). The gold surface of the sensor chip was first thoroughly modified with antibody alone (6 μg/mL for anti-β-tubulin and anti-actin; 23.6 μg/mL for anti-chicken IgY; 300 μg/mL for anti- $MSP1_{19}$), protein A (10 μg/mL), DSP-protein A (10 μg/mL), or ZZ-BNC (10 μg/mL) (designated patterns 1, 2, 3, and 4, respectively, in Figure 4.4A), the latter three of which were then fully reacted with the same antibody. The QCM equipment had a limit of detection (LOD) of a weight change of 2 ng/cm^2 (corresponding to ΔF of –3.3 Hz). Therefore, to compare the sensitivities of the sensor chip in the four patterns, the lowest concentrations of antigens necessary to give this LOD were determined. With tubulin, the lowest concentrations were ~31, 100, 328, and 7 ng/mL (Figure 4.4B); with actin, the concentrations were ~6200, 1205, 1491, and 49 ng/mL (Figure 4.4C); with chicken IgY, the concentrations were ~213, 11, 1.5, and 1.3 ng/mL (Figure 4.4D), in patterns 1, 2, 3, and 4 (Figure 4.4A), respectively. With $MSP1_{19}$, the concentrations were ~6600 and 0.001 ng/mL (Figure 4.4E), in patterns 1 and 4, respectively. Thus, the sensitivity of the sensor chip increased dramatically in all cases by adsorbing antibodies onto ZZ-BNC. The antigen-binding capacity of each sensor chip was compared in terms of the upper limit of antigen binding (calculated from the maximum ΔF). The sensor chip modified with ZZ-BNC could bind the largest amount of antigens for all cases examined. Consequently, the use of ZZ-BNC significantly expanded the dynamic concentration ranges of antigens (*ca.* 20–2200, 220–7700, 2–2200, and 0.006–0.666 ng/mL for tubulin, actin, chicken IgY, and $MSP1_{19}$, respectively; Figures 4.4B–E).

Immobilization of antibodies on ZZ-BNC was also effective for increasing their antigen-binding efficiencies (avidities) [26] as judged from the amounts of bound antigen per immobilized antibody. For example, 0.03, 0.11, 0.10, and 0.89 mol of tubulin bound per 1 mol of an anti-β-tubulin mouse monoclonal IgG2b immobilized in patterns 1, 2, 3, and 4, respectively (Figure 4.4A). The 33.1-fold (*vs.* antibody alone), 8.3-fold (*vs.* protein A) and 8.7-fold (*vs.* DSP-protein A) increases in antigen-binding efficiency of the antibody immobilized on ZZ-BNC far exceeded those reported for conventional orientation-controlled antibody immobilization methods (*e.g.*, protein

A-coated plasma-polymerized film (PPF) (5.35-fold, *vs.* antibody alone) [27, 28], protein A-coated SAM (2.1-fold, *vs.* antibody alone) [29], protein A-coated nanopatterned PPF (1.2-fold, *vs.* antibody alone) [30], and Fab′ fragment-coated PPF [31]). Based on the significant increases in sensitivities and antigen-binding capacities, ZZ-BNC might provide immunosensors with more efficient oriented immobilization of antibodies.

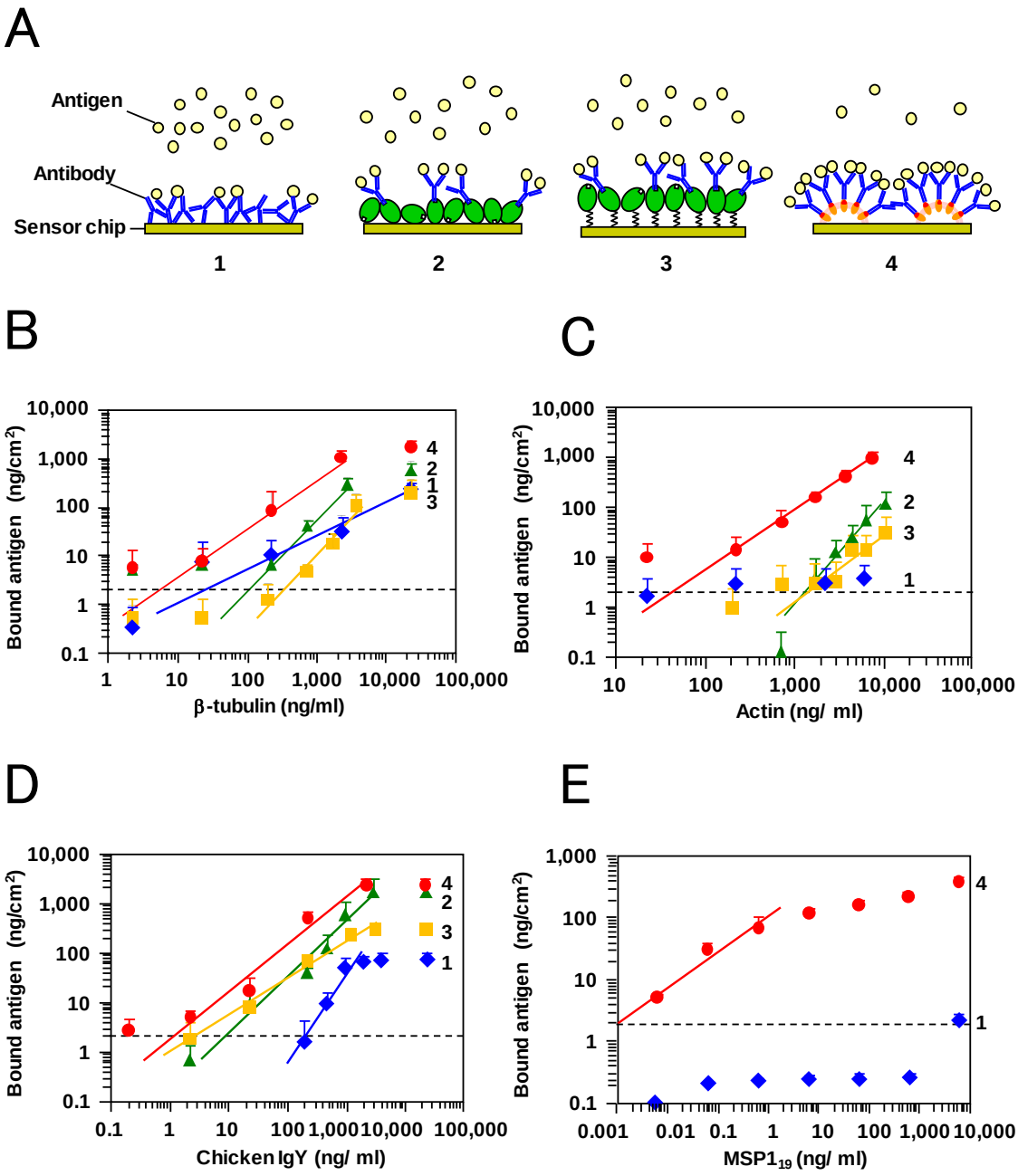

Figure 4.4 Effect of antibody immobilization on sensitivity and antigen-binding capacity. (A) Schematic representation of antibody immobilization on the sensor chip with an antibody alone, protein A, DSP-protein A or ZZ-BNC (patterns 1, 2, 3, and 4, respectively). The amounts of bound antigen calculated from frequency changes in QCM were plotted against concentrations of the injected antigen (B, tubulin; C, actin; and D, chicken IgY; E, $MSP1_{19}$) for immobilization patterns 1 (blue diamonds), 2 (green triangles), 3 (orange squares), and 4 (red circles). LOD (2 ng/cm^2) is indicated by dashed lines. Dynamic concentration ranges of measured antigens are shown approximately with lines for each immobilization pattern.

4.3.5. Effect of serum on the ZZ-BNC-coated sensor chip in QCM

To expand the possibility of using ZZ-BNC-coated gold surfaces on various immunosensors used in clinical fields, the antigen-binding capacity was measured using tubulin (2–20,000 ng/mL) in PBS and fetal bovine albumin (FBS) by QCM. The presence of 100% (v/v) FBS did not have a significant influence on the background nor antigen-binding capacity of the anti-β-tubulin mouse IgG2b immobilized onto ZZ-BNC-coated sensor chips (Figure 4.5A). Similar results were obtained using anti-actin IgG2a (Figure 4.6A).

4.3.6. Repetitive use of ZZ-BNC-coated sensor chips in QCM

The stability of ZZ-BNC-coated sensor chips was examined by repetition of the antibody adsorption and regeneration of ZZ-BNCs. The sensor chip was coated with ZZ-BNC and subsequently skimmed milk as described in the "**Materials and Methods**" section. After stabilization of ΔF (less than ± 3 Hz for >1 min), anti-chicken IgY rabbit polyclonal IgG (11.8 μg/mL) was injected into the measuring bath (*squares* in Figure 4.5B). After 5-min measurement, the chip was rinsed twice with 2N HCl (20 μL) for stripping bound antibodies (*arrows*), washed three times with PBS, and then used for blocking with skimmed milk (first cycle, *left dashed box* in Figure 4.5B). The cycle of adsorption and removal of antibodies was repeated 21 times (21st cycle, *right dashed box*). The frequency change (ΔF) observed in the 21st cycle was >98% of ΔF in the first cycle. A similar result was obtained using mouse total IgG (Figure 4.6B). Even after removal of bound antibodies by washing under harsh conditions (*e.g.*, pH 2–12, 50°C, 1 M NaCl, 2N HCl), the sensor chip fully retained the ZZ-BNCs and could be used repeatedly for immobilization of antibodies. Thus, ZZ-BNC is stably adsorbed onto the gold surface of a sensor chip, presumably by forming Au–S covalent linkages with some of the 14 Cys residues in the S region of the ZZ-L protein.

A

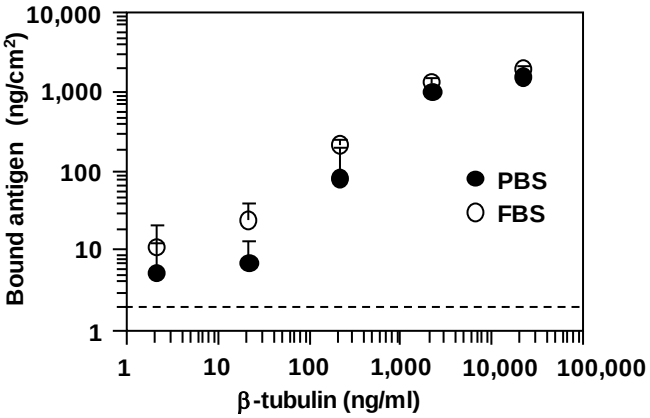

B

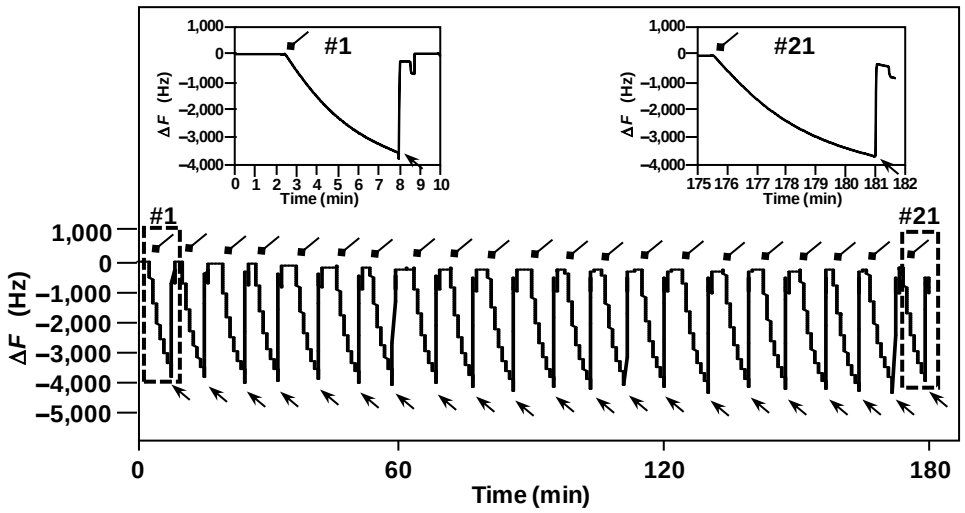

Figure 4.5 Effects of fetal bovine serum and repetitive use on the function of ZZ-BNC-coated sensor chips. (A) The antigen-binding capacity of anti-β-tubulin mouse IgG2b immobilized onto ZZ-BNC-coated sensor chips. PBS alone (closed circles) and 100% (v/v) FBS (open circles). (B) Anti-chicken IgY rabbit polyclonal IgG (squares) was injected onto the ZZ-BNC-coated sensor chip. After 5-min measurement, the chip was rinsed twice with 2N HCl (arrows) to strip bound antibodies. The cycle of adsorption and removal of antibody was repeated 21 times. Insets, frequency changes in the 1st and 21st cycle are shown.

A

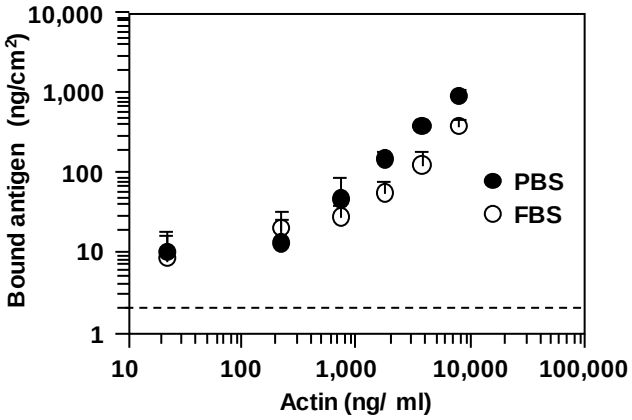

B

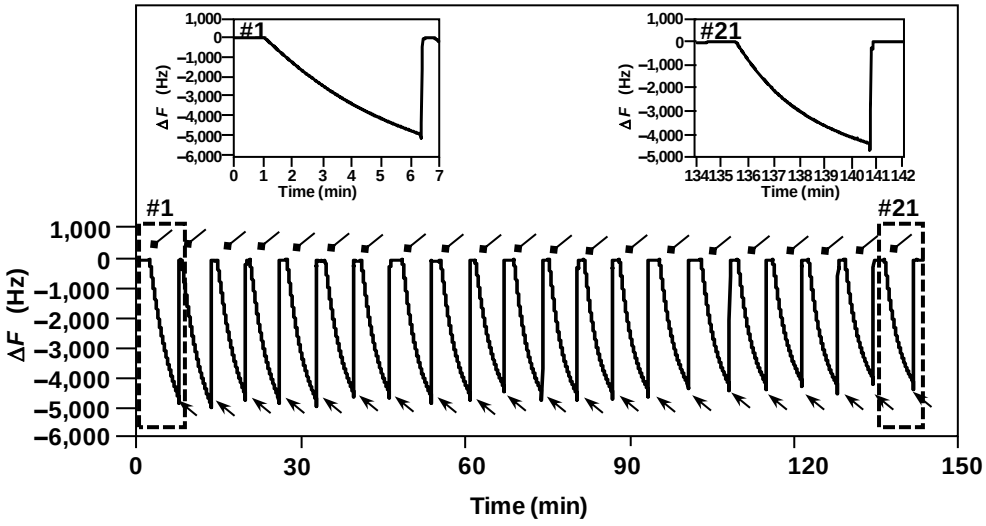

Figure 4.6 Effects of fetal bovine serum and repetitive use on the function of ZZ-BNC-coated sensor chips. (A) The antigen-binding capacity of anti-actin mouse IgG2a immobilized onto ZZ-BNC-coated sensor chips. PBS alone (closed circles) and 100% (v/v) FBS (open circles). (B) Mouse total IgG (squares, 11.8 μg/mL) was injected onto the ZZ-BNC-coated sensor chip. After 5-min measurement, the chip was rinsed twice with 2N HCl (arrows) to strip bound antibodies. The cycle of adsorption and removal of antibody was repeated 21 times. Insets, frequency changes of the 1st and 21st cycle are shown.

4.3.7. Effect of ZZ-BNC on the antigen-binding affinity of immunosensors in SPR

The advantages of ZZ-BNC in QCM immunosensors led us to use ZZ-BNC in SPR [32]. First, ZZ-BNC (50 μg/mL, channel 3) or protein A (50 μg/mL, channel 1) was adsorbed onto the surface of a bare gold sensor chip in each channel of SPR using distilled water at a flow rate of 30 μL/min for 10 min. Subsequently, anti-actin mouse IgG2a (12.5 nM) or anti-chicken IgY rabbit polyclonal IgG (7.5 nM) was immobilized to protein A- or ZZ-BNC-coated gold sensor chips using the running buffer (20 mM NaH_2PO_4 pH 8.0, 300 mM NaCl and 0.005% (v/v) Tween-20) for 3 min, and then subjected to the interaction analysis of the antigen with its respective antibody (Figure 4.7). The maximal response if all available ligand binding sites are occupied (R_{max}) induced by antigen binding to gold sensor chips based on ZZ-BNC (actin, 56.3 RU; IgY 38.4 RU) were, respectively, 2.3- and 1.5-times higher if compared with the signals obtained for protein A. This indicated that the antigen-binding sites on protein A were partially blocked due to an incorrect binding position of the antibody whereas, on ZZ-BNC, the antigen-binding sites were more readily accessible from the solution front, which agreed well with the results observed in QCM (*see* Figure 4.4). To determine the kinetic rate constant for association and dissociation, the simple 1:1 kinetic model was fitted to each dataset with terms for the on-rate constant (k_a) and off-rate constant (k_d). These kinetic constants were fitted globally for each assay set. The kinetic interaction of antigens for each antibody (K_D) was of a higher affinity when analyzed on a ZZ-BNC-coated sensor chip (actin, 3.09 nM; chicken IgY, 43.2 nM) compared with on a protein A-coated sensor chip (actin, 8.93 nM; chicken IgY, 151.6 nM), respectively (Table 4.2). The on-rate constants (k_a) of these interactions were nearly identical for both gold sensor chips. However, the off-rate constant (k_d) exhibited a slower dissociation from the ZZ-BNC-coated sensor chip (actin, 6.28×10^{-5} s^{-1}; chicken IgY, 4.57×10^{-5} s^{-1}) when compared with a protein A-coated sensor chip (actin, 2.06×10^{-4} s^{-1}; chicken IgY, 1.7×10^{-4} s^{-1}). These data indicated that ZZ-BNC mainly contributes to reduce the dissociation rates of antigens from each antibody. The steric hindrance around antigen-binding sites may be decreased by the oriented immobilization of antibodies on ZZ-BNC, thereby stabilizing the antigen–antibody complexes.

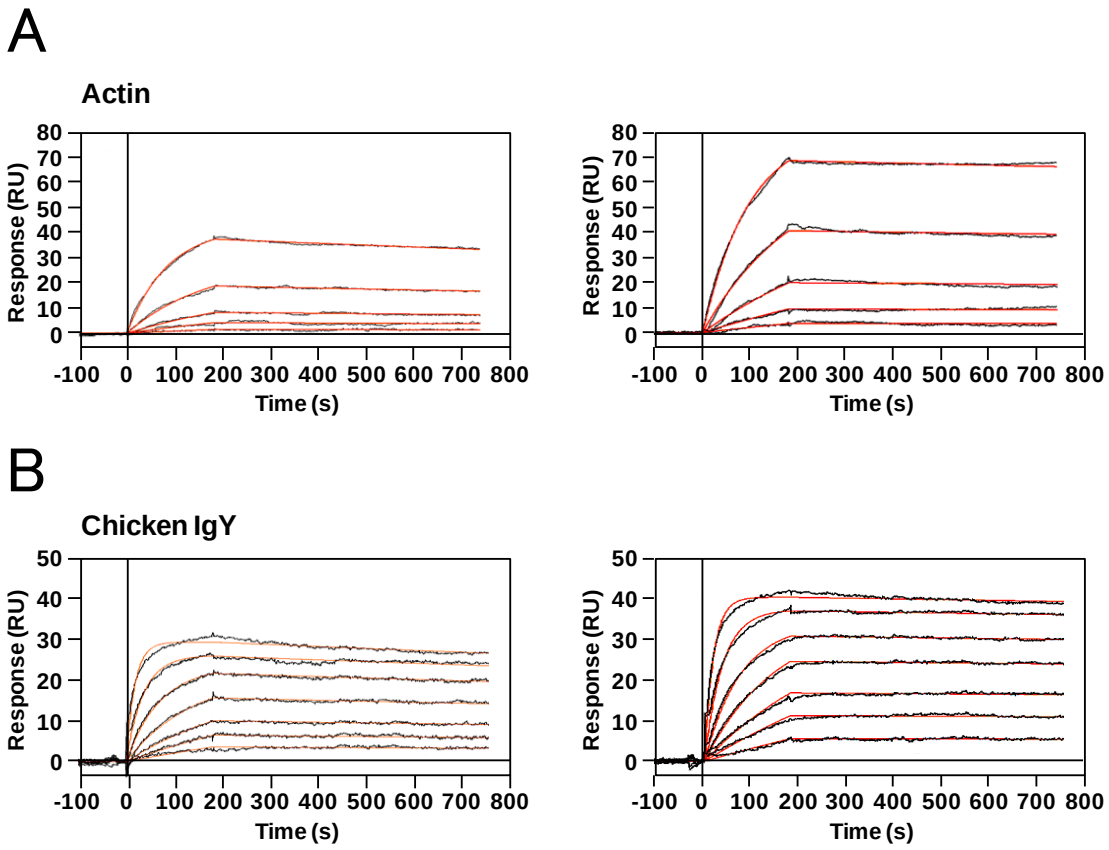

Figure 4.7 Kinetic analyses of antigen–antibody interactions on protein A- (left panels) and ZZ-BNC-coated (right panels) sensor chips using SPR. The doubling dilution series of each antigen ((A) actin, 0–500 nM; (B) chicken IgY, 0–50 nM) were injected for 3 min and dissociation monitored for 10 min. The response curves were overlaid and double-referenced by subtracting the reference curve signal and the signal of a buffer blank. The simple 1:1 kinetic model (red lines) was fitted to each dataset with terms for the on-rate constant (k_a) and off-rate constant (k_d). These kinetic constants were fitted globally for each assay set.

Table 4.2 Comparison of association (k_a), and dissociation (k_d), and estimated equilibrium dissociation (K_D) constants for the interaction of actin and chicken IgY with respective antibodies immobilized onto protein A- and ZZ-BNC-coated sensor chips

	Actin (analyte)			Chicken IgY (analyte)		
	k_a ($M^{-1}s^{-1}$)	k_d (s^{-1})	K_D (nM)	k_a ($M^{-1}s^{-1}$)	k_d (s^{-1})	K_D (nM)
IgG/Protein A	2.31×10^4	2.06×10^{-4}	8.93	1.12×10^6	1.7×10^{-4}	151.6
IgG/ZZ-BNC	2.03×10^4	6.28×10^{-5}	3.09	1.06×10^6	4.57×10^{-5}	43.2

4.3.8. Repetitive use of ZZ-BNC-coated sensor chips in SPR

I examined if ZZ-BNC-coated gold surfaces could be used multiple times for antibody immobilization in SPR. A doubling dilution series of anti-actin mouse IgG2a or anti-chicken IgY rabbit polyclonal IgG was prepared from a stock concentration of 50 nM (anti-actin) and 100 nM (anti-chicken IgY) in running buffer. Each concentration of the antibody dilution series was injected for 3 min at a flow rate of 30 μL/min and dissociation during buffer flow monitored for 10 min. The sensor surface was regenerated by injecting 10 mM HCl for 1 min. Duplicate injections of anti-actin and anti-chicken IgY were performed for determining the overall change in antibody-binding activity of the protein A- and ZZ-BNC-coated gold sensor chips (Figure 4.8). The assay cycles were carried out at random to eliminate systematic artifacts. The mean percentage differences were calculated using the following formula:

$[(R2 - R1)/ R_{max}] \times 100\ (\%)$

where R2 is the second of two responses at a given concentration and R1 is the first of two responses. The R_{max} induced by antibody binding to these sensor chips was 114 RU (anti-actin vs. protein A), 257 RU (anti-chicken IgY vs. protein A), 131 RU (anti-actin vs. ZZ-BNC), and 312 RU (anti-chicken IgY vs. protein A). The result showed that ZZ-BNC possesses a better overall stability and tends to degrade at a much slower rate. Furthermore, ZZ-BNC-coated sensor chips were assumed to be robust because appreciable dissociation of ZZ-BNC was not observed over 2 days.

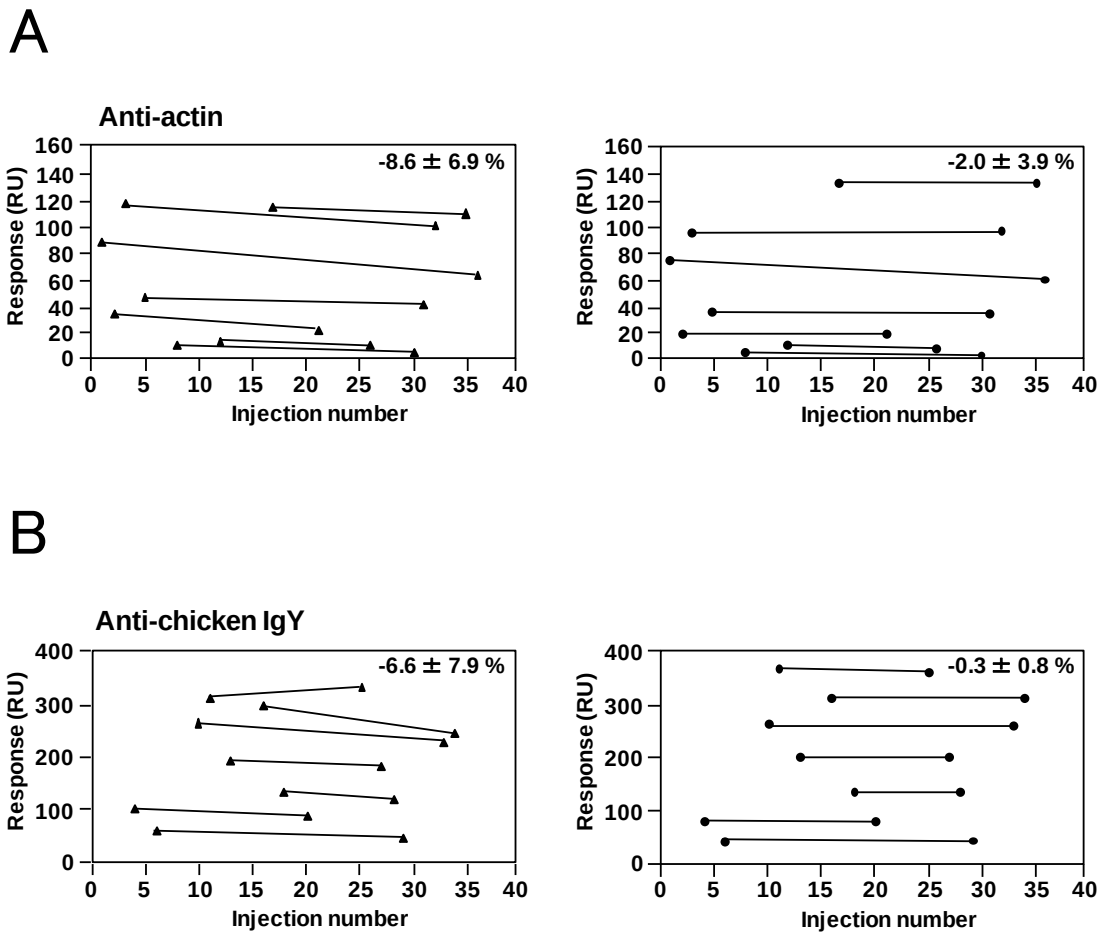

Figure 4.8 Repetitive use of ZZ-BNC-coated sensor chips in SPR. The doubling dilution series of each antibody ((A) anti-actin mouse IgG2a, 0–50 nM; (B) anti-chicken IgY rabbit polyclonal IgG, 0–100 nM) were injected for 3 min and the dissociation monitored for 10 min. The sensor surface was regenerated with 10 mM HCl for 1 min. Duplicate injections of each antibody were performed for determining the overall change in the antibody-binding activity of each sensor chip. The mean percentage differences (upper right) were calculated using the following formula: $[(R2 - R1)/ R_{max}] \times 100$ (%), where R2 is the second of two responses at a given concentration and R1 is the first of two responses.

4.3.9. Conclusions

This study demonstrated that ZZ-BNCs are a promising scaffold for displaying antibodies on a solid phase. They improve the sensitivity, antigen-binding capacity, and affinity of immunosensors, presumably in the manner of oriented immobilization of antibodies. ZZ-BNCs also associate firmly with glass and plastic surfaces (unpublished results). The extraordinarily high stability of ZZ-BNC-bound chips makes them an ideal sensor applicable for various immunosensing technologies, including QCM and SPR, but also surface acoustic wave (SAW) [1], laser nephelometry [33], fluorescence anisotropy [34] and immunologically modified field effect transistors (ImmunoFET) [35].

4.4. References

1. Gizeli E, Lowe CR. Immunosensors. Curr Opin Biotechnol 1996;7:66–71.
2. Rao SV, Anderson KW, Bachas LG. Oriented immobilization of proteins. Mikrochim Acta 1998;128:127–143.
3. Prieto-Simón B, Campàs M, Marty J-L. Biomolecule immobilization in biosensor development: tailored strategies based on affinity interactions. Protein Pept Lett 2008;15:757–763.
4. Wink T, van Zuilen SJ, Bult A, van Bennkom WP. Self-assembled monolayers for biosensors. Analyst 1997;122:43R–50R.
5. Johnsson B, Löfås S, Lindquist G, Edström A, Müller Hillgren RM, Hansson A. Comparison of methods for immobilization to carboxymethyl dextran sensor surfaces by analysis of the specific activity of monoclonal antibodies. J Mol Recog 1995;8:125–131.
6. Geckeler KE, Müller B. Polymer materials in biosensors. Naturwissenschaften 1993;80:18–24.
7. Suzuki N, Quesenberry MS, Wang JK, Lee RT, Kobayashi K, Lee YC. Efficient immobilization of proteins by modification of plate surface with polystyrene derivatives. Anal Biochem 1997;247:412–416.
8. Jordan CE, Corn RM. Surface plasmon resonance imaging measurement of electrostatic biopolymer adsorption onto chemically modified gold surfaces. Anal Chem 1997;69:1449–1456.
9. Yamada T, Iwasaki Y, Tada H, Iwabuki H, Chuah MK, VandenDriessche T, et al. Nanoparticles for the delivery of genes and drugs to human hepatocytes. Nat Biotechnol 2003;21:885–890.
10. Kuroda S, Otaka S, Miyazaki T, Nakao M, Fujisawa Y. Hepatitis B virus envelope L protein particles. J Biol Chem 1992;267:1953–1961.
11. Nilsson B, Moks T, Jansson B, Abrahmsén L, Elmblad A, Holmgren E, et al. A synthetic IgG-binding domain based on staphylococcal protein A. Protein Eng 1987;1:107–113.
12. Tsutsui Y, Tomizawa K, Nagita M, Michiue H, Nishiki T, Ohmori I, et al. Development of bionanocapsules targeting brain tumors. J Control Release 2007;122:159–164.
13. Kurata N, Shishido T, Muraoka M, Tanaka T, Ogino C, Fukuda H, et al. Specific protein delivery to target cells by antibody-displaying bionanocapsules. J Biochem 2008;144:701–707.

14. Iijima M, Matsuzaki T, Kadoya H, Hatahira S, Hiramatsu S, Jung G, et al. Bionanocapsule-based enzyme-antibody conjugates for enzyme-linked immunosorbent assay. Anal Biochem 2010;396:257–261.
15. Kanno T, Yamada T, Iwabuki H, Tanaka H, Kuroda S, Tanizawa K, et al. Size distribution measurement of vesicles by atomic force microscopy. Anal Biochem 2002;309:196–199.
16. Yamada T, Iwabuki H, Kanno T, Tanaka H, Kawai T, Fukuda H, et al. Physicochemical and immunological characterization of hepatitis B virus envelope particles exclusively consisting of the entire L (pre-S1 + pre-S2 + S) protein. Vaccine 2001;19:3154–3163.
17. Okafor CM, Anumudu CI, Omosun YO, Uthaipibull C, Ayede I, Awobode HO, et al. Cellular responses to modified Plasmodium falciparum $MSP1_{19}$ antigens in individuals previously exposed to natural malaria infection. Malar J 2009;8:263–271.
18. Schmid AH, Stanca SE, Thakur MS, Thampi KR, Suri CR. Site-directed antibody immobilization on gold substrate for surface plasmon resonance sensors. Sens Actuators B Chem 2006;113:297–303.
19. Hiemenz PC. Light scattering by polymer solutions. In: Polymer Chemistry. The basic concepts. Chpt 10. New York: Marcel Decker Inc, 1984. p. 659–722.
20. Kobayashi M, Asano T, Utsunomiya M, Itoh, Y, Fujisawa Y, Nishimura O, et al. Recombinant hepatitis B virus surface antigen carrying the pre-S2 region derived from yeast: purification and characterization. J Biotech 1988;8:1–21.
21. Hui SW, Viswanathan R, Zasadzinski JA, Israelachvili JN. The structure and stability of phospholipid bilayers by atomic force microscopy. Biophys J 1995;68:171–8.
22. Shons A, Dorman F, Najarian JJ. An immunospecific miclobalance. J Biomed Mater Res 1972;6:565–570.
23. Björck L, Kronvall G. Purification and some properties of streptococcal protein G, a novel IgG-binding reagent. J Immunol 1984;133:969–974.
24. Ohnishi S, Murata M, Hato M. Correlation between surface morphology and surface forces of protein A adsorbed on mica. Biophys J 1998;74:455–465.
25. Thomson NH. The substructure of immunoglobulin G resolved to 25 kDa using amplitude modulation AFM in air. Ultramicroscopy 2005;105:103–110.
26. Coe Clough NE, Hauer PJ. Using polyclonal and monoclonal antibodies in regulatory testing of biological products. ILAR J 2005;46:300–306.

27. Nakanishi K, Muguruma H, Karube I. A novel method of immobilizing antibodies on a quartz crystal microbalance using plasma-polymerized films for immunosensors. Anal Chem 1996;68:1695–1700.
28. Wang H, Liu Y, Yang Y, Deng T, Shen G, Yu R. A protein A-based orientation-controlled immobilization strategy for antibodies using nanometer-sized gold particles and plasma-polymerized film. Anal Biochem 2004;324:219–226.
29. Briand E, Salmain M, Compère C, Pradier CM. Anti-rabbit immunoglobulin G detection in complex medium by PM-RAIRS and QCM influence of the antibody immobilization method. Biosens Bioelectron 2007;22:2884–2890.
30. Valsesia A, Colpo P, Mannelli I, Mornet S, Bretagnol F, Ceccone G, et al. Use of nanopatterned surfaces to enhance immunoreaction efficiency. Anal Chem 2008;80:1418–1424.
31. Wang H, Wu J, Li J, Ding Y, Shen G, Yu R. Nanogold particle-enhanced oriented adsorption of antibody fragments for immunosensing platforms. Biosens Bioelectron 2005;20:2210-2217.
32. Liedberg B, Nylander C, Lundström I. Biosensing with surface plasmon resonance-how it all standard. Biosens Bioelectron 1995;10:i-ix.
33. Whicher JT, Price CP, Spencer K. Immunonephelometric and immunoturbidimetric assays for proteins. Crit Rev Clin Lab Sci 1983;18:213-260.
34. Baldini F, Carloni A, Giannetti A, Porro G, Trono C. A new optical platform for biosensing based on fluorescence anisotropy. Anal Bioanal Chem 2008;391:1837-1844.
35. Eteshola E, Keener MT, Elias M, Shapiro J, Brillson LJ, Bhushan B, et al. Engineering functional protein ingerfaces for immunologically modified field effect transistor (ImmunoFET) by molecular genetic means. J R Soc Interface 2008;5:123-127.

Chapter V

Fluorophore-labeled nanocapsules displaying IgG Fc-binding domains for the simultaneous detection of multiple antigens

5.1. Introduction

The simultaneous detection of multiple antigens in one specimen by immunological methods (*e.g.*, western blot analysis, immunocytochemistry, flow cytometric analysis, and immunohistochemistry) has been considered as a powerful tool for the elucidation of functions and cellular localizations of various biomolecules. However, primary antibodies derived from the same host species cannot be used simultaneously, because one secondary antibody may cross-react with multiple primary antibodies. Usually, we have chosen primary antibodies from different or non-crossreactive species/subclasses [1]. Such convenient pairs of antibodies are not always available. Even if we have excellent primary antibodies, the cross-reactivity limitation has hampered the expansion of possibilities of these immunological methods. Generally, 'sequential immunolabeling methods' have been applied to enable the detection of multiple antigens with primary antibodies from the same host species. Each immunolabeling step is carried out using a secondary antibody labeled with a distinct fluorophore [1], enzyme, or hapten [2], which are sometimes coupled by heat treatment [3, 4], low pH, and detergent [5] to eliminate the residual antibodies on the specimen for subsequent immunolabeling steps. Tyramide signal amplification (TSA) [6] is also used to reduce the amount of primary antibodies in the first immunolabeling step. Alternatively, each primary antibody used in the first immunolabeling step is blocked by anti-IgG Fab fragments to reduce the cross-reaction of secondary antibodies in the second immunolabeling step [7, 8]. Fluorophore-labeled anti-IgG Fab fragments [9], enzyme-labeled anti-IgG Fab/$F(ab')_2$ fragments [10], and fluorophore-labeled anti-IgG $F(ab')_2$ fragments [11] could be used for the immunolabeling of primary antibodies in the first step. However, these methods are time-consuming, not applicable for the simultaneous immunolabeling of multiple antigens, and practically limited to two immunolabelings. False-positive signals may also occur by the cross-reaction of secondary antibodies. To overcome these problems, 'simultaneous immunolabeling methods' have been developed to detect multiple antigens with primary antibodies from the same host species as follows; (a) direct labeling, where each primary antibody is directly labeled with a distinct enzyme [12] or fluorophore [13]; (b) protein A complex,

where each primary antibody is conjugated with fluorophore-labeled *Staphylococcus aureus* protein A [14]; and (c) anti-IgG or anti-Fc Fab fragment, where each primary antibody is conjugated with a fluorophore-labeled anti-Fc or anti-IgG Fab fragment [15, 16]. These methods could facilitate the simultaneous immunolabeling for multiple antigens in one step. However, in the case of 'direct labeling method,' the chemical modifications of each primary antibody are laborious and require a large amount of antibodies, which may damage the antigen-binding activity and stability of primary antibodies. The 'protein A method' is applicable for a variety of IgGs, but it does not sufficiently exclude the possibility that primary antibodies on protein A are replaced by other primary antibodies, which may increase the cross-reactions of the primary antibodies. Additionally, the amount of fluorophore per one molecule of primary antibody cannot be increased significantly over that of conventional methods. The 'anti-IgG or anti-Fc Fab fragment method' requires the preparation of Fab fragments for each animal species and IgG subclass, which is time-consuming and laborious. The signal intensity is also comparable to that of conventional methods [15, 17].

Our group has previously generated a nanocapsule of ~30 nm diameter by expressing the hepatitis B virus surface antigen (HBsAg) L gene in *Saccharomyces cerevisiae* [18]. The nanoparticle (abbreviated later as BNC, bio-nanocapsule) is composed of about 110 molecules of HBsAg L proteins embedded in a liposome. Our collaborators have recently made a derivative of BNC in which the N-terminal region (amino acid residue from 51 to 159) of L protein is replaced with a tandem sequence of the IgG Fc-interacting region (Z domain) derived from protein A [19] and designated it ZZ-BNC (Figure 5.1) [20]. ZZ-BNC displays about 120 molecules of the ZZ-L protein (N-terminally ZZ-fused L protein) on its surface, and can capture ~60 mouse total IgG molecules, as well as displaying all the IgG Fv regions outwardly for effective antigen binding [21]. When ZZ-BNCs were used as a scaffold of antibodies for the immunosensor chip of quartz crystal microbalance (QCM) and surface plasmon resonance (SPR), they markedly improved the sensitivity, antigen-binding capacity, and affinity of the antibodies on the gold surface of immunosensor chip, presumably by the oriented immobilization of the antibodies. Furthermore, in conventional enzyme-linked immunosorbent assays (ELISAs) and western blot analyses, the addition of ZZ-BNCs with secondary antibodies in the aqueous phase enhanced the sensitivities of antigen detection by 10-fold and 50-fold, respectively [22]. These results indicated that ZZ-BNC contributes not only to the clustering of antibodies and labeling molecules, but also to the oriented immobilization of the antibodies.

In this paper I present a study of the capacity of fluorophore-labeled ZZ-BNCs

to enhance the sensitivity and signal intensity of various immunological assays and the possibility of establishing simultaneous immunolabeling methods for multiple antigens.

5.2. Experimental Procedures

5.2.1. BNCs

ZZ-BNCs were overexpressed in *S. cerevisiae* AH22R$^-$ cells carrying the ZZ-BNC-expression plasmid pGLD-ZZ50 [18, 20]. According to the preparation method for BNC [23, 24], ZZ-BNCs were extracted by the disruption with glass beads and purified by affinity chromatography on porcine IgG and gel filtration equipped on an AKTA system (GE Healthcare, Amersham, UK).

5.2.2. Reagents

Cy2-, Cy3-, Cy5-, and Cy7-bis-reactive Dye were from GE Healthcare. Rabbit muscle actin was from Sigma-Aldrich Inc. (Saint Louis, MO, USA). Recombinant human desmin and recombinant human vimentin were from Progen Biotechnik GmbH (Heidelberg, Germany). Tubulin from porcine brain was from Cytoskeleton Inc. (Denver, CO, USA). Cy2- or Cy5-labeled goat-derived anti-mouse IgG were from Jackson ImmunoResearch Laboratories, Inc. (West Grove, PA, USA). Zenon Cy2 mouse IgG2a labeling kit was from Molecular Probes, Inc. (Eugene, OR, USA). The primary antibodies used in this study are listed in Table 5.1. Glutathione-*S* transferase (GST) was expressed in *Escherichia coli* BL21 carrying the GST-expression plasmid pGEX6P-1 (GE Healthcare), and was purified by affinity chromatography on glutathione (GE Healthcare).

5.2.3. Conventional western blot analysis

Each antigen (actin, desmin, GST, vimentin; 0.5–500 ng) was separated by a 0.1% (w/v) sodium dodecyl sulfate-12.5% (w/v) polyacrylamide gel (12.5% SDS-PAGE), and blotted onto an Immobilon-FL polyvinylidene fluoride (PVDF) membrane (Millipore, Billerica, MA, USA). The membrane was blocked with 5% (w/v) skimmed milk (Nacalai Tesque, Kyoto, Japan) in TBST (20 mM Tris-HCl, 140 mM NaCl, 0.05% (v/v) Tween-20, pH 7.4) at room temperature for 30 min, and then incubated at room temperature for 1 h with each primary antibody (anti-actin mouse IgG2a, anti-desmin mouse IgG2a, anti-GST mouse IgG2a, and anti-vimentin mouse IgG2a; 1 μg/mL). These membranes were washed three times with TBST, and incubated with the Cy2-labeled goat-derived anti-mouse IgG (2 μg/mL) secondary antibody at

room temperature for 1 h. After washing three times with TBST, the Cy2-derived fluorescence (emission 506 nm) was visualized under a Typhoon FLA-9000 fluorescence image analyzer (GE Healthcare) equipped with 473-nm laser. In the case of visualization of immunoreactive bands with chemiluminescence, I used Immobilon-P PVDF membrane (Millipore), horseradish peroxidase (HRP)-conjugated rabbit anti-mouse IgG (Sigma-Aldrich), ECL Western blotting detection reagent (GE Healthcare), and a luminescence image analyzer (LAS-4000mini, Fujifilm, Tokyo, Japan).

5.2.4. Western blot analysis using fluorophore-labeled Fab fragments

The western blots were prepared and blocked as described in section 2.3. Each primary antibody (1 μg) was incubated with 5 μL of Zenon labeling reagent (Cy2-labeled anti-mouse IgG2a Fab fragment) at room temperature for 5 min, mixed with 5 μL of Zenon blocking reagent (mouse IgG) at room temperature for 5 min, and then diluted in 1 mL of TBST. The western blots were immersed into the buffer, incubated at room temperature for 1 h, and then washed three times with TBST. The Cy2-labeled bands were visualized under a Typhoon FLA-9000 fluorescence image analyzer.

5.2.5. Western blot analysis using single fluorophore-labeled ZZ-BNCs

The western blots were prepared and blocked as described in section 2.3. For immunolabeling with a single fluorophore, Cy2-labeled ZZ-BNCs (5 μg as protein) were preincubated with each primary antibody (1 μg) in 50 μL of PBS at room temperature for 30 min, and then diluted in 1 mL of TBST. The western blots were immersed into the buffer, incubated at room temperature for 1 h, and then washed three times with TBST. The Cy2-labeled bands were visualized under a Typhoon FLA-9000 fluorescence image analyzer.

5.2.6. Western blot analysis using multiple fluorophore-labeled ZZ-BNCs

To reduce the spontaneous release of IgGs from each Cy-labeled ZZ-BNC/IgG complex, 50 μM of BS^3 (bis-sulfosuccinimidyl suberate) cross-linker (Thermo Fisher Scientific Inc. (Rockford, IL, USA)) was added to each Cy-labeled ZZ-BNC/IgG complex (5 μg of BNC and 1 μg of primary antibody in 50 μL PBS) and incubated at

room temperature for 30 min. To eliminate the unbound IgGs, the complex was passed through 100 μL (50% slurry) of nProtein A Sepharose 4 Fast Flow resin (GE Healthcare), followed by the addition of ZZ-BNC (5 μg as protein). The western blots containing four antigens (GST, actin, tubulin, and desmin) were prepared as described in section 2.3. The membrane was immersed in the mixture of four types of Cy-labeled ZZ-BNC/IgG complexes (Cy2-labeled ZZ-BNC/anti-GST mouse IgG2a, Cy3-labeled ZZ-BNC/anti-actin mouse IgG2a, Cy5-labeled ZZ-BNC/anti-β-tubulin mouse IgG2b, and Cy7-labeled ZZ-BNC/anti-desmin mouse IgG2a), incubated at room temperature for 1 h, and then washed with TBST three times. The following fluorescent signals were visualized separately under a Typhoon FLA-9000 fluorescence image analyzer: Cy2-derived fluorescence (emission 506 nm) by a 473-nm laser, Cy3-derived fluorescence (emission 570 nm) by a 532-nm laser, Cy5-derived fluorescence (emission 670 nm) by a 635-nm laser, and Cy7-derived fluorescence (emission 776 nm) by a 785-nm laser.

5.2.7. Immunocytochemistry

Human breast cancer MDA-MB435 cells (ATCC, HTB-129) (approximately 1 × 10^5 cells) were cultured in 8-well chamber slides (Nalge Nunc International, Rochester, NY, USA) for 24 h, and washed three times with PBS. Cells were then fixed with ice-cold 100% methanol on ice for 10 min, washed three times with PBS, and blocked with blocking buffer (2.5% (w/v) BSA in PBS) at room temperature for 30 min. One μg of each primary antibody (anti-β-tubulin, anti-vimentin, anti-Tom20 (translocase of outer membrane 20), anti-LAMP2 (lysosomal-associated membrane protein 2), and anti-PML (promyelocytic leukemia)) was diluted with 250 μL of blocking buffer, added to each well, incubated at room temperature for 1 h, and then washed three times with PBS. One μg of Cy2-labeled goat-derived anti-mouse IgG and Hoechst 33342 (1:10000 dilution) were diluted with 250 μL of blocking buffer, added to each well, incubated at room temperature for 1 h, and then washed three times with PBS. The fluorescent images were acquired using a FluoView FV1000D confocal laser scanning microscope (Olympus, Tokyo, Japan). Hoechst 33342-derived fluorescence (emission 461 nm) was excited by 457-nm laser, and Cy2-derived fluorescence (emission 506 nm) by a 488-nm laser. For the immunocytochemistry using multiple Cy-labeled ZZ-BNCs, the preparation of multiple Cy-labeled ZZ-BNC/IgG complexes was as described in section 2.5. The Cy3-derived fluorescence (emission 570 nm) was excited by a 543-nm laser, and the Cy5-derived fluorescence (emission 670 nm) by a

633-nm laser.

5.2.8. Flow cytometry

Human epithelial carcinoma A431 cells (Riken, RCB0202) (approximately 1 × 10^6 cells) were incubated in 1 mL blocking buffer on ice for 30 min. The 100 μL aliquot of cell suspension was mixed with 1 μg of each primary antibody (anti-EGFR mouse IgG2a, anti-integrin β1 mouse IgG2a, and mouse total IgG (negative control)), incubated on ice for 30 min, washed three times with blocking buffer, and then mixed with 1 μg of secondary antibody (Cy2-labeled anti-mouse IgG or Cy5-labeled anti-mouse IgG). After incubation on ice for 30 min, the cells were washed three times with blocking buffer, and then subjected to quantitative analysis by using a flow cytometer (BD FACScan Canto II; BD Biosciences, San Jose, CA, USA) with linear amplification for forward/side scatter and logarithmic amplification for Cy2 and Cy5 fluorescence. The Cy2-derived fluorescence (emission 506 nm) was excited by a 488-nm laser and Cy5-derived fluorescence (emission 670 nm) was excited by a 633-nm laser. Acquisition data analysis was performed on 20,000 cells/sample using FACSDiva Software (BD Biosciences).

Table 5.1 Primary antibodies used in this study

Antigen	Species	Manufacturer [a]	Binding affinity to ZZ-BNC (%) [b]
Actin	Mouse IgG2a	Sigma-Aldrich	29
Desmin	Mouse IgG2a	Abnova	29
GST	Mouse IgG2a	Nacalai Tesque	29
Vimentin	Mouse IgG2a	Progen	29
β-tubulin	Mouse IgG2b	Millipore	31
Tom20	Mouse IgG2a	Santa Cruz	29
LAMP2	Mouse IgG2a	Santa Cruz	29
PML	Mouse IgG1	Santa Cruz	6
EGFR	Mouse IgG2a	Katayama	29
Integrin β1	Mouse IgG2a	Santa Cruz	29
	Mouse total IgG	Sigma-Aldrich	100
	Human total IgG	Sigma-Aldrich	80
	Rat total IgG	Sigma-Aldrich	10
	Mouse IgG1	Sigma-Aldrich	6
	Mouse IgG2a	Sigma-Aldrich	29
	Mouse IgG2b	Sigma-Aldrich	31

[a]Sigma-Aldrich, Inc. (Saint Louis, MO, USA); Abnova Corporation (Taipei, Taiwan); Nacalai Tesque, Inc. (Kyoto, Japan); Progen Biotechnik GmbH (Heidelberg, Germany); Millipore Corporation (Bedford, MA, USA); Santa Cruz Biotechnology, Inc. (Santa Cruz, CA, USA); Katayama Chemical Industries Co., Ltd. (Osaka, Japan).

[b]Binding affinity to each antibody was defined as percentage (%) of that of ZZ-BNC to mouse total IgG [21].

5.3. Results and Discussion

5.3.1. Cy-labeled ZZ-BNC/IgG complex for western blot analysis

ZZ-BNC contains ~120 molecules of ZZ-substituted L (ZZ-L) protein as a lipid bilayer-embedding form, and can bind ~60 molecules of mouse total IgGs per single ZZ-BNC (Figure 5.1) [21]. When using the ZZ-BNC in ELISA and immunosensors, as described in the Introduction, ZZ-BNC has shown to improve both sensitivity and antigen binding capacity by clustering antibodies by oriented immobilization [21, 22]. Therefore, I first examined whether the fluorophore-labeled ZZ-BNC could be applicable to enhance the intensity and sensitivity of western blot analysis. ZZ-BNC was labeled with Cy2-, Cy3-, Cy5-, and Cy7-dye using NHS (N-hydroxysuccinimide) chemistry, and the molar ratio of Cy-dye/ZZ-L was estimated at 1–3 by spectrophotometry. Although one ZZ-L protein molecule displays at least 15 primary amine residues derived from 15 Lys residues localized outside of the lipid bilayer, the antibody-binding activity of ZZ-BNC was slightly affected by Cy-dye-conjugation. For example, in the case of Cy5-labled ZZ-BNC, the number of antibodies displayed on the ZZ-BNC was changed from 43 to 28 by Cy5-conjugation.

Then, three fluorophore-labeling techniques, including conventional fluorophore-labeled secondary antibody (Figure 5.2A), the fluorophore-labeled Fab fragment (Figure 5.2B), and the fluorophore-labeled ZZ-BNC (Figure 5.2C), were examined to compare the sensitivity and the signal intensity in western blot analysis using a membrane containing four antigens (actin, desmin, GST, and vimentin; 0.5–500 ng/lane). Both the Cy2-labeled secondary antibody and Cy2-labeled Fab fragment showed comparable levels of sensitivity (*e.g.*, 50 ng in actin, desmin, GST, and vimentin), while prolonged exposure allowed us to detect 5 ng of GST and vimentin. Under the same condition, Cy2-labeled ZZ-BNC showed about 10-fold higher levels of sensitivity for desmin, GST, and vimentin without prolonged exposure (*e.g.*, 5 ng). The signal intensities were also improved by the use of Cy2-labeled ZZ-BNC (*e.g.*, 3.4- and 5.1-fold enhancement in 50 ng of actin and desmin). As demonstrated in our previous study [22], the Cy-labeled ZZ-BNC could cluster antibodies on its surface by oriented immobilization, which may improve the avidity and antigen recognition of antibodies.

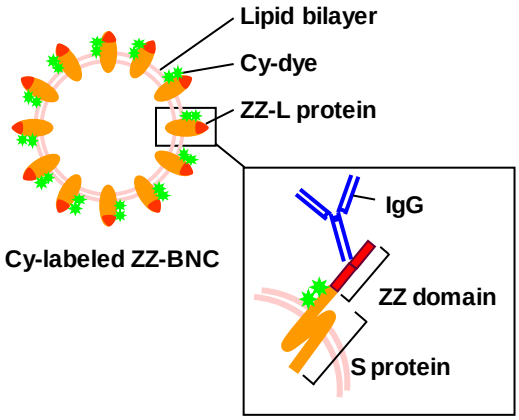

Figure 5.1 Capsular structure of Cy-labeled ZZ-BNC. One ZZ-BNC particle consists of ~120 ZZ-L proteins and a lipid bilayer.

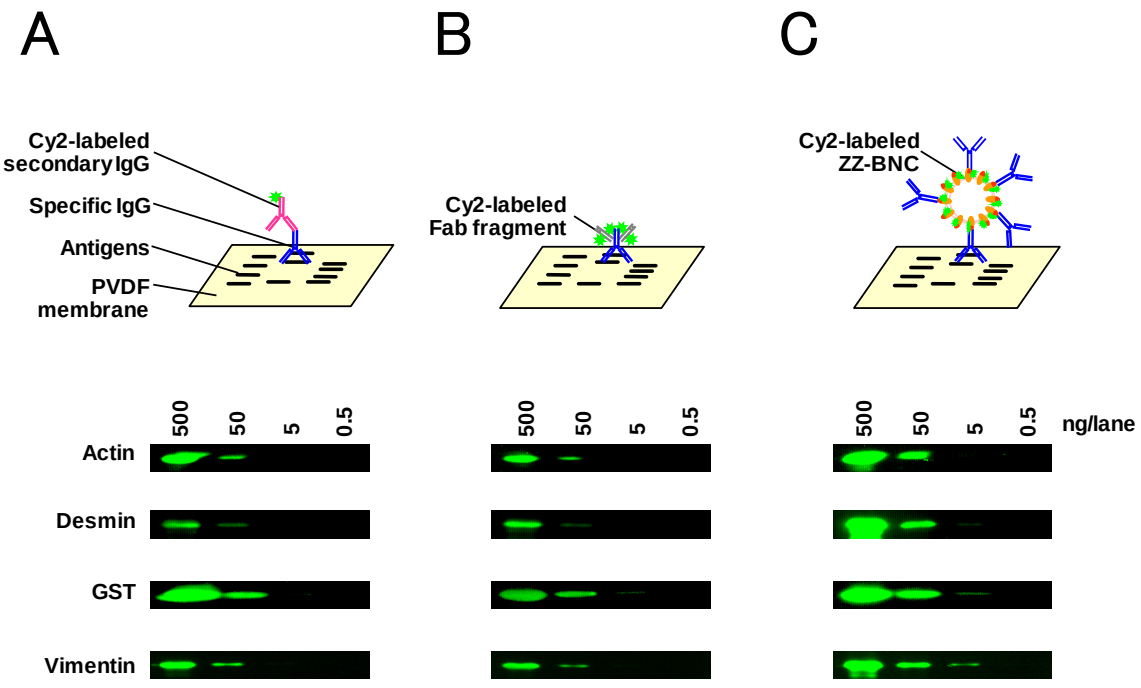

Figure 5.2 Western blot analyses using three distinct fluorophore-labeling methods. (A) Conventional Cy2-labeled secondary antibody, (B) Cy2-labeled Fab fragment, and (C) Cy2-labeled ZZ-BNC/IgG complex. Western blots containing 0.5–500 ng/lane of actin, desmin, GST, and vimentin were used.

5.3.2. Generation of stable ZZ-BNC/IgG complex by crosslinking

When multiple Cy-labeled ZZ-BNC/IgG complexes are used for simultaneous immunolabeling methods, it has not been sufficiently excluded that IgGs on ZZ-BNCs are replaced by other IgGs spontaneously, which may increase the background in immunoassays. I therefore added BS^3 cross-linker (0–1.0 mM) to the mixture of ZZ-BNC (300 ng) and mouse total IgG (300 ng), and examined the degree of crosslinking between IgGs and ZZ-BNCs by western blot analysis. As shown in Figure 5.3A, the immunoreactive bands of ZZ-L protein (lane 1, arrow) and mouse total IgG heavy and light chains (lane 2, arrowheads) were detected at approximately 48-, 50- and 25-kDa, respectively. When ZZ-BNC/IgG complex was incubated with various concentrations of BS^3 for 30 min, smeared bands (>100 kDa, asterisk in lanes 4–7) appeared with increasing BS^3 concentration, indicating that IgGs and ZZ-BNCs form stable complexes when crosslinked with BS^3. Next, I prepared ZZ-BNCs labeled with various Cy dyes (Cy2, Cy3, Cy5, and Cy7), mixed with mouse IgGs against GST, actin, desmin, and β-tubulin, respectively, and subjected them to simultaneous immunolabeling of multiple antigens by western blot analysis (Figure 5.3B). Although non-specific immunoreactive bands (*see* arrowheads in upper panels) were observed in each blot when using a non-crosslinked ZZ-BNC/IgG complex, the specificity of the western blot analysis was significantly improved by 50 μM BS^3-mediated crosslinking (*see* asterisks in lower panels). Based on the results, the optimal concentration of BS^3 was determined at 50 μM for further experiments.

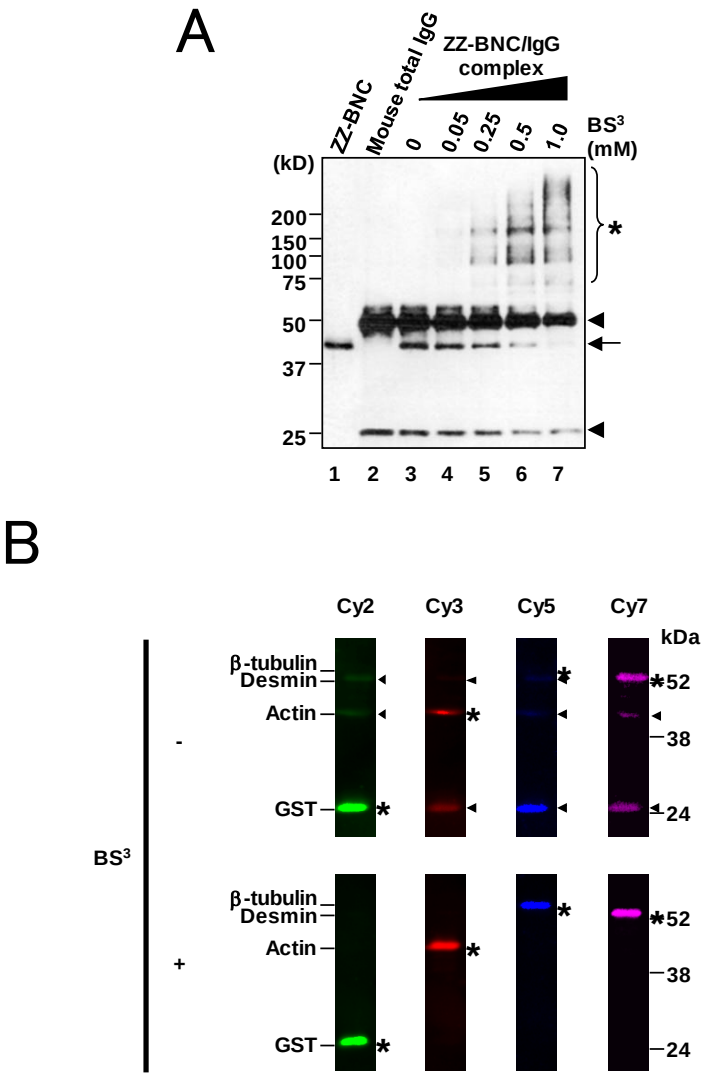

Figure 5.3 Optimization of the crosslinking reaction of the ZZ-BNC/IgG complex. (A) Western blot analysis of ZZ-BNC (lane 1), mouse total IgG (lane 2), ZZ-BNC/IgG complexes with BS^3 (0–1.0 mM, lanes 3–7). ZZ-L protein (arrow), mouse total IgG heavy chain (upper arrowhead), light chains (lower arrowhead), and ZZ-BNC/IgG complex (asterisk) were observed. Molecular sizes (kDa) are indicated in the left margin. The ZZ-L proteins on the blot were visualized with HRP-conjugated anti-mouse IgG. (B) Simultaneous immunolabeling of multiple antigens by various Cy-labeled ZZ-BNC/IgG complexes with (+) or without (-) the crosslinking reaction with BS^3. The blots containing various antigens (GST, actin, β-tubulin, and desmin; each 500 ng/lane) were treated with the mixture of Cy2-labeled ZZ-BNC/mouse anti-GST IgG2a, Cy3-labeled ZZ-BNC/mouse anti-actin IgG2a, Cy5-labeled ZZ-BNC/mouse anti-β-tubulin IgG2b, and Cy7-labeled ZZ-BNC/mouse anti-desmin IgG2a complexes. Specific bands and non-specific bands are shown with asterisks and arrowheads, respectively. Molecular sizes (kDa) are indicated in the right margin.

5.3.3. Evaluation of antibody swapping of ZZ-BNC/IgG complexes

As shown in Figure 5.3B, the combination of ZZ-BNC and BS^3 crosslink reaction facilitated the simultaneous immunolabeling of multiple antigens using antibodies derived from the same animal species. However, the antibodies displayed on ZZ-BNC should not be replaced by free antibodies in an antibody-swapping manner. Thus, I evaluate the incidence of antibody swapping using human epithelial carcinoma A431 cells and anti-EGFR IgG (mouse IgG2a). I first mixed Cy5-labeled ZZ-BNC/anti-EGFR IgG (mouse IgG2a, 20 μg/mL as IgG) complexes with known amounts of non-specific antibodies derived from various animal species (0–160 μg/mL) at room temperature for 30 min, and allowed the mixtures to contact with A431 cells on ice for 30 min (Figure 5.4A). The Cy5-derived fluorescence in A431 cells was measured by a flow cytometer. When using mouse and human total IgG, both exhibited high binding affinity to the ZZ-L protein [21]. The relative fluorescence intensity was decreased to 82% by 40 μg/mL mouse total IgG, presumably by antibody swapping (Figure 5.4B); however, this suddenly increased to 150% by the addition of 80 μg/mL mouse total IgG. The sudden increase of fluorescence intensity was attributed to the aggregation of ZZ-BNCs. The Cy5-labeled ZZ-BNC/anti-EGFR IgG complexes crosslinked with 50 μM BS^3 showed stable fluorescence, even after the addition of 160 μg/mL mouse total IgG. Since one Fc region could interact with two Z domains [19], excess amounts of IgGs might induce crosslinking of ZZ-BNCs. The BS^3 treatment would modify the ZZ-BNC surface to reduce the non-specific binding of IgGs. Likewise, the relative fluorescence intensity was not changed by 80 μg/mL human total IgG, and suddenly increased to 115% by 160 μg/mL human total IgG (Figure 5.4C). The BS^3 treatment enabled the use of 160 μg/mL human total IgG. On the other hand, when using low affinity IgGs to ZZ-BNC (rat total IgG and mouse IgG1) and moderate affinity IgGs to ZZ-BNC (mouse IgG2a and mouse IgG2b), the relative fluorescence intensities did not change significantly by the addition of 160 μg/mL of respective IgG, regardless of BS^3 treatment (Figures 4D-G). Taken together, the results demonstrate that antibody swapping on the ZZ-BNC/IgG complexes could not be observed in a 2-fold excess of free IgGs and was substantially abolished by BS^3 treatment, even in the presence of an 8-fold excess of free IgGs.

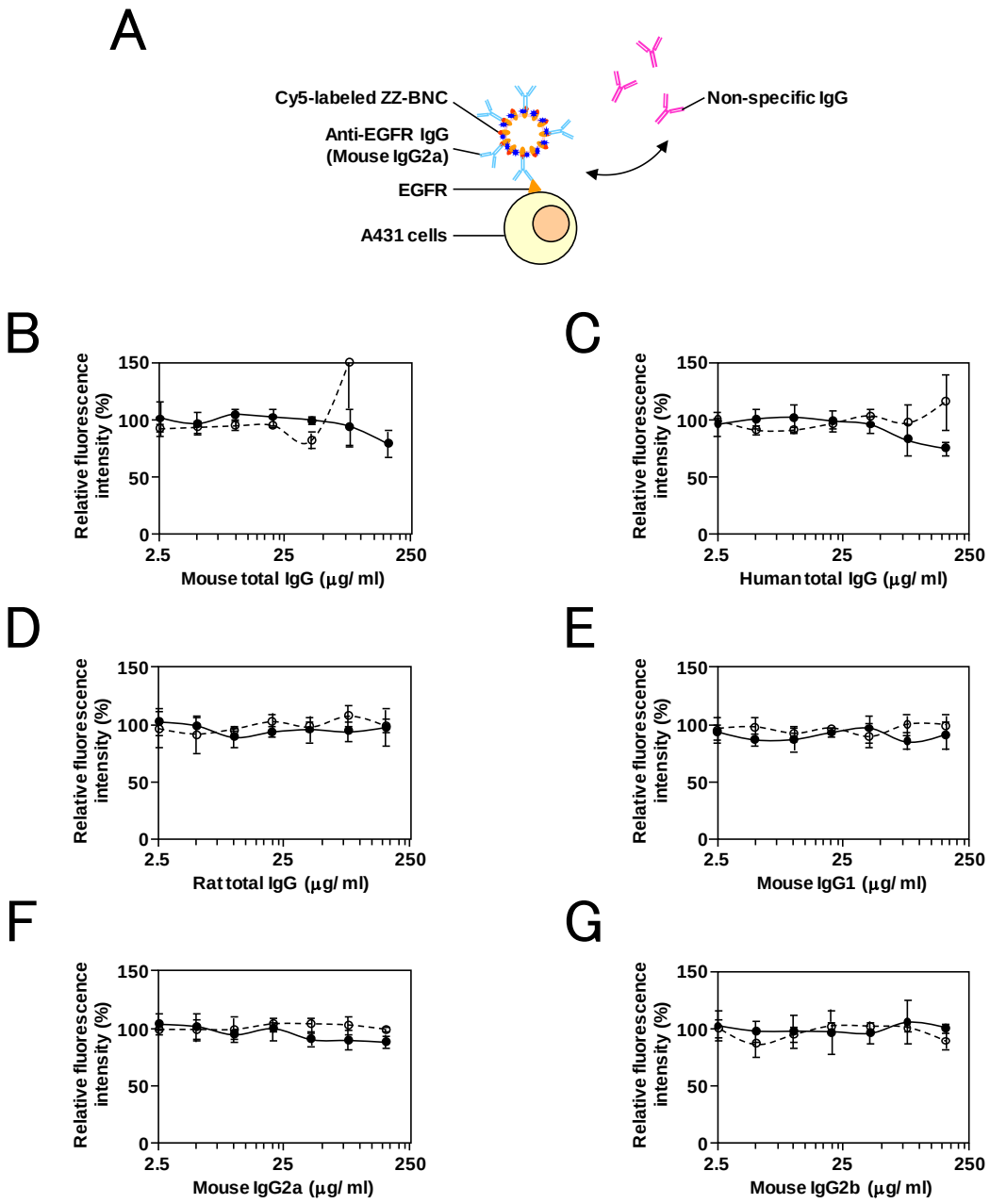

Figure 5.4 Evaluation of antibody swapping of ZZ-BNC/mouse anti-EGFR IgG2a complexes. (A) Schema for the competition assay of Cy5-labeled ZZ-BNC/mouse anti-EGFR IgG2a complexes on A431 cells with non-specific IgGs. (B-G) Relative fluorescence intensities (%) of Cy5-labeled ZZ-BNC/mouse anti-EGFR IgG2a/A431 cells in 2.5–160 μg/mL of various non-specific IgGs ((B) mouse total IgG, (C) human total IgG, (D) rat total IgG, (E) mouse IgG1, (F) mouse IgG2a, and (G) mouse IgG2b). The relative fluorescence intensity of Cy5-labeled ZZ-BNC/mouse anti-EGFR IgG2a/A431 cells in the absence of non-specific IgGs was defined as 100%. The Cy5-labeled ZZ-BNC/mouse anti-EGFR IgG2a complexes were treated with (closed circles) or without (open circles) 50 μM BS^3.

5.3.4. Cy-labeled ZZ-BNC/IgG complexes for simultaneous immunolabeling of multiple antigens in western blot analysis

Simultaneous immunolabeling of multiple antigens (GST, actin, β-tubulin, and desmin) was performed using primary antibodies of the same animal species or the same IgG subclass (mouse anti-GST IgG2a; mouse anti-actin IgG2a; mouse anti-β-tubulin IgG2b; mouse anti-desmin IgG2a) and ZZ-BNCs labeled with multiple Cy dyes (Cy2-, Cy3-, Cy5-, and Cy7-, respectively) in western blot analysis (Figure 5.5A). To reduce the likelihood of antibody swapping of each Cy-labeled ZZ-BNC/IgG complex, each Cy-labeled ZZ-BNC/IgG complex crosslinked with 50 μM of BS^3. The mixture of four Cy-labeled ZZ-BNC/IgG complexes was then subjected to western blotting for multiple antigens. As shown in Figure 5.5B, I succeeded in the simultaneous immunolabeling of four antigens using mouse primary antibodies, with no nonspecific bands.

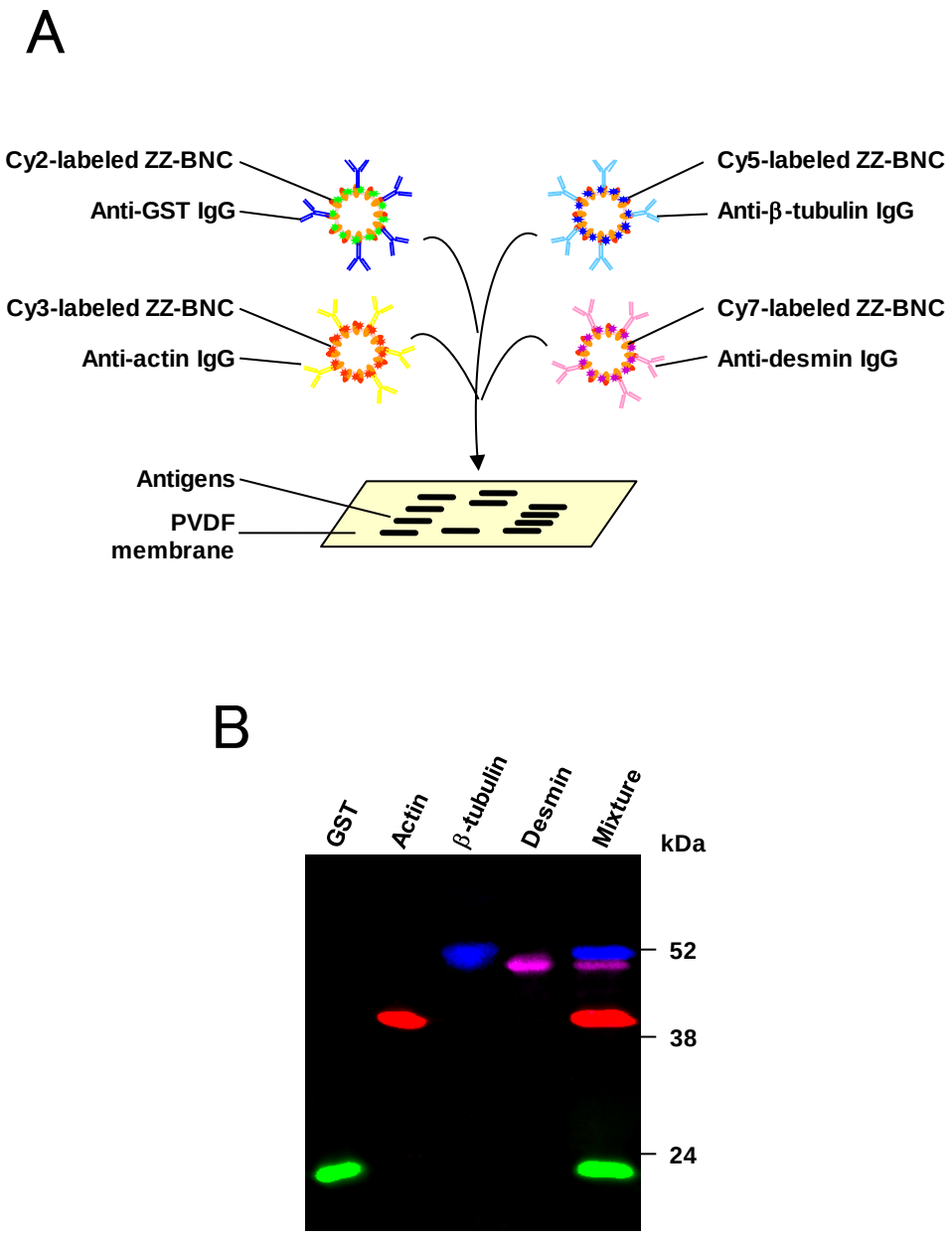

Figure 5.5 Simultaneous immunolabeling of multiple antigens by western blot analysis with various Cy-labeled ZZ-BNC/IgG complexes. (A) Schema for simultaneous detection of GST, actin, β-tubulin, and desmin by the mixture of Cy2-labeled ZZ-BNC/mouse anti-GST IgG2a, Cy3-labeled ZZ-BNC/mouse anti-actin IgG2a, Cy5-labeled ZZ-BNC/mouse anti-β-tubulin IgG2b, and Cy7-labeled ZZ-BNC/mouse anti-desmin IgG2a complexes. (B) Western blot analysis of GST (lane 1, green), actin (lane 2, red), β-tubulin (lane 3, blue), desmin (lane 4, cyan), and mixture (lane 5). Molecular sizes (kDa) are indicated in the right margin.

5.3.5. Cy-labeled ZZ-BNC/IgG complexes for simultaneous immunolabeling of multiple antigens in immunocytochemistry

Simultaneous immunolabeling of multiple antigens by Cy-labeled ZZ-BNCs in western blot analysis led us to examine whether the Cy-labeled ZZ-BNC/IgG complexes are applicable for immunocytochemistry. Cy2-labeled ZZ-BNC was used to detect two cytoskeletal proteins (β-tubulin and vimentin), one mitochondrial protein (Tom20), one endosomal protein (LAMP2), and one nuclear protein (PML) in human breast cancer MDA-MB435 cells. Each primary antibody (mouse anti-β-tubulin IgG2b; mouse anti-vimentin IgG2a; mouse anti-Tom20 IgG2a; mouse anti-LAMP2 IgG2a; mouse anti-PML IgG1) was mixed with Cy2-labeled ZZ-BNC, and then each complex was applied to fixed and permeabilized cells, followed by staining with Hoechst 33342 (Figure 5.6B). As a control, the same antibodies were used for conventional immunocytochemistry using Cy2-labeled anti-mouse IgG secondary antibody (Figure 5.6A). Both methods could visualize the intracellular localizations of cytoskeletal proteins (β-tubulin and vimentin), mitochondrial protein (Tom20), lysosomal protein (LAMP2), and nuclear protein (PML) to a similar extent. Although the ZZ-BNC/IgG complex is ~53 nm in diameter (by dynamic light scattering), the Cy2-labeled ZZ-BNC/IgG complex could pass through the nuclear membrane. Moreover, for the IgG subclass, while mouse IgG1 shows lower affinity to ZZ-BNC than other mouse IgG subclasses (*see* Table 5.1), it is noteworthy that mouse IgG1 can be used for the Cy-labeled ZZ-BNC complex as a primary antibody, without BS^3 treatment. I then examined the applicability of Cy-labeled ZZ-BNCs for simultaneous immunolabeling of multiple antigens in immunocytochemistry (Figure 5.7A). After preparation of Cy2-labeled ZZ-BNC/mouse anti-β-tubulin IgG2b and Cy5-labeled ZZ-BNC/mouse anti-Tom20 IgG2a complexes without BS^3 treatment, both complexes were combined into a single tube, and then added to fixed and permeabilized cells, followed by staining with Hoechst 33342 (Figure 5.7B). The specimen clearly showed the localization of β-tubulin and Tom20 in cells without any non-specific signal.

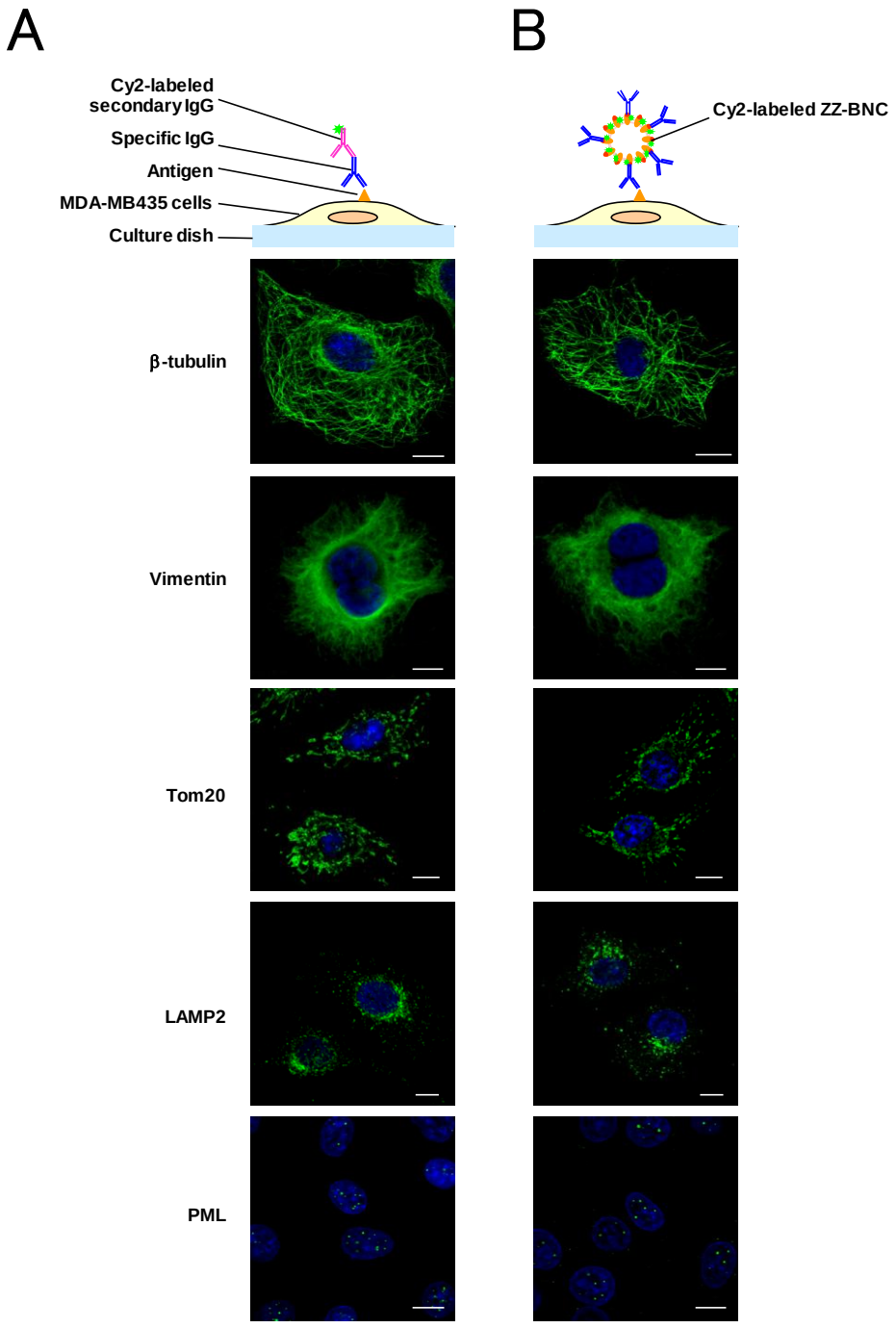

Figure 5.6 Evaluation of each Cy2-labeled ZZ-BNC/IgG complex for immunocytochemistry. (A) Conventional Cy2-labeled secondary antibody method. (B) Cy2-labeled ZZ-BNC/IgG complex method. Schemas for the immunocomplexes formed on MDA-MB435 cells (upper panels). Immunocytochemical images obtained using antibodies against β-tubulin (2nd panels), vimentin (3rd panels), Tom20 (4th panels), LAMP2 (5th panels), and PML (bottom panels). Nuclei were stained with Hoechst 33342. Bars, 10 μm.

A

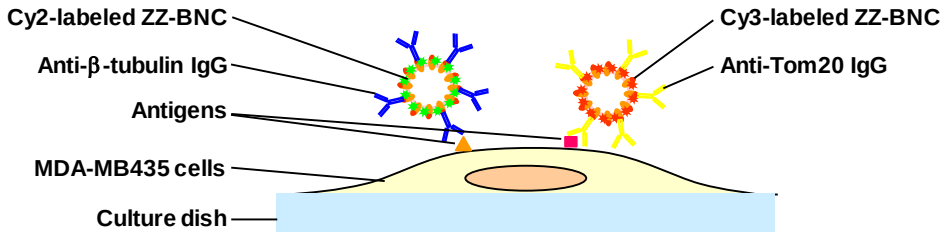

B

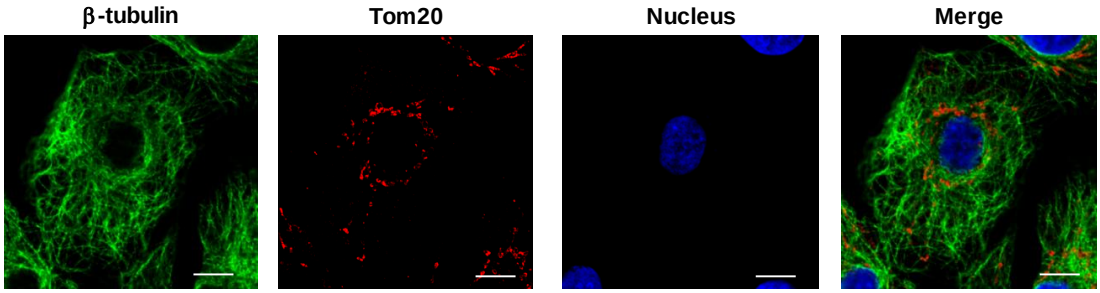

Figure 5.7 Simultaneous immunolabeling of multiple antigens by immunocytochemistry with various Cy-labeled ZZ-BNC/IgG complexes. (A) Schemas for the immunocomplexes of Cy2-labeled ZZ-BNC/mouse anti-β-tubulin IgG2b and Cy3-labeled ZZ-BNC/mouse anti-Tom20 IgG2a formed on MDA-MB435 cells. (B) Immunocytochemical images obtained by using antibodies against β-tubulin (green) and Tom20 (red). Nuclei were stained with Hoechst 33342. Bars, 10 μm.

5.3.6. Cy-labeled ZZ-BNC/IgG complexes for simultaneous immunolabeling of multiple antigens in flow cytometric analysis

The potential for multiple immunolabeling with Cy-labeled ZZ-BNC/IgG complexes was investigated in the context of flow cytometry. As described in Figure 5.4, the Cy5-labeled ZZ-BNC/IgG complex could work in flow cytometry. The expressions of EGFR and integrin β1 on the surface of A431 cells were measured by mouse anti-EGFR IgG2a and mouse anti-integrin β1 IgG2a, respectively, using a flow cytometric analysis (Figure 5.8A). After trypsinization, A431 cells were contacted with either Cy2-labeled ZZ-BNC/anti-EGFR antibody or Cy5-labeled ZZ-BNC/anti-integrin β1 antibody, and then analyzed with a flow cytometer (Figure 5.8B and C, dark areas). The fluorescent intensity was comparable to that of the conventional method (Figure 5.8A, left panel; Figure 5.8B and C, light areas). When applying both Cy-labeled ZZ-BNC/IgG complexes (Figure 5.8A, right panel), each fluorescent-intensity was obtained without signal attenuation (Figure 5.8D). Moreover, each Cy-labeled ZZ-BNC/IgG complex was observed at the cell surface under confocal laser scanning microscope (Figure 5.8E), strongly suggesting that the complexes bound to specific antigens.

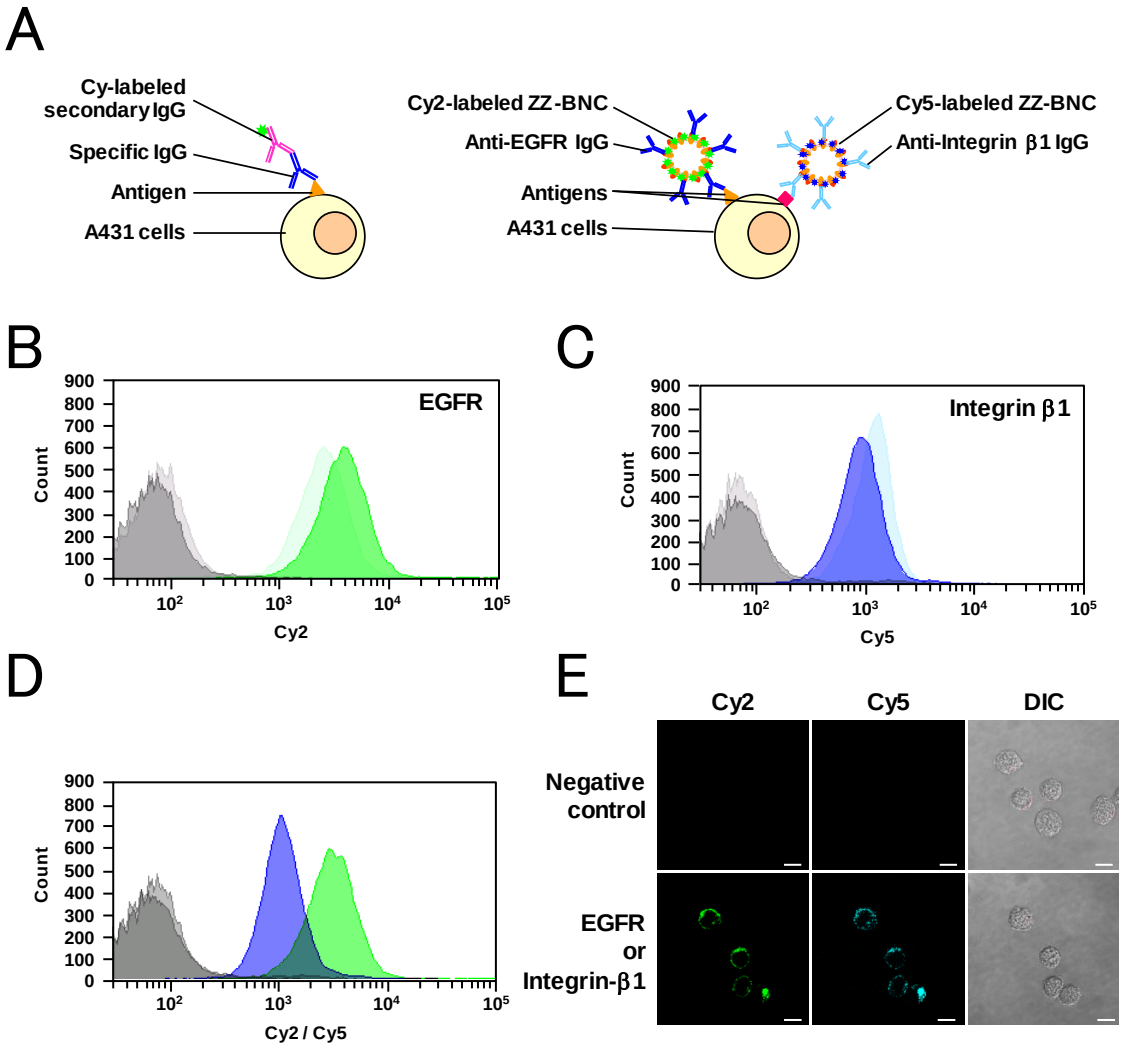

Figure 5.8 Flow cytometric analyses using various Cy-labeled ZZ-BNC/IgG complexes. (A) Schemas for the immunocomplexes formed on A431 cells. Conventional Cy-labeled secondary antibodies (left panel), and Cy-labeled ZZ-BNC/IgG complexes (right panel). (B) Flow cytometric analysis of EGFR on A431 cells. Histogram plots of expression levels of EGFR obtained with mouse anti-EGFR IgG2a in combination with Cy2-labeled secondary antibody (light green) and Cy2-labeled ZZ-BNC/IgG complex (dark green). Negative controls were obtained with mouse total IgG in combination with Cy2-labeled secondary antibody (light gray) and Cy2-labeled ZZ-BNC/IgG complex (dark gray). (C) Flow cytometric analysis of integrin β1 on A431 cells. Histogram plots of expression levels of integrin β1 obtained with mouse anti-integrin β1 IgG2a in combination with Cy5-labeled secondary antibody (light blue) and Cy5-labeled ZZ-BNC/IgG complex (dark blue). Negative controls were obtained with mouse total IgG in combination with Cy5-labeled secondary antibody (light gray) and Cy5-labeled ZZ-BNC/IgG complex (dark gray). (D) Simultaneous flow cytometric analysis of EGFR and integrin β1 on A431 cells. Histogram plots of expression levels of EGFR and integrin β1

obtained with Cy2-labeled ZZ-BNC/mouse anti-EGFR IgG2a (dark green) and Cy5-labeled ZZ-BNC/mouse anti-integrin β1 IgG2a (dark blue) complexes. Negative controls were obtained with Cy2-labeled ZZ-BNC/mouse total IgG (light gray) and Cy5-labeled ZZ-BNC/mouse total IgG (dark gray) complexes. (E) Immunocytochemical and differential interference constant images (DIC) of A431 cells stained with Cy2-labeled ZZ-BNC/mouse anti-EGFR IgG2a (green) and Cy5-labeled ZZ-BNC/mouse anti-integrin β1 IgG2a (blue) complexes. Both Cy2-labeled ZZ-BNC/mouse total IgG and Cy5-labeled ZZ-BNC/mouse total IgG complexes were used as negative controls. Bars, 10 μm.

5.3.7. Significance of Cy-labeled ZZ-BNC/IgG complexes as biomaterials

When the Cy-labeled ZZ-BNCs are compared with the fluorophore-labeled Fab fragments (also known as Zenon labeling reagent) [15], our method requires only ZZ-BNCs labeled with various fluorescent dyes. However, the Zenon method requires many kinds of Fab fragments specific to Fc regions (dependent on animal species and IgG subclass), which must be labeled with various fluorescent dyes, requiring many more reagents than the ZZ-BNC method. Additionally, a ZZ-BNC could function as a scaffold for oriented immobilization of antibodies [21], resulting in enhanced sensitivity and antigen binding capacity. Recently, several types of nanoparticles have been introduced as bio-imaging probes with higher stability and stronger fluorescence intensity, such as semiconductor nanoparticles (quantum dots) [25], silica spheres [26], and lipidic nanoparticles [27]. However, it has been difficult to control the direction of bio-recognition molecules (especially, antibodies) on their surfaces. If these nanoparticles are incorporated into ZZ-BNCs by liposomal fusion, as described previously [28], these ZZ-BNC-coated nanoparticles, including the fluorophore-labeled ZZ-BNCs, become promising bio-imaging probes for immunofluorescence techniques, facilitating both oriented immobilization of antibodies and simultaneous immunolabeling of multiple antigens.

Because hepatitis B virus infects with human liver cells specifically, our group previously developed BNC (*i.e.*, HBsAg L particle) as a novel carrier for the *in vivo* pinpoint delivery of genes and drugs [29]. BNCs efficiently deliver encapsulated materials to tissues derived from the human liver *in vivo* by exploiting the infection mechanism of hepatitis B virus. These data strongly suggested that Cy-labeled ZZ-BNC/IgG complexes function as bio-imaging probes applicable not only *in vitro* but also *in vivo*.

5.3.8. Conclusions

This study demonstrated that a series of Cy-labeled ZZ-BNCs improves both the sensitivity and signal intensity of western blot analysis, presumably by oriented immobilization of the antibodies. Where the available antibodies are derived from the same animal species, the Cy-labeled ZZ-BNCs enable the simultaneous immunolabeling of multiple antigens in western blot analysis, immunocytochemistry, and flow cytometric analysis.

5.4. References

1. Tidman N, Janossy G, Bodger M, Granger S, Kung PC, Goldstein G. Delineation of human thymocyte differentiation pathways utilizing double-staining techniques with monoclonal antibodies. Clin Exp Immunol 1981;45:457–467.
2. Falini B, Abdulaziz Z, Gerdes J, Canino S, Ciani C, Cordell JL, et al. Description of a sequential staining procedure for double immunoenzymatic staining of pairs of antigens using monoclonal antibodies. J Immunol Methods 1986;93:265–273.
3. Lan HY, Mu W, NG YY, Nikolic-Paterson DJ, Atkins RC. A simple, reliable, and sensitive method for nonradioactive in situ hybridization: use of microwave heating to improve hybridization efficiency and preserve tissue morphology. J Histochem Cytochem 1996;44:281–287.
4. Tornehave D, Hougaard DM, Larsson L. Microwaving for double indirect immunofluorescence with primary antibodies from the same species and for staining of mouse tissues with mouse monoclonal antibodies. Histochem Cell Biol 2000;113:19–23.
5. Pirici D, Mogoanta L, Kumar-Singh S, Pirici I, Margaritescu C, Simionescu C, et al. Antibody elution method for multiple immunohistochemistry on primary antibodies raised in the same species and of the same subtype. J Histochem Cytochem 2009;57:567–575.
6. Shindler KS, Roth KA. Double immunofluorescent staining using two unconjugated primary antisera raised in the same species. J Histochem Cytochem 1996;44:1331–1335.
7. Lewis Carl SA, Gillete-Ferguson I, Ferguson DG. An indirect immunofluorescence procedure for staining the same cryosection with two mouse monoclonal primary antibodies. J Histochem Cytochem 1993;41:1273–1278.
8. Franzusoff A, Redding K, Crosby J, Fuller RS, Schekman R. Localization of components involved in protein transport and processing through the yeast Golgi apparatus. J Cell Biol 1991;112:27–37.
9. Wessel GM, McClay DR. Two embryonic, tissue-specific molecules identified by a double-label immunofluorescence technique for monoclonal antibodies. J Histochem Cytochem 1986;34:703–706.
10. Negoescu A, Labat-Moleur F, Lorimier P, Lamarcq L, Guillermet C, Chambaz E, et al. F(ab) secondary antibodies: a general method for double immunolabeling with primary antisera from the same species. Efficiency control by chemiluminescence. J Histochem Cytochem 1994;42:433–437.

11. Owen GR, Häkkinen L, Wu C, Larjava H. A reproducible technique for specific labeling of antigens using preformed fluorescent molecular IgG-F(ab')2 complexes from primary antibodies of the same species. Microsc Res Tech 2010;73:623–630.
12. Boorsma DM. Direct immunoenzyme double staining applicable for monoclonal antibodies. Histochemistry 1984;80:103–106.
13. Tsurui H, Nishimura H, Hattori S, Hirose S, Okumura K, Shirai T. Seven-color fluorescence imaging of tissue samples based on Fourier spectroscopy and singular value decomposition. J Histochem Cytochem 2000;48:653–662.
14. Morris TJ, Stanley EF. A simple method for immunocytochemical staining with multiple rabbit polyclonal antibodies. J Neurosci Methods 2003;127:149–155.
15. Bradford JA, Buller G, Suter M, Ignatius M, Beechem JM. Fluorescence-intensity multiplexing: simultaneous seven-marker, two-color immunophenotyping using flow cytometry. Cytometry A 2004;61:142–152.
16. Brown JK, Pemberton AD, Wright SH, Miller HR. Primary antibody-Fab fragment complexes: a flexible alternative to traditional direct and indirect immunolabeling techniques. J Histochem Cytochem 2004;52:1219–1230.
17. Tang X, He J, Partin J, Vafai A. Comparative analysis of direct fluorescence, Zenon labeling, and quantum dot nanocrystal technology in immunofluorescence staining. J Immunoassay Immunochem 2010;31:250–257.
18. Kuroda S, Otaka S, Miyazaki T, Nakao M, Fujisawa Y. Hepatitis B virus envelope L protein particles. Synthesis and assembly in Saccharomyces cerevisiae, purification and characterization. J Biol Chem 1992;267:1953–1961.
19. Nilsson B, Moks T, Jansson B, Abrahmsén L, Elmblad A, Holmgren E, et al. A synthetic IgG-binding domain based on staphylococcal protein A. Protein Eng 1987;1:107–113.
20. Kurata N, Shishido T, Muraoka M, Tanaka T, Ogino C, Fukuda H, Kondo A. Specific protein delivery to target cells by antibody-displaying bionanocapsules. J Biochem 2008;144:701–707.
21. Iijima M, Kadoya H, Hatahira S, Hiramatsu S, Jung G, Martin A, et al. Nanocapsules incorporating IgG Fc-binding domain derived from Staphylococcus aureus protein A for displaying IgGs on immunosensor chips. Biomaterials 2011;32:1455–1464.
22. Iijima M, Matsuzaki T, Kadoya H, Hatahira S, Hiramatsu S, Jung G, et al. Bionanocapsule-based enzyme-antibody conjugates for enzyme-linked immunosorbent assay. Anal Biochem 2010;396:257–261.
23. Yamada T, Iwabuki H, Kanno T, Tanaka H, Kawai T, Fukuda H, et al.

Physicochemical and immunological characterization of hepatitis B virus envelope particles exclusively consisting of the entire L (pre-S1 + pre-S2 + S) protein. Vaccine 2001;19:3154–3163.

24. Jung J, Iijima M, Yoshimoto N, Sasaki M, Niimi T, Tatematsu K, et al. Efficient and rapid purification of drug- and gene-carrying bio-nanocapsules, hepatitis B virus surface antigen L particles, from Saccharomyces cerevisiae. Protein Expression and Purification 2011;78:149–155.
25. Medintz IL, Uyeda HT, Goldman ER, Mattoussi H. Quantum dot bioconjugates for imaging, labelling and sensing. Nat Mater 2005;4:435–446.
26. van Blaaderen A, Vrij A. Synthesis and characterization of colloidal dispersions of fluorescent, monodisperse silica spheres. Langmuir 1992;8:2921–2931.
27. Mulder WJ, Strijkers GJ, van Tilborg GA, Cormode DP, Fayad ZA, Nicolay K. Nanoparticulate assemblies of amphiphiles and diagnostically active materials for multimodality imaging. Acc Chem Res 2009;42:904–914.
28. Jung J, Matsuzaki T, Tatematsu K, Okajima T, Tanizawa K, Kuroda S. Bio-nanocapsule conjugated with liposomes for in vivo pinpoint delivery of various materials. J Control Release 2008;126:255–264.
29. Yamada T, Iwasaki Y, Tada H, Iwabuki H, Chuah MKL, VandenDriessche T, et al. Nanoparticles for the delivery of genes and drugs to human hepatocytes. Nat Biotech 2003;21:885–890.

Chapter VI

6.1. Comprehensive Discussion

Several strategies have been reported to improve the sensitivity, antigen-binding capacity and specificity of immunoassay systems by introducing the oriented immobilization of antibodies to bio-sensing probes. However, conventional strategies (*e.g.*, chemical crosslinking without any control of orientation through single or mixed self-assembled monolayers (SAMs), an immunoglobulin G Fc-interacting protein A or G, a biotin/(strept)avidin complex, or synthetic polymers) [1, 2] have still harbored potential problems as described in the Introduction of Chapter IV. Therefore, the aim of this study is to develop new strategies accomplishing the completely oriented immobilization of antibodies without affecting the function of antibodies. On the other hand, our groups have developed a hollow nanocapsule consisting hepatitis B virus surface antigen L protein (known as BNC, bio-nanocapsule) as a new drug delivery system (DDS) carrier. In the course of the improvement of BNC, we generated BNC displaying the ZZ domain (IgG Fc-binding region) derived *Staphylococcus aureus* protein A (known as ZZ-BNC) for the antibody-dependent pinpoint DDS. These situations led me to investigate if ZZ-BNC could be a scaffold for the completely oriented immobilization of antibodies in bio-sensing probes.

Since the availability of BNC has so far been limited due to the inefficiency of purification process, as described in Chapter II, I have established the new purification process for BNCs, which utilized heat treatment and affinity chromatography. Especially, I found that heat treatment at 70°C at pH 7.4 for 20 min completely inactivated the yeast proteinases resided in the crude extract (see Figures 2.1 and 2.4). Consequently, both yield and purity of BNCs have been significantly improved and the time required for whole purification process has been shortened from 1 week to 2 days. Furthermore, lyophilization with sucrose was found to preserve the function of BNC at 4°C for at least 14 months. Thus, these improvements have broadened the versatility of BNC in the biomaterial field.

In Chapter III, I demonstrated that ZZ-BNC could assemble antibodies on their surface even without chemical modification. Then, ZZ-BNC could enhance the signals in the detection of antigens and antibodies through the formation of ZZ-BNC-antibody complex when added to the aqueous phase of conventional ELISA and Western blot analysis. Combination of the avidin-biotin complex (ABC) system and biotinylated ZZ-BNC significantly improved the sensitivity of conventional ELISA and Western blot

analysis. ZZ-BNC was postulated to tether the Fc regions of IgG on the ZZ domain so that all the Fv regions are displayed outwards for effective formation of immunocomplexes. Since our group previously reported that BNC (including ZZ-BNC) can incorporate various materials by electroporation [3] and liposome fusion [4], ZZ-BNC might be applicable for the immunoassays utilizing various labeling molecules (*e.g.*, fluorophores, radioisotopes, quantum dots, chromophores).

Our group previously reported that BNCs could adsorb onto a mica surface without the disruption of its particle structure [5]. In Chapter IV, I tried to utilize ZZ-BNC as a scaffold of antibodies for immunosensors, and demonstrated that ZZ-BNC enhanced the sensitivities and antigen-binding capacities on the immunosensor chips by the oriented immobilization of antibodies. ZZ-BNC could associate firmly not only mica and gold but also with glass and plastics (unpublished results). The extraordinarily high stability of ZZ-BNC-bound chips makes them an ideal bio-sensing probe applicable for various immunosensing technologies, including QCM and SPR, but also surface acoustic wave (SAW) [6], laser nephelometry [7], fluorescence anisotropy [8] and immunologically modified field effect transistors (ImmunoFET) [9].

Finally, to expand the applications of ZZ-BNC in immunofluorescence techniques, in Chapter V, I prepared various types of fluorophore-labeled ZZ-BNC as bio-imaging probes. As described in Chapter IV, I found the improvement of sensitivity and antigen-binding capacity of antibodies by conjugating with ZZ-BNC fluorophore-labeled ZZ-BNCs, and established the simultaneous immunolabeling methods for multiple antigens. Where the available antibodies are derived from the same animal species, the fluorophore-labeled ZZ-BNCs enable the simultaneous immunolabeling of multiple antigens in western blot analysis, immunocytochemistry, and flow cytometric analysis. These data strongly suggested that the fluorophore-labeled ZZ-BNC/IgG complexes function as bio-imaging probes applicable not only *in vitro* but also *in vivo*.

In conclusion, I demonstrated that ZZ-BNC is an ideal scaffold for the oriented immobilization of antibodies in the bio-sensing probes. Although the interaction of biomolecules is not only antigen-antibody but also ligand-receptor [10], lectin-sugar chain [11], DNA-nucleotide binding protein [12], and so on. Recently, biosensors [13, 14] have been utilized to detect these specific interactions, which are very important to maintain the biological activity in the fields of food analysis [15], bioterrorism [16, 17], environmental survey [16-18] and in the area of human health monitoring and diagnostics [19, 20]. In the near future, ZZ-BNC could display various biomolecules (e.g., antibodies, ligands, lectins, DNAs) by using the IgG-Fc-fusion technique [21] in

an oriented immobilization manner, which would facilitate the development of new bio-sensors and new applications for these fields.

6.2. References

1. Lu B, Smyth MR, O'Kennedy R. Oriented immobilization of antibodies and its applications in immunoassays and immunosensors. Analyst 1996;121:29R–32R.
2. Rao SV, Anderson KW, Bachas LG. Oriented immobilization of proteins. Mikrochim Acta 1998;128:127–143.
3. Yamada T, Iwasaki Y, Tada H, Iwabuki H, Chuah MKL, VandenDriessche T, Fukuda H, Kondo A, Ueda M, Seno M, Tanizawa K, Kuroda S. Nanoparticles for the delivery of genes and drugs to human hepatocytes. Nat Biotechnol 2003;21:885–890.
4. Jung J, Matsuzaki T, Tatematsu K, Okajima T, Tanizawa K, Kuroda S. Bio-nanocapsule conjugated with liposomes for *in vivo* pinpoint delivery of various materials. J Control Release 2008;126:55–264.
5. Kanno T, Yamada T, Iwabuki H, Tanaka H, Kuroda S, Tanizawa K, Kawai T. Size distribution measurement of vesicles by atomic force microscopy. Anal Biochem 2002;309:196–199.
6. Gizeli E, Lowe CR. Immunosensors. Curr Opin Biotechnol 1996;7:66–71.
7. Whicher JT, Price CP, Spencer K. Immunonephelometric and immunoturbidimetric assays for proteins. Crit Rev Clin Lab Sci 1983;18:213–260.
8. Baldini F, Carloni A, Giannetti A, Porro G, Trono C. A new optical platform for biosensing based on fluorescence anisotropy. Anal Bioanal Chem 2008;391:1837–1844.
9. Eteshola E, Keener MT, Elias M, Shapiro J, Brillson LJ, Bhushan B, et al. Engineering functional protein ingerfaces for immunologically modified field effect transistor (ImmunoFET) by molecular genetic means. J R Soc Interface 2008;5:123–127
10. Loetscher H, Pan YC, Lahm HW, Gentz R, Brockhaus M, Tabuchi H, Lesslauer W. Molecular cloning and expression of the human 55 kd tumor necrosis factor receptor. Cell 1990;61:351–359.
11. Horejsí V, Tichá M, Kocourek J. Studies on lectins. XXXI. Determination of dissociation constants of lectin. Sugar complexes by means of affinity electrophoresis. Biochim Biophys Acta 1977;499:290–300.
12. Bickle TA, Krüger DH. Biology of DNA restriction. Microbiol Rev 1993;57:434–450.

13. Prieto-Simín B, Campàs M, Marty JL. Biomolecule immobilization in biosensor development: tailored strategies based on affinity interactions. Protein Pept Lett 2008;15:757–763.
14. Arlett JL, Myers EB, Roukes ML. Comparative advantages of mechanical biosensors. Nat Nanotechnol 2011;6:203–215.
15. Eden-Firstenberg R, Schaertel BJ. Biosensor in the food industry: Present and Future. J Food Prot 1988;51:811–820.
16. Lindner D. Profile: The μChemLabTM project: micro total analysis system R&D at Sandia National Laboratories. Lab Chip 2001;1:15N–20N.
17. Burkle FM. Measures of effectiveness in large scale bioterrorism events. Prehosp Disaster Med 2003;18:258–262.
18. Maseini M. Affinity electrochemical biosensors for pollution control. Pure Appl Chem 2001;73:23–30.
19. Malhotra BD, Chaube A. Biosensors for clinical diagnostics industry. Sens Actuators B Chem 2003;91:117–126.
20. Anjum V, Pundir CS. Biosensors: Future analytical tools. Sensors and Transducers 2007;76:937–944.
21. Brown SJ, Becherer KA, Blumeyer K, Kautzer C, Axelrod F, Le H, McConnell SJ, Whalley A, Spinella DG. Expression and ligand binding assays of soluble cytokine receptor-immunoglobulin fusion proteins. Protein Expr Purif 1998;14:120–124.

Acknowledgments

This is a thesis to be submitted to the Graduate School of Bioagricultural Science, Nagoya University for the Ph.D. of agriculture. The works described in this thesis have been performed under the directions of Prof. Shun'ichi Kuroda at the Department of Structural Molecular Biology, the Institute of Scientific and Industrial Research, Osaka University (from 2007 to 2009) and the Laboratory of Industrial Bioscience, Division of Biotechnology, Department of Bioengineering Sciences, the Graduate School of Bioagricultural Science, Nagoya University (from 2009 to 2011).

First of all, my deepest and heartfelt appreciation goes to Prof. Shun'ichi Kuroda whose comments and suggestions were innumerably valuable throughout the course of my study. I am grateful to Prof. Katsuyuki Tanizawa for his valuable advices and warm encouragements. I would like to acknowledge Prof. Tohru Yoshimura, Prof. Hideo Nakano and Assistant Prof. Tomoaki Niimi whose comments made enormous contributions toward my work, Assistant Prof. Takashi Matsuzaki for giving his valuable suggestions to my work, Dr. Joohee Jung, Dr. Hiroyasu Kadoya, Dr. Takeshi Kasuya and Ms. Yoko Matsushita for their technical supports and warm encouragements, Prof. Takeshi Arakawa at University of the Ryukyus for providing antigens and antibodies of $MSP1_{19}$, Dr. Giman Jung, Mr. Shingo Hiramatsu and Ms. Satoko Hatahira at Toray Industries, Inc., Dr. Aaron Martin and Dr. John Quinn at ICx Nomadics for their collaboration and helpful advice, and As One Corporation, Tanaka Kikinzoku Kogyo K.K. and KOBELCO Research Institute, Inc. for their technical supports. I sincerely express my thanks to all member of Prof. Kuroda's laboratory.

Finally, I would also like to express my gratitude to my family for their mental supports and warm encouragements.

List of Publications

Original papers

1. **Iijima M**, Matsuzaki T, Kadoya H, Hatahira S, Hiramatsu S, Jung G, Tanizawa K, Kuroda S. Bionanocapsule-based enzyme-antibody conjugates for enzyme-linked immunosorbent assay. *Anal Biochem* 2010;396:257–261. (M.I. performed all experiments and prepared the entire manuscript)

2. **Iijima M**, Kadoya H, Hatahira T, Hiramatsu S, Jung, G., Martin A, Quinn J, Jeong SY, Choi EK, Arakawa T, Hinako F, Kusunoki M, Yoshimoto N, Niimi T, Tanizawa T, Kuroda S. Nanocapsules incorporating IgG Fc-binding domain derived from *Staphylococcus aureus* protein-A for displaying IgGs on immunosensor chips. *Biomaterials* 2011;32:1455–1464. (M.I. performed all experiments and prepared the entire manuscript)

3. Jung J, **Iijima M**, Yoshimoto N, Sasaki M, Niimi T, Tatematsu K, Jeong SY, Choi EK, Tanizawa K, Kuroda S. Efficient and rapid purification of drug- and gene-carrying bio-nanocapsules, hepatitis B virus surface antigen L particles, from *Saccharomyces cerevisiae*. *Protein Expression and Purification* 2011;78:149–155. (M.I. performed a part of the experiment and prepared most of the manuscript)

4. **Iijima M**, Matsuzaki T, Yoshimoto N, Niimi T, Tanizawa K, Kuroda S. Fluorophore-labeled nanocapsules displaying IgG Fc-binding domains for the simultaneous detection of multiple antigens. *Biomaterials in press.* (DOI: 10.1016/j.biomaterials.2011.08.012) (M.I. performed all experiments and prepared the entire manuscript)

Reference

1. Kasuya T, Jung J, Kinoshita R, Goh Y, Matsuzaki T, **Iijima M**, Yoshimoto N, Tanizawa K, Kuroda S. Chapter 8 - Bio-nanocapsule-liposome conjugates for *in vivo* pinpoint drug and gene delivery. *Methods in Enzymology* 2009;464:147–166. (M.I. performed a part of the experiment)

International and Domestic Meetings

Presentations at international conferences (*Speaker)

1. ***Iijima M**, Matsuzaki T, Tanizawa K, Kuroda S. Protein A-derived ZZ domain-displaying bio-nanocapsules for drug and gene delivery systems and hypersensitive immunoassay systems: determination of IgG-binding capacity. *4th Handai Nanoscience and Nanotechnology International Symposium*, 2008, September 29–October 1, Osaka, Japan.

2. ***Iijima M**, Kuroda S. Efficiently oriented display of antibodies in immunoassay systems. *International Workshop on Nanomedicine, Geneva University*, 2010, June 1, Geneva, Switzerland.

3. ***Iijima M**, and Kuroda S. Bio-nanocapsules for oriented immobilization of IgGs on immunosensor chips. *5th European Conference of the International Federation for Medical and Biological Engineering*, 2011, September 14–18, Budapest, Hungary.

Presentations at domestic meetings (*Speaker)

1. ***Iijima M**, Jung J, Matsuzaki T, Okajima T, Kondo A, Kuroda S, Tanizawa K. Qualitative and quantitative analyses of antibody-binding ability of bio-nanocapsule displaying ZZ-tag. *The 30th Annual Meeting of the Molecular Biology Society of Japan*, 2007, December 11–15, Yokohama.

2. ***Iijima M**, Matsuzaki T, Tanizawa K, Kuroda S. Characterization analysis of bio-nanocapsule displaying antibodies. *The 24th Annual Conference of The Japan Drug Delivery System Research Society*, 2008, June 29–30, Tokyo.

3. ***Iijima M,** Matsuzaki T, Tanizawa K, Kuroda S. Bio-imaging technique for simultaneous detection of multiple antigens using ZZ tag-displaying bio-nanocapsule. *The 32nd Annual Meeting of the Molecular Biology Society of Japan*, 2009, December 9–12, Yokohama.

4. ***Iijima M.**, Tanizawa K, Kuroda S. Bio-nanocapsules for effective oriented immobilization of antibodies. *The 8th Annual Meeting of Society of Nano Science and Technology*, 2010, May 13–15, Okazaki.

5. ***Iijima M.**, Kuroda S. Bio-nanocapsules for efficiently oriented immobilization of antibodies. *62th Annual Meeting of the Society for Biotechnology, Japan*, 2010, October 27–29, Miyazaki.

6. ***Iijima M.**, Kuroda S. Bio-nanocapsules for efficiently oriented immobilization of antibodies. *Nagoya University Women Faculty & Students Science forum*, 2010, November 13, Nagoya.

7. *__Iijima M.__, Kuroda S. Improvement of biosensors by using new scaffold for oriented antibody immobilization (bio-nanocapsules). *63rd Annual Meeting of the Society for Biotechnology, Japan*, 2011, September 26–28, Tokyo.

Other Publications, Patents and Awards

1. Kashima Y, **Iijima M**, Okamoto A, Koizumi Y, Udaka S, Yanagida F. Purification and characterization of the two intracellular esterases related to ethylacetate formation in *Acetobactor pasteurianus*. *J Ferment Bioeng* 1998;85:584–588.

2. Kashima Y, **Iijima M**, Nakano T, Tayama K, Koizumi Y, Udaka S, Yanagida F. The role of intercellular esterases in the production of esters by *Acetobactor pasteurianus*. *J Biosci Bioeng* 2000;89:81–83.

3. Sasaki T, Matsumoto T, Yamamoto K, Sakata K, Baba T, Katayose Y, Wu J, Niimura Y, Cheng Z, Nagamura Y, Antonio B, A, Kanamori H, Hosokawa S, Masukawa M, Arikawa K, Chiden Y, Hayashi M, Okamoto M, Ando T, Aoki H, Arita K, Hamada M, Harada C, Hijishita S, Honda M, Ichikawa Y, Idonuma A, **Iijima M**, Ikeda M, Ikeno M, Ito S, Ito T, Ito Y, Ito Y, Iwabuchi A, Kamiya K, Karasawa W, Katagiri S, Kikuta A, Kobayashi N, Kono I, Machita K, Maehara T, Mizuno H, Mizubayashi T, Mukai Y, Nagasaki H, Nakashima M, Nakama Y, Nakamichi Y, Nakamura M, Namiki N, Negishi M, Ohta I, Ono N, Saji S, Sakai K, Shibata M, Shimokawa T, Shomura A, Song J, Takazaki Y, Terasawa K, Tsuji K, Waki K, Yamagata H, Yamane H, Yoshiki S, Yoshihara R, Yukawa K, Zhing H, Iwama H, Endo T, Ito H, Nahn, JH, Kim HI, Eun MY, Yano M, Jiamg J, Gojobori T. The genome sequence and structure of rice chromosome 1. *Nature* 2002;420:312–326.

4. Miki K, Komase K, Mgone CS, Kawanishi R, **Iijima M,** Mgone JM, Asuo PG, Alpers PM, Takasu T, Mizutani T. Molecular analysis of measles virus genome derived from SSPE and acute measles patients in Papua New Guinea. *J Med Virol* 2002;68:105–112.

5. Komase K, Nakayama T, **Iijima M,** Miki K, Kawanishi R, Uejima H. The phosphoprotein of attenuated measles AIK-C vaccine strain contributes to its temperature-sensitive phenotype. *Vaccine* 2006;24:826–834.

6. Hasebe A, Tashima H, Ide T, **Iijima M**, Yoshimoto N, Ting K, Kuroda S, Niimi T. Efficient production and characterization of recombinant human NELL1 protein in human embryonic kidney 293-F cells. *Mol. Biotechnol in press.* (DOI: 10.1007/s12033-011-9440-4)

Patents

1. エステラーゼ構造遺伝子、その形質転換株 およびその構造遺伝子を用いた食酢の製造方法 (特許公開平 11-75860)

2. 抗体／抗原結合能を有する高感度免疫学測定用ナノ粒子 (特願 2008-269000)

3. 多抗原同時検出用ナノ粒子 (特願 2009-57199)

Awards

1. 平成 15 年 6 月（社）北里研究所研究奨励賞「麻疹ウイルスの N 蛋白に関する研究」

2. 平成 16 年 6 月（社）北里研究所研究奨励賞「麻疹ウイルスの N 蛋白の機能解析」